CRANFIELD UNIVERSITY

XUDONG QIU

EFFECT OF ROLLING ON FATIGUE CRACK GROWTH RATE OF WIRE AND ARC ADDITIVE MANUFACTURE (WAAM) PROCESSED TITANIUM

SCHOOL OF ENGINEERING

MSc By Research

MSc Thesis

Academic Year: 2012 - 2013

Supervisor: Dr. Xiang Zhang

November 2013

CRANFIELD UNIVERSITY

SCHOOL OF ENGINEERING
MSc By Research

MSc Thesis

Academic Year 2012 - 2013

XUDONG QIU

Effect of rolling on fatigue crack growth rate of Wire and Arc Additive Manufacture (WAAM) processed Titanium

Supervisor: Dr. Xiang Zhang
November 2013

This thesis is submitted in partial fulfilment of the requirements for the degree of MSc

ABSTRACT

Titanium (Ti) alloys have been commonly used in the aerospace industry, not only because they have a high strength-to-weight ratio (comparing to the steels) but also their satisfactory corrosion resistance. Furthermore, they can be assembled with the carbon fibre composite parts. However, conventional manufacturing methods cause high material scrap rate and require lots of machining to obtain the final shape and size, which increases both the manufacturing time and cost. In order to improve the efficiency and reduce the cost of Ti parts, Additive Manufacturing (AM) has been developed.

Rolled Wire and Arc Additive Manufacturing (rolled WAAM) is one of the AM processes. The main characteristics of this technology is the reduced β grain size to refine the alloy's microstructure. Both the ultimate tensile strength and yield strength of Ti alloy made by rolled WAAM are at least 10% higher than traditional wrought Ti.

This project is to investigate the fatigue crack growth rates of the Ti-6Al-4V built by rolled WAAM process in both the longitudinal and transverse orientations to study the effect of rolling on fatigue crack growth rate of WAAM processed Ti. The project was carried out by testing the fatigue crack growth rates for 4 compact tension specimens. The test results of different orientations were compared with each other, and scatters in fatigue life and fatigue crack growth rate were found. Fatigue crack growth rate is lower in the longitudinal specimens. The results are also compared with those of the unrolled WAAM specimens tested in a previous project. It was found that rolling can significantly improve the fatigue crack growth behaviour in WAAM processed Ti, and can reduce the difference between the two orientations, i.e. achieving better isotropic material properties. Recorded scatters may be caused by the process induced residual stresses, error in measurement, and the test machine load range being much higher than the applied loads. More specimens can be tested to validate above observations further.

Keywords:

Additive Manufacturing, Fatigue Crack Growth Rate, Ti-6Al-4V, Compact Tension Specimen, Rolling

ACKNOWLEDGEMENTS

I would like to thank Dr. Xiang Zhang for her advises and availability during this project. Her help was decisive in the achievement of this project.

I also would like to express my gratitude to Dr. Fude Wang for his guidance and assistance in the metallography of this project.

I would like to acknowledge Mr. Filomeno Martina for his availability and his kindness. I would not have been able to carry out all the tests I did without his hard working on building the specimens used in this project.

I am grateful to Mr. Ian Hakon for his help to machine the specimens used in this project.

I would like to show my gratitude to Mr. Barry Walker for his availability and his kindness. I would not have been able to carry out all the tests I did without his help.

I would like to thank Mr. Xueyuan Wang for his support in this project.

I would like to thank my family and all the friends for all the support they have been giving me.

Finally, I would like to thank my newly born son for his birth giving me hopes and confidence.

TABLE OF CONTENTS

ABSTRACT i
ACKNOWLEDGEMENTS iii
LIST OF FIGURES vii
LIST OF TABLES xi
LIST OF EQUATIONS xiii
LIST OF ABBREVIATIONS xiv
1 INTRODUCTION 1
1.1 Background 2
1.2 Layered deposition techniques 4
1.3 Scope 5
2 LITERATURE REVIEW 7
2.1 Additive manufacturing technologies 7
2.2 Microstructure of Ti-6Al-4V 12
2.2.1 Microstructure of traditional Ti-6Al-4V 13
2.2.2 Microstructure of WAAM Ti-6Al-4V 17
2.2.3 Microstructure of rolled WAAM Ti-6Al-4V 20
2.3 Mechanical properties of additive manufactured materials 24
2.3.1 Mechanical properties of DLD material 25
2.3.2 Mechanical properties of EBM material 26
2.3.3 Mechanical properties of WAAM material 27
2.3.4 Mechanical properties of rolled WAAM material 28
2.4 Fatigue behaviour 32
2.4.1 S-N curve 33
2.4.2 Fatigue crack propagation rates properties 33
2.4.3 Fatigue properties of AM manufactured materials 35
2.5 Fracture toughness 39
3 MATERIALS AND TESTING PROCEDURES 45
3.1 Original material and manufacturing method 45
3.2 Specimen machining 49
3.3 Test method 53
3.3.1 Measurement 53
3.3.2 Equipment for the fatigue crack growth rate tests 54
3.3.3 Parameters of the fatigue crack growth rate tests 56
3.3.4 Testing 57
4 TEST RESULTS 59
4.1 Results of L-T specimens 60
4.1.1 Crack growth life 61
4.1.2 Fatigue crack growth rates 62
4.2 Results of T-L specimens 65
4.2.1 Crack growth life 68

4.2.2 Fatigue crack growth rates 68
5 DISCUSSION 73
5.1 Comparison between L-T and T-L 73
5.1.1 a-N curves 74
5.1.2 da/dN curves 79
5.2 Comparison between unrolled and rolled WAAM 81
6 CONCLUSIONS 87
7 SUGGESTION FOR FUTURE WORK 89
REFERENCES 91
APPENDICES 97

LIST OF FIGURES

Figure 1-1 Producer price index trend for titanium mill products, 1971–2006 [8] 3

Figure 1-2 Surface integrity of machined sample at magnification 500X [10] 4

Figure 1-3 AM Ti-6Al-4V component used on F-35 [11] 4

Figure 2-1 SLD schematics 8

Figure 2-2 Process of EBM [14] 9

Figure 2-3 Process of SMD [15] 9

Figure 2-4 Principle of additive layer manufacturing [2] 10

Figure 2-5 Principle of rolled WAAM [18] 10

Figure 2-6 Directions of the parts [19] 11

Figure 2-7 Structure transformation of Ti [4] 12

Figure 2-8 Alloying effects on titanium phase diagram [3] 13

Figure 2-9 Prior and secondary alpha phase in Ti-6Al-4V after heat treatment in the (α+β) field and post-deformation quenching [2] 15

Figure 2-10 Relationship between α and β in Ti-6Al-4V, α inside β [23, 24] 15

Figure 2-11 Widmanstätten microstructure of Ti-6Al-4V [26] 16

Figure 2-12 The growth of lamellae [19] 16

Figure 2-13 Microstructure with different cooling rates. A: 1 ^{O}C/min, B: 100 ^{O}C/min, C: 800 ^{O}C/min [27] 17

Figure 2-14 Coordinate system defined for WAAM [29] 17

Figure 2-15 A WAAM processed wall [30] 18

Figure 2-16 Orientation of prior β grains at the top and bottom of the wall [2] .. 18

Figure 2-17 Differences in the microstructure of top and bottom regions [2] 19

Figure 2-18 Microstructure of a WAAM component, near the top (a, b), and in the central region (c, d) [31] 19

Figure 2-19 β grains in WAAM processed component [19] 20

Figure 2-20 Rolling equipment at the Welding Engineering Research Centre, Cranfield University [17] 21

Figure 2-21 Microstructures from the refined region from the centre of the wall a) without rolling, b) 50 kN load, c) 75 kN load [33] 22

Figure 2-22 Y-Z sections a without rolling, b 50 kN load, c 75 kN [18] 23

Figure 2-23 Grain sizes change with different loads, control means the unrolled one [19] 23

Figure 2-24 Microstructures of a) common low-carbon steel [34], b) 75 kN WAAM [33] 24

Figure 2-25 a) microstructure in longitudinal direction, b) microstructure in transverse direction [38] 27

Figure 2-26 Roller designs applied to the WAAM deposits [33] 29

Figure 2-27 Effects on residual stress in longitudinal direction 30

Figure 2-28 Effects on residual stress in transverse direction 30

Figure 2-29 Comparison of tension properties of various load rolled WAAM and wrought Ti-6Al-4V [19] 31

Figure 2-30 Comparison of the tensile properties by different processes 32

Figure 2-31 Constant amplitude fatigue crack growth under small-scale yielding conditions [44] 34

Figure 2-32 Typical fatigue crack growth behaviour in metals [44] 34

Figure 2-33 Fatigue crack growth rate results of SLM parts (as-built), [edited from Ref 36] 36

Figure 2-34 Fatigue crack growth rate test results of WAAM, [edited from Ref 2] 37

Figure 2-35 Crack growth in L-T specimen [2] 37

Figure 2-36 Fatigue characteristics of EBM specimens, [edited from Ref 38] .. 38

Figure 2-37 Variation of measured fracture toughness with specimen thickness for an unspecified alloy [44] 39

Figure 2-38 Effect of specimen thickness on fracture surface [44] 39

Figure 2-39 C (T) specimens used by Lorant [2] 40

Figure 2-40 DC Current System [45] 41

Figure 2-41 Specimen dimension requirement in ASTM E399 [46] 42

Figure 2-42 C (T) specimen and Displacement Gage used in 43

Figure 2-43 Directions of the specimens, (a) L-T, (b) T-L [2] 44

Figure 2-44 Crack propagation in compact tension specimen a） L-T specimen, b) T-L specimen [2] 44

Figure 3-1 Current signal used in the VBC Interpulse Tungsten Inert Gas Welding 45

Figure 3-2 TIG COMMANDER 400AC/DC 46
Figure 3-3 Machine used to build the wall 47
Figure 3-4 Roller used to build the wall 47
Figure 3-5 Final dimensions of the wall 48
Figure 3-6 The initial wall 48
Figure 3-7 Unrolled WAAM processed Ti-6Al-4V wall [2] 49
Figure 3-8 Dimensions requirements in ASTM E647 [45] 50
Figure 3-9 Wave surface of the initial wall 50
Figure 3-10 Layout of the specimens 51
Figure 3-11 Dimensions of the specimens 52
Figure 3-12 Scribing the specimens using the vernal gauge 53
Figure 3-13 Scores in the specimens 54
Figure 3-14 Clevis used in the tests 55
Figure 3-15 C (T) specimen, microscope, levis and grips in the INSTRON machine 55
Figure 3-16 Scribed lines observed from the microscope 56
Figure 3-17 Pre-crack requirement in ASTM E647 [45] 57
Figure 4-1 Fatigue crack in the test observed through a microscope (vertical lines indicate the scribes at 1 mm distance) 59
Figure 4-2 Definition of L-T specimen 60
Figure 4-3 Locations of L-T specimens as they were cut off from the “wall”; crack in L1 specimen was from the wall’s top to bottom, crack in L2 specimen was from the wall’s bottom (near the substrate plate) 61
Figure 4-4 Photo of the L1, L2 specimens 61
Figure 4-5 Test measured *a-N* curves of L1 and L2 62
Figure 4-6 Fatigue crack growth rate curves of L1 and L2 63
Figure 4-7 Specimen L1 after the test 65
Figure 4-8 Specimen L2 after the test 65
Figure 4-9 Definition of T-L specimen 66
Figure 4-10 Locations of T-L specimens, crack in T1 was from left to right, crack in T2 was from left to right 67

Figure 4-11 Final shapes of T1, T2 67

Figure 4-12 a-N curves of T1 and T2 68

Figure 4-13 Fatigue crack growth rate curves of T1 and T2 69

Figure 4-14 Specimen T1 after the test 70

Figure 4-15 Specimen T2 after the test 71

Figure 5-1 Summary of a-N 74

Figure 5-2 (a) Microstructure observed in the top of the initial wall and (b) microstructure observed in the rest of the wall [47] 75

Figure 5-3 The range of top the area [47] 75

Figure 5-4 Distance between the top of initial wall and the specimen 76

Figure 5-5 Longitudinal residual stress in measured area [47] 77

Figure 5-6 Residual stress in the longitudinal (LD) direction [48] 78

Figure 5-7 Distance between the specimen and the bottom of the wall 78

Figure 5-8 Fracture profiles a) L2, b) T1 79

Figure 5-9 Summary for the *da/dN* curves 80

Figure 5-10 (a) unrolled L-T specimen (b) rolled L-T specimen 82

Figure 5-11 Crack growth path in the unrolled specimen [2] 83

Figure 5-12 Comparison of the *da/dN* curves between the rolled and unrolled Ti-6Al-4V specimens, also compare with Ti64 wrought 83

LIST OF TABLES

Table 1-1 Titanium alloy properties compared to Fe, Ni, and Al [3] 2

Table 2-1 Summary of advantages and disadvantages of Additive Layer Manufacturing processes 11

Table 2-2 Characteristics of Ti alloys 13

Table 2-3 Composition of Ti-6Al-4V [22] 14

Table 2-4 Mechanical property requirements for wrought Ti-6Al-4V in AMS 4911 [22] 24

Table 2-5 AMS 4999 – Titanium Alloy Laser Deposition Products 6Al-4V Annealed [35] 25

Table 2-6 Ultimate tensile strength, yield strength and elongation at break of SLM produced Ti-6Al-4V [36] 26

Table 2-7 Tensile test result [37] 26

Table 2-8 Tensile test results [38] 27

Table 2-9 Tensile tests results [2] 28

Table 2-10 Parameters used for the rolling experiments [33] 29

Table 2-11 Tensile test results [19] 31

Table 2-12 Fatigue properties of AM processed Ti-6Al-4V 38

Table 2-13 Load range ΔP and fracture toughness K_{IC} for each specimen tested [2] 43

Table 3-1 Parameters used to build the wall 46

Table 3-2 Parameters of specimens used in fatigue crack growth rate tests ... 58

Table 4-1 The Paris Law constants of the L-T specimens 64

Table 4-2 The Paris Law constants of the T-L specimens 69

Table 5-1 Tensile properties and hardness of rolled WAAM processed Ti-6Al-4V 73

Table 5-2 Comparison of the Paris Law parameter 80

Table 5-3 Comparison between fatigue crack growth rates of the four specimens 81

Table 5-4 Comparison of fatigue crack growth rates of rolled and unrolled Ti .. 84

LIST OF EQUATIONS

(2-1)..... 34
(2-2)..... 35
(2-3)..... 35
(2-4)..... 35
(2-5)..... 41
(2-6)..... 42
(2-7)..... 42
(2-8)..... 42
(2-9)..... 42
(3-1)..... 56
(4-1)..... 59
(4-2)..... 63
(4-3)..... 64

LIST OF ABBREVIATIONS

a	Crack length
AM	Additive Manufacturing
AMS	Aerospace Material Specification
ASTM	American Society for Testing and Materials
BCC	Body Centred Cubic
BTF	Buy-To-Fly
C (T)	Compact Tension
CAD	Computer Aided Design
DLD	Direct Laser Deposition
E	Modulus of Elasticity
EADS	European Aeronautic Defence and Space Company N.V.
EASA	European Aviation Safety Agency
EBD	Electron Beam Deposition
EBM	Electron Beam Melting
FAA	Federal Aviation Administration
FCC	Face Centred Cubic
HCF	High Cycle Fatigue
HCP	Hexagonal Close Packed
IMS	Integral Metallic Structures
K	Stress intensity factor
K_{IC}	Fracture Toughness
K_{max}	Maximum stress intensity factor
K_{min}	Minimum stress intensity factor
LCF	Low Cycle Fatigue
PSBs	Persistent Slip Bands
RP	Rapid Prototyping
RUAM	Ready-to-Use Additive Manufacturing
SLD	Supersonic Laser Deposition
SMD	Shaped Metal Deposition
Ti	Titanium
TIG	Tungsten Inert Gas
TMF	Thermal Mechanical Fatigue

VBC	VBC Group Ltd
WAAM	Wire and Arc Additive Manufacturing
WELPC	Welding Engineering and Laser Processing Centre
ε	Elongation at Break
σ_b	Ultimate Tensile Strength
σ_y	Yield Tensile Strength

1 INTRODUCTION

With the rapid increasing competition in aircraft industry especially in commercial aircraft, a successful commercial aircraft must meet the strict requirements not only from the airworthiness, but also from the environment, safety, market and so on. So it has become more and more important to try best to meet all the requirements and simultaneously reduce the cost as much as possible. The cost of Ti material is expensive, and the machining cost is also expensive.

The "Buy-To-Fly" (BTF) ratio is a frequently-used factor in the aerospace field (the ratio of material bought to material that eventually goes to the aircraft). This ratio is at a range of 10-20:1 in a conventional process [1]. Effective ways that can reduce this ratio and substitute the conventional processes efficiently are being investigated.

Additive Manufacturing (AM) is generated as a consequence of developments of Rapid Prototyping used in a variety of industries to describe a process that directly fabricates a model using a three-dimensional Computer Aided Design system without the need for process planning. This technology is widely used in prototypes, tooling components, and manufacturing parts with different materials, etc [1]. AM can reduce the BTF ratio by 35%-45%. EADS research team in Filton forecasted that 25 meter-length or approximate component parts of an Airbus airplane could be made by using AM, saving around 3000 tons in weight and a $300 billion is saving for airlines [1].

Damage tolerant design manages the extension of cracks in structures is used in aircraft design to ensure the safety of an aircraft and reduce maintenance costs. Materials which have good fatigue properties are desired in order to improve the damage tolerance. Choosing a material with lower fatigue crack growth rate can improve the damage tolerance of the structure.

WAAM uses a welding process to manufacture 3D metal geometries. It can greatly reduce the manufacturing cost and decrease the "Buy-To-Fly" ratio

nearly to 1:1 [1]. The high efficiency of the WAAM process for Ti alloy parts has been proved in Lorant's work [2].

Rolled WAAM is a newer process developed from the WAAM. It is proved that rolling the structure normal to the surface can significantly decrease the longitudinal residual stress. This project investigates the rolling effects over the fatigue crack growth rate of the WAAM processed Ti-6Al-4V.

1.1 Background

In 1795, Klaproth, a German scientist, identified an oxide of an unknown element, which was subsequently determined to be the same as discovered earlier by Gregor. The metal was bestowed with the name “titanium” in reference to the titans of Greek mythology [3]. Titanium is named after the Titans, the powerful sons of the earth in Greek mythology. Titanium is the forth abundant metal on earth crust (~ 0.86%) after aluminium, iron and magnesium [4]. Titanium alloys possess a combination of mechanical properties and corrosion resistance which makes them very attractive for the airframe applications. It can be seen from Table 1-1 that titanium has a high strength to weight ratio – only less than 60% of the density of iron. And better corrosion resistance than aluminium. Titanium also has lower thermal conductivity than iron and high strength –around 55% of the Young's modulus of iron.

Table 1-1 Titanium alloy properties compared to Fe, Ni, and Al [3]

	Ti	Fe	Ni	Al
Melting Temperature (^{o}C)	1670	1538	1455	660
Allotropic Transformation (^{o}C)	$\beta \xrightarrow{882} \alpha$	$\gamma \xrightarrow{912} \alpha$	–	–
Crystal Structure	$\mathrm{BCC} \rightarrow \mathrm{HCP}$	$\mathrm{FCC} \rightarrow \mathrm{BCC}$	FCC	FCC
Room Temperature *E* (GPa)	115	215	200	72
Yield Stress Level (MPa)	880(Ti-6Al-4V)	1517(300M)	1034（Inconel 718）	455（7075）
Density (g/cm^3)	4.5	7.9	8.9	2.7
Comparative Corrosion	Very	Low	Medium	High

Resistance	High			
Comparative Reactivity with Oxygen	Very High	Low	Low	High
Comparative Price of Metal	Very High	Low	High	Medium

The use of titanium in commercial airliners has continued to grow from only 5% weight on the DC 7 in 1953 [5] to the latest generation of jetliners such as the Boeing 787 and Airbus A350 containing more than 15% [6]. The advantages of its excellent comprehensive mechanical properties, such as high strength, excellent fracture toughness and good corrosion-resistance as mentioned above makes it compatible with the carbon fibre composites.

However, it is quite expensive to make titanium and its alloy. The cost is almost 6 times more than aluminium and 10 times more than stainless steel to produce a titanium part [7]. The cost is rising at a rapid rate in these years as shown in Figure 1-1.

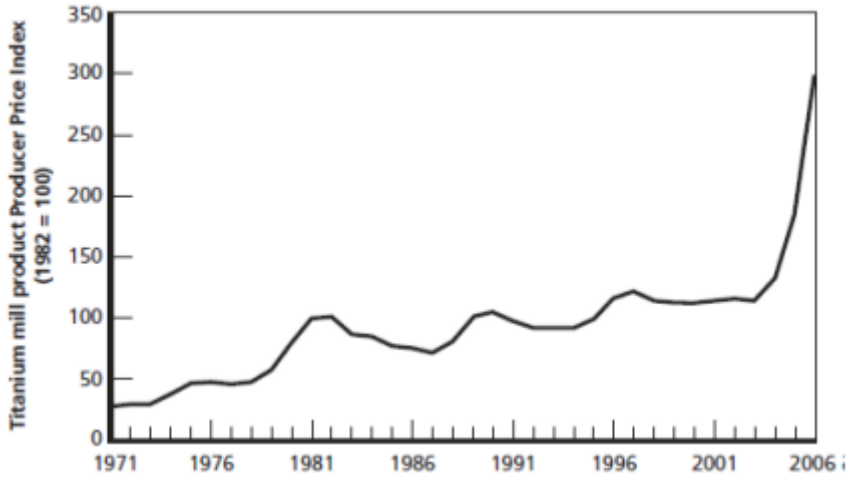

Figure 1-1 Producer price index trend for titanium mill products, 1971–2006 [8]

Finding a low cost and high efficient manufacturing process has become a hot topic. Traditional manufacturing techniques cause material scrap and require lots of machining to get the final shape (90% of the initial material block is wasted), which increases both manufacturing time and cost. Beside this, the sharp tools like milling cutters during traditional process could cause micro cracks on the alloy surface which limits the service life of structures or cause

premature failures. Airbus found scratches less than 200 μm deep are capable of severely reducing the fatigue life performance under service load [9]. Scratches can be seen in Figure 1-2.

Wrought blocks used in traditional process also could have internal defects which also reduce the fatigue properties of the structure. An efficient and low cost method is always being sought for in Ti manufacturing.

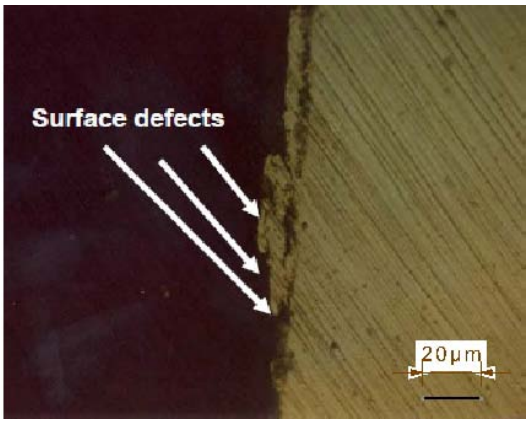

Figure 1-2 Surface integrity of machined sample at magnification 500X [10]

1.2 Layered deposition techniques

Over the past decade, layered deposition techniques have turned to a true manufacturing platform. Layered deposition technologies can drastically reduce the manufacturing costs and material scrap of components for the aerospace industry. Applications of metal Additive Manufacturing (AM) have concentrated on the high value materials such as Ti-6Al-4V. Figure 1-3 shows the Ti-6Al-4V part manufactured by AM used on the F-35 aircraft.

Figure 1-3 AM Ti-6Al-4V component used on F-35 [11]

As a rapid prototyping technique, layered deposition technology is a process based on welding. Short lead-time is obtained and design changes can easily be incorporated [2].

1.3 Aim and objectives

The aim of this study is to investigate the effect of rolling on fatigue crack growth rate of WAAM processed Ti.

The objective of this study is to determine the fatigue crack propagation behaviour of the Ti-6Al-4V specimens built by rolled WAAM process through fatigue crack growth rate tests, and compare the test results with the unrolled ones by Emilie Lorant [2], then find the effect of rolling on fatigue crack growth rate. The testing method follows the specification ASTM Standard E647 (standard test method for measurement of fatigue crack growth rates).

2 LITERATURE REVIEW

This chapter describes the manufacture technologies used in this project and other Additive Manufactures under developing. The microstructures of Ti-6Al-4V especially the microstructures of both the unrolled and rolled WAAM processed Ti-6Al-4V are also described in this chapter. The mechanical properties of the materials made by different manufacture technologies are compared in this chapter as well.

2.1 Additive manufacturing technologies

AM is the fabrication of functional net or near net shape products directly from CAD solid models [1]. AM technologies combine high flexibility and low cost manufacture with the advantages of RP. Due to the short product development cycles, increased components complexity and product variability, AM technologies have become more competitive than traditional manufacturing technologies in recent years. These technologies are now being developed to producing Ti-6Al-4V parts to lower the manufacturing cost. Different from the traditional manufacturing through cutting, machining and turning to gain the final shape of the parts, AM technologies build the parts by adding the materials layer by layer. So AM technologies can save a lot of materials. On the other hand, Ti-6Al-4V is a kind of alloys with great hardness. Special tools of great hardness are required to treat the alloys during the traditional manufacturing, but AM technologies which are based on melting, do not need such expensive tools. So AM technologies can reduce the manufacturing cost.

The possibility of using AM technologies to substitute for traditional manufacturing technologies is being investigated. Since the materials must meet the strict regulation such as European Aviation Safety Agency (EASA) and Federal Aviation Administration (FAA), it is important to know the microstructures and mechanical properties of Ti-6Al-4V made by AM technologies.

Direct Laser Deposition (DLD) is a technique creating metal parts usually by direct sintering in a powder bed like a 3D printer. Wire instead of powder also

can be used in order to solve the dust problems and high prices of high quality powders. DLD process can obtain a good surface finish, but the products volumes are limited to the size of the bed and the average production rate is 50 grams per hour [2, 12]. Beside these, the equipment generally is large, requires large investments, and many safety measures have to be incorporated. Figure 2-1 shows one of the DLD processes, Supersonic Laser Deposition (SLD). A high pressure nitrogen gas supply is split and delivered to a converging–diverging nozzle both directly and via a speed. The powder stream impacts a region of the substrate that is simultaneously illuminated by a laser and sintered to the aimed shape in a process chamber [13].

Electron Beam Melting (EBM) or Electron Beam Deposition (EBD) is also based on powders. EBM is of 95 percent efficiency in its use of energy—5 to 10 times higher than DLD technology [14]. But surface finish quality is not as good as for DLD technology and high vacuum environment is demanded. EBM process is a complex process depending on different parameters of the system, ranging from beam power and beam size to scanning speed and scanning direction / scanning strategy. Figure 2-2 shows the process of EBM.

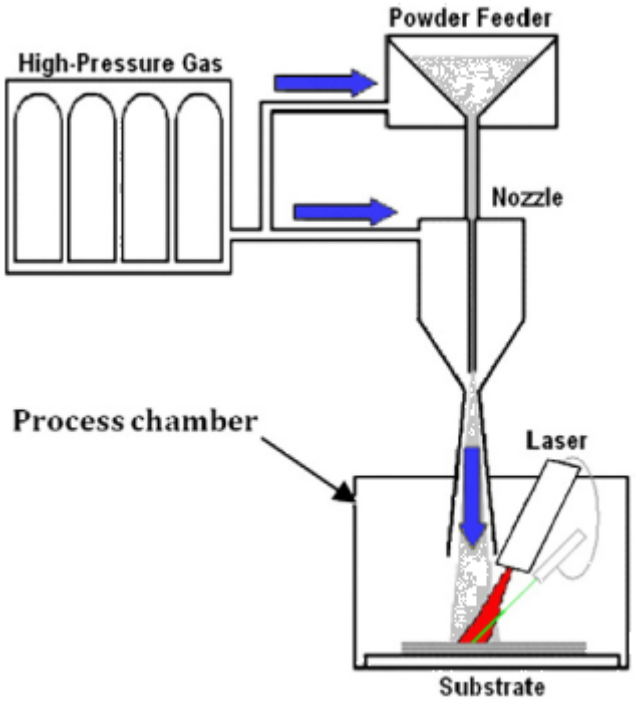

Figure 2-1 SLD schematics

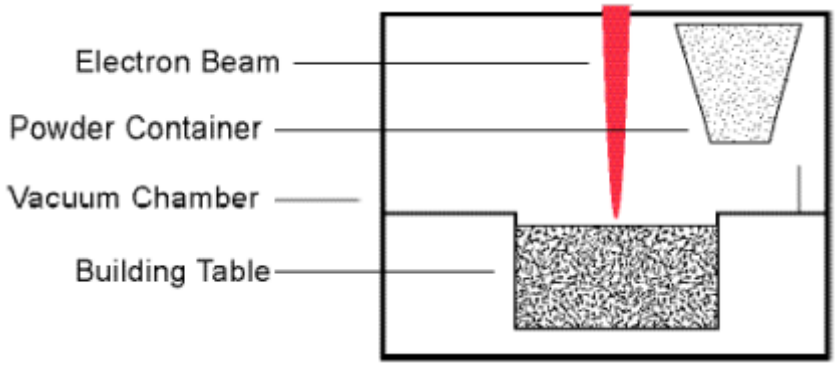

Figure 2-2 Process of EBM [14]

Shaped Metal Deposition (SMD) is a prototyping technique which creates near-net shape metal pieces layer by layer. SMD uses arc lased welding technologies and wire to produce parts in a protected atmosphere. The surface quality of the products is not as good as EBM processed parts. But the speed is faster than EBM. Also SMD can use any material which can be welded. The SMD process is shown in Figure 2-3.

Figure 2-1 Process of SMD [15]

Wire and Arc Additive Manufacture (WAAM) using Tungsten Inert Gas (TIG) welding is a technique that manufacture parts or components by adding material in the form of wire without the need of tooling [16]. The parts are manufactured layer by layer in a protected atmosphere and the welding machine is operated according to a Computer Aided Design (CAD) model. WAAM can produce large size parts and has a much higher deposition rate (up to 1 kg per hour can be deposited [12]) and lower cost comparing with DLD and EBM. Additionally, unlike the case of EBD it needs no vacuum. However, the

accuracy and surface quality are not as good as for DLD or EBM. Figure 2-4 shows the principle of WAAM manufacturing.

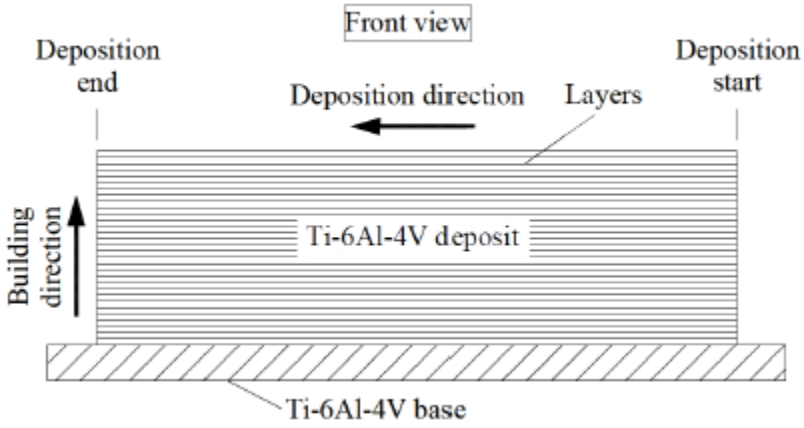

Figure 2-4 Principle of additive layer manufacturing [2]

Rolled Wire and Arc Additive Manufacture (rolled WAAM) or rolled Wire and Arc Additive Layer Manufacture (rolled WAALM) is a much newer manufacture based on the type of electric arc torch used to melt and fuse the wires. Rolled WAAM has a high deposition efficiency and low cost[17], so it has gained a lot of interest in recent years. The manufacturing is developed from normal WAAM mentioned above, a rolling process is introduced after each layer being deposited. The principle is shown in figure 2-5. Figure 2-6 illustrates the directions defined in WAAM. The advantages and disadvantages are listed in Table 2-1.

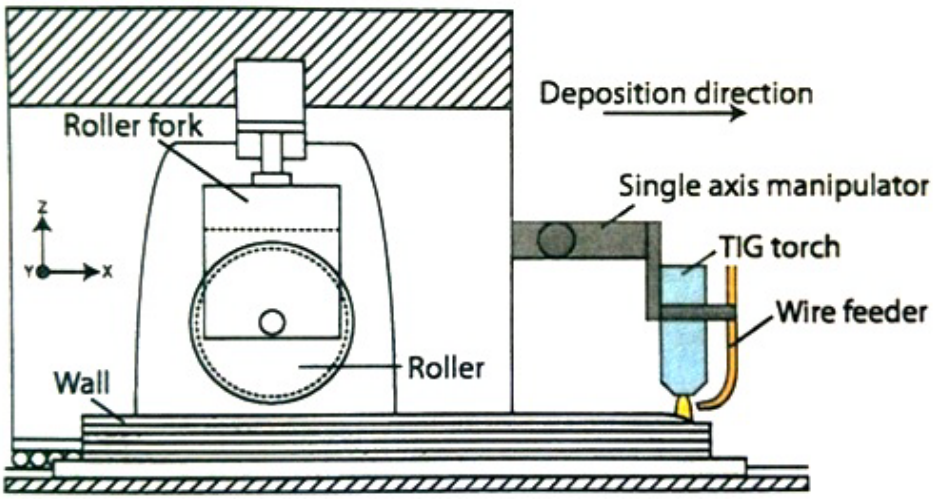

Figure 2-5 Principle of rolled WAAM [18]

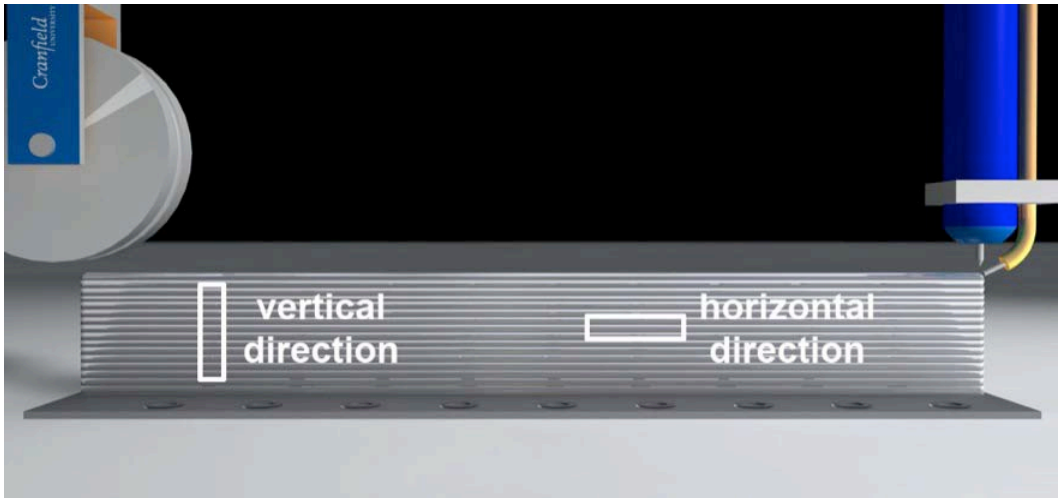

Figure 2-6 Directions of the parts [19]

Table 2-1 Summary of advantages and disadvantages of Additive Layer Manufacturing processes

Process	Advantages	Disadvantages
DLD	• Good surface quality	•Depend on the powder quality •The orientation of the part in the bed has an influence •Size of the part limited to the bed dimensions •Low production rate •High investments •Anisotropic
EBM	• Can be used for conductive metals and reflective alloys • Good mechanical properties	•Poorer surface finish than parts built by Direct Laser Deposition •High investments
WAAM	• Possibility to weld superalloys • Creation of large parts possible • Fastest Additive Layer Manufacturing process	•Poorer surface quality •Anisotropic
Rolled WAAM	• Possibility to weld superalloys • residual stress can be reduced • Faster Additive Layer Manufacturing process than DLD and EBD	•Products thickness depend on the roller gap •residual stress depends on rolling load

2.2 Microstructure of Ti-6Al-4V

Titanium is an allotropic element that has two primary crystallographic phases: alpha (α) is a hexagonal close packed structure (HCP) and beta (β) is a body centred cubic structure (BCC). It is in the α at ambient temperature. The structure changes when the temperature rises. The crystal structure transforms to β at 882.5 ^{o}C. Figure 2-7 presents the structure transformation.

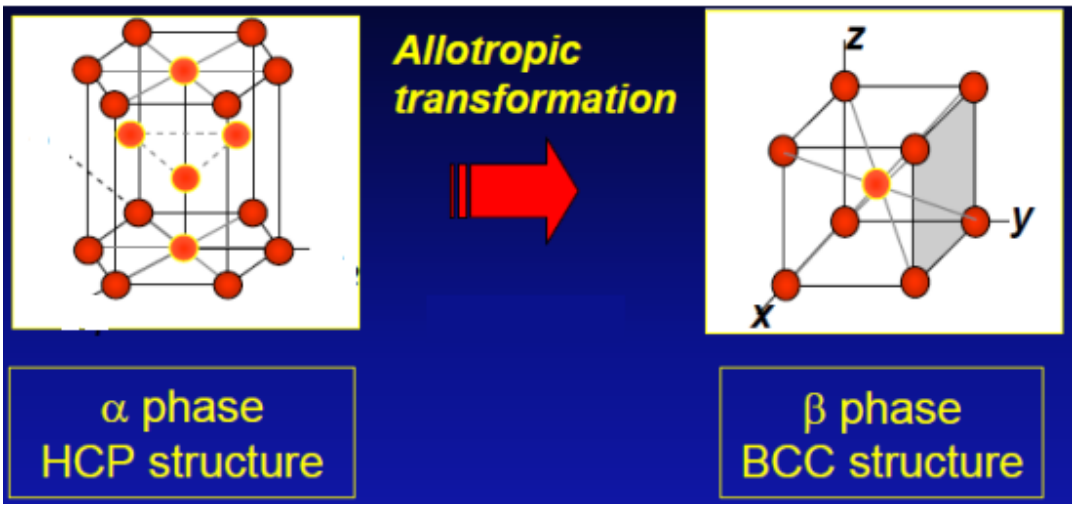

Figure 2-7 Structure transformation of Ti [4]

The morphology of the two crystallographic allotropic phases can be controlled to refine the structure and produce desirable mechanical properties combinations with different proportions of α and β. So the material property of titanium and its alloys can be optimized and tailored by designing the microstructure via control of chemistry, processing route, and heat treatment. Different phases have different characteristics. Increasing α phase can improve the creep strength and corrosion resistance, and increasing β phase can improve the tensile strength.

The exact temperature for transformation between the two phases is influenced by the purity of the metal. So the alloying elements for titanium can be divided into two categories according to their effects on "the transus temperature". One is called Alpha stabilizers which raise the β transus temperature with increasing the content, such as Al, O and N [20]. The other is called Beta stabilizers which decrease the β transus temperature with raising the content, such as V, Mo,

and niobium (Nb) [21]. The influence caused by different stabilizers is shown in figure 2-8. The characteristics of different Ti alloys are summarized in Table 2-2.

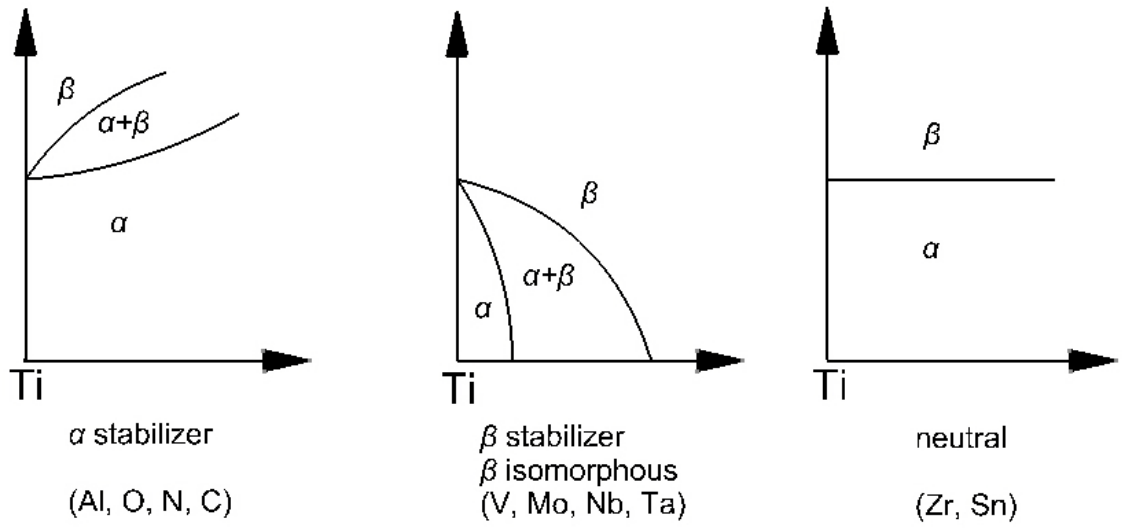

Figure 2-8 Alloying effects on titanium phase diagram [3]

Table 2-1 Characteristics of Ti alloys

Phase	Advantages	Disadvantages
α titanium alloys	Weldable Good creep strength Good corrosion resistance Good notch toughness	Non-heat treatable
β titanium alloys	Heat treatable High tensile strength	Low ductility
α+β titanium alloys	Heat treatable Good forming properties Good creep strength	

2.2.1 Microstructure of traditional Ti-6Al-4V

Ti-6Al-4V as one of the most widely used Ti alloys in the aerospace industry, is a typical α+β alloy .The composition percentages by weight are listed in Table 2-3.

Table 2-3 Composition of Ti-6Al-4V [22]

Element	min	max
Aluminium	5.5	6.75
Vanadium	3.5	4.5
Iron	--	0.3
Oxygen	--	0.2
Carbon	--	0.08
Nitrogen	--	0.05 (500 ppm)
Hydrogen	--	0.015 (150 ppm)
Yttrium	--	0.005 (50 ppm)
Other Elements, each	--	0.1
Other Elements, total	--	0.4
Titanium	remainder	

Annealing from the β phase field (β annealed) causes a transformation from β to α microstructure. This α structure called secondary α or "transformed β" is different from the α mentioned before. The former one called primary α (α ') is present during prior hot working and remains through heat treatment. The secondary α (α ") can have several microstructures (lamellar, acicular, serrated, platelike or basket weaves which is also called Widmanstätten) depending on cooling rate and alloy composition. Alloys with increasing β stabilizers have a higher tendency to form α " [20]. Figure 2-9 shows the prior and secondary alpha phase in Ti-6Al-4V after hot working in the (α+β) field and post-deformation quenching. Figure 2-10 is a simple explanation of the relationship between α " and β.

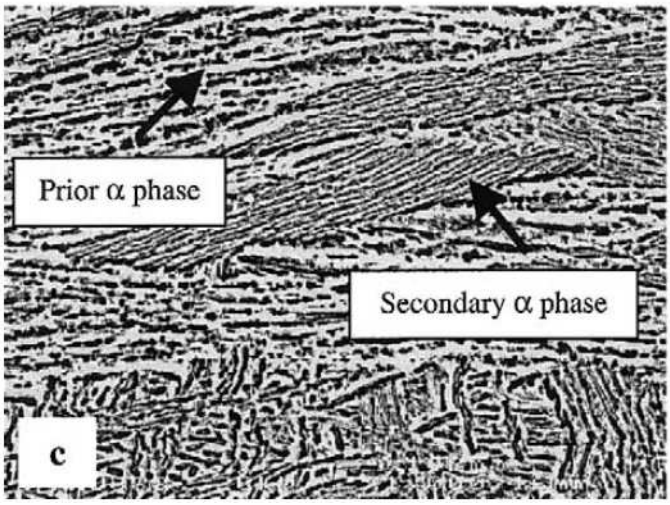

Figure 2-9 Prior and secondary alpha phase in Ti-6Al-4V after heat treatment in the (α+β) field and post-deformation quenching [2]

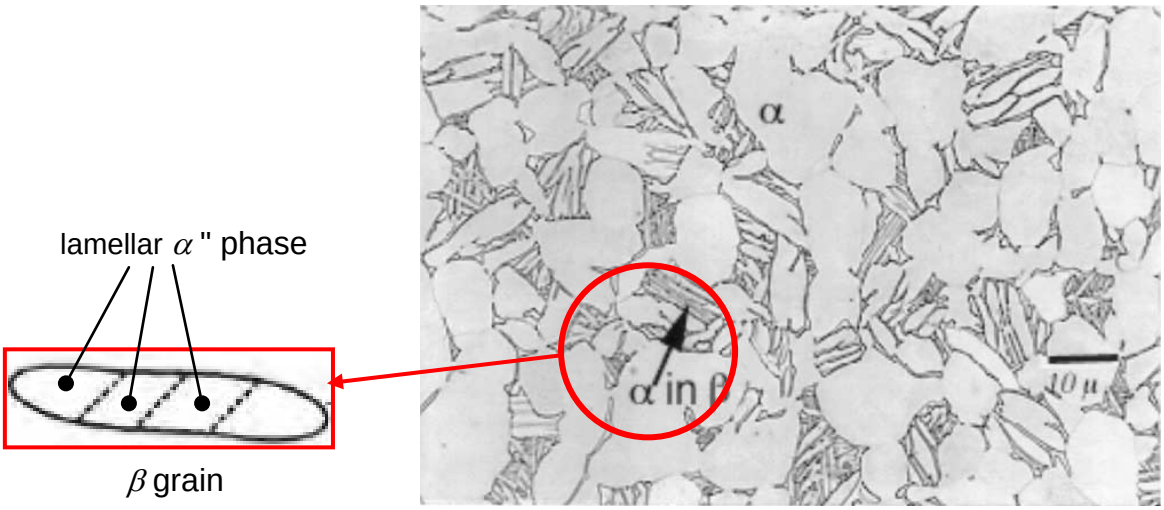

Figure 2-10 Relationship between α and β in Ti-6Al-4V, α inside β [23, 24]

β phase also has two types. They are equilibrium β and nonequilibrium (or metastable) β. The latter should be avoided by limiting their content in β stabilizers, because the metastable β can reduce the elastic modulus of the alloy [25].

The most common microstructure of Ti-6Al-4V used is a basketweave structure, called the “Alpha Widmanstätten structure” or Widmanstätten, which is obtained by cooling from above the beta transus temperature. Figure 2-11 shows the Widmanstätten structure of Ti-6Al-4V. In this structure, α phase (α lamellae) nucleates perpendicular to prior β grain boundaries as shown in Figure 2-12.

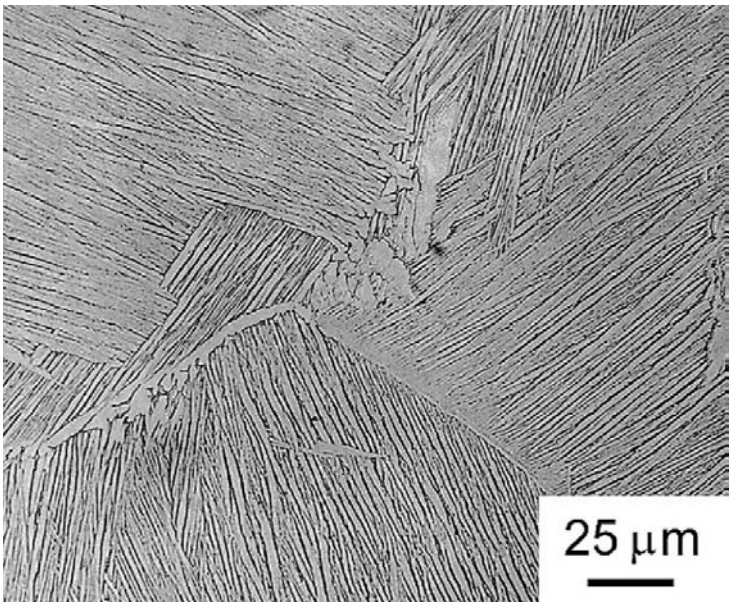

Figure 2-11 Widmanstätten microstructure of Ti-6Al-4V [26]

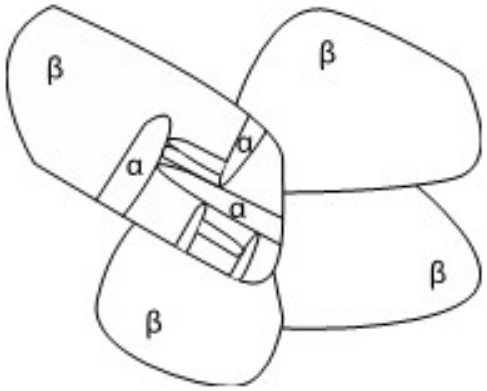

Figure 2-12 The growth of lamellae [19]

Widmanstätten structure increases yield stress of the alloy. The morphology can be changed from a colony of similarly aligned α laths to a Widmanstätten by raising the cooling rate or altering the alloy composition. With an increase in cooling rate, the α colony is decreased with a corresponding reduction in effective slip length and comparable increase in yield stress [3]. Figure 2-13 shows the microstructures with different cooling rates. It can be seen that with the increase in cooling rate the structure becomes much finer.

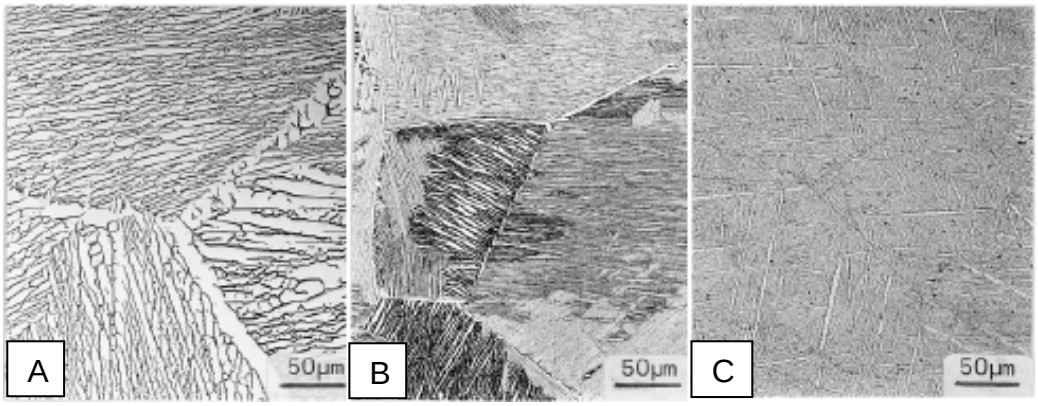

Figure 2-13 Microstructure with different cooling rates. A: 1 ^{O}C/min, B: 100 ^{O}C/min, C: 800 ^{O}C/min [27]

Finer microstructures slow crack nucleation and exhibit increased strength and ductility. Coarse microstructures are more resistant to fatigue-crack growth and creep [28].

2.2.2 Microstructure of WAAM Ti-6Al-4V

Since WAAM is a process from which a layered structure is produced, a coordinate system is defined, as shown Figure 2-14.

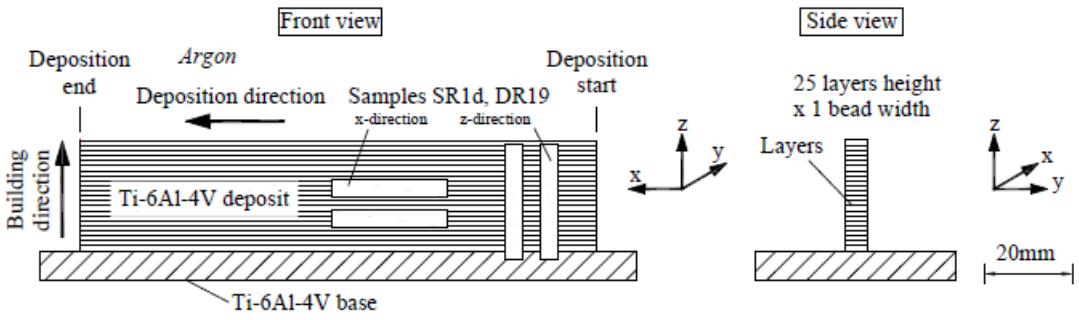

Figure 2-14 Coordinate system defined for WAAM [29]

The X-direction is the deposition direction (or the so-called longitudinal direction, "L") and z direction is the building direction (or the so-called transverse direction, "T"). Y is for the thickness (t). Figure 2-15 is a panel manufactured by WAAM. The dimension 1000 (L)*200 (T)*4 (t) mm and the original wire used is 1.2 mm in diameter. Figure 2-16 shows the β grains in the panel.

Figure 2-15 A WAAM processed wall [30]

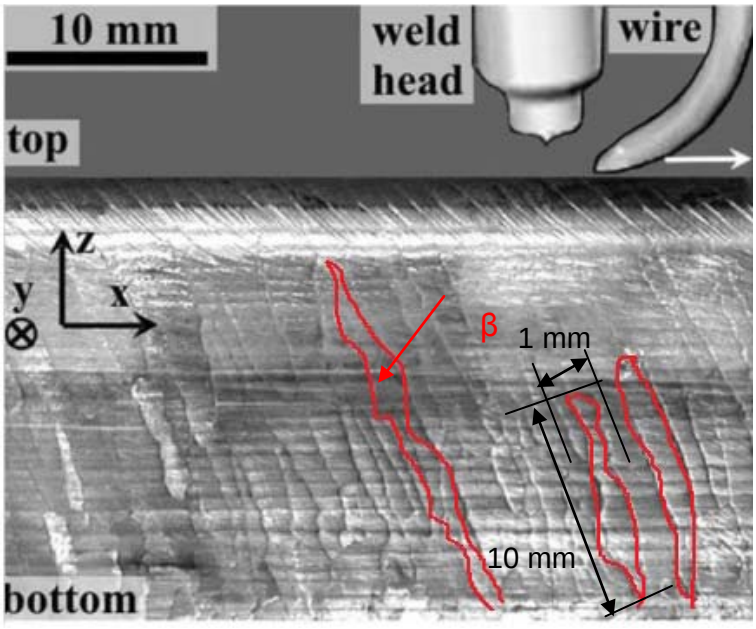

Figure 2-16 Orientation of prior β grains at the top and bottom of the wall [2]

The microstructure of a part built by WAAM process depends on its location in the wall. It can be seen from Figure 2-17, Figure 2-18 and Figure 2-19, top and bottom regions have different appearance. In the top area, the phases are much smaller than the phases in the bottom area.

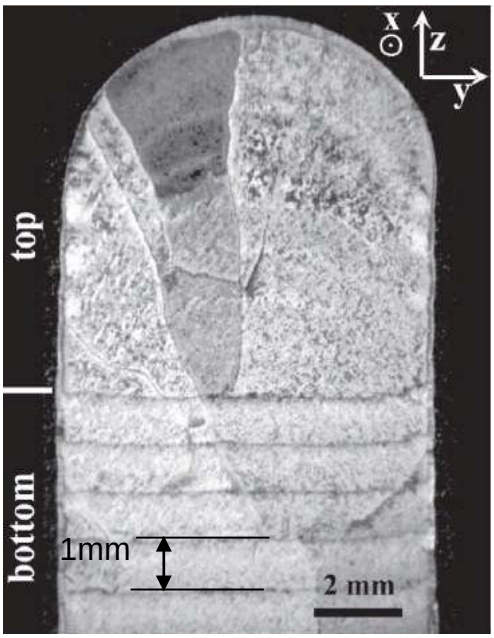

Figure 2-17 Differences in the microstructure of top and bottom regions [2]

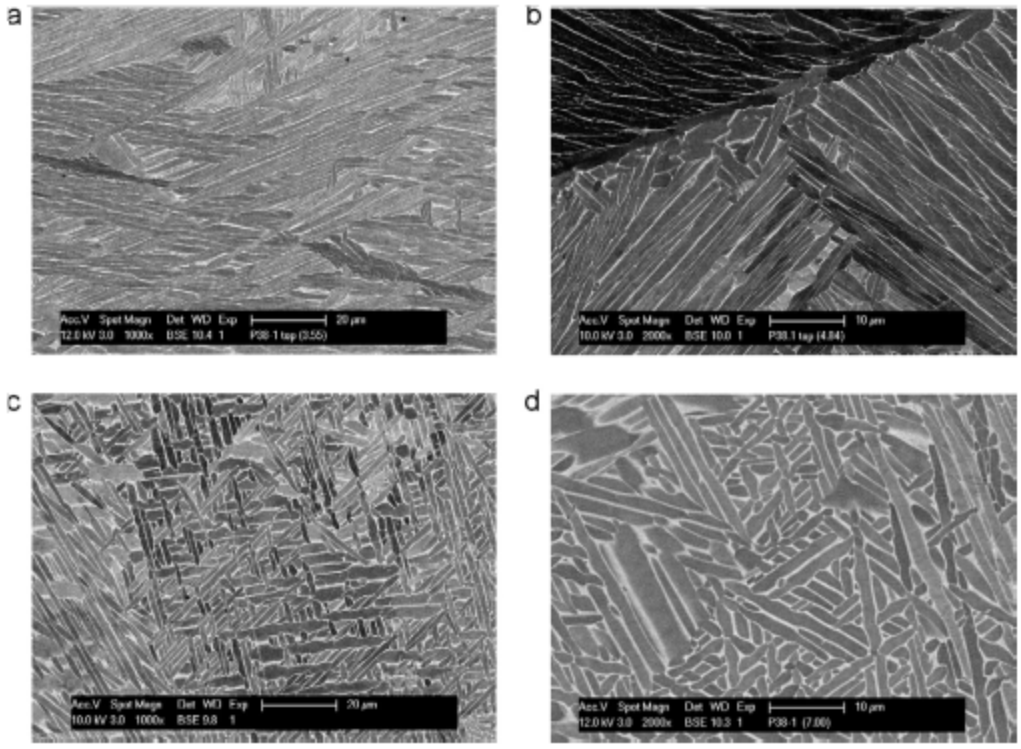

Figure 2-18 Microstructure of a WAAM component, near the top (a, b), and in the central region (c, d) [31]

The top and bottom both get an (α+β) microstructure and they are both Widmanstätten structure, but fine needles appear at the top and thicker laths are obtained at the bottom. In the study by Bernd Baufeld and Omer VanderBiest (2009) they explain that the top region represents the area which

was within the β phase field during the very last deposition, and this region is led to fine α needles within a β matrix resulting from the fast cooling after the last deposition. In contrast, the bottom region was subjected to repeated heat treatments within the (α+β) phase field by subsequent welding steps, which leads to the coarsening of the α laths [32]. In another word, it means that the bottom region is annealed several times, which causes α laths becoming coarser. On the other hand, the top region was cooled quite fast. For these characteristics, the alloy gets an anisotropic microstructure. Annealing can cause an increase of the ultimate tensile strength and a decrease of the ductility.

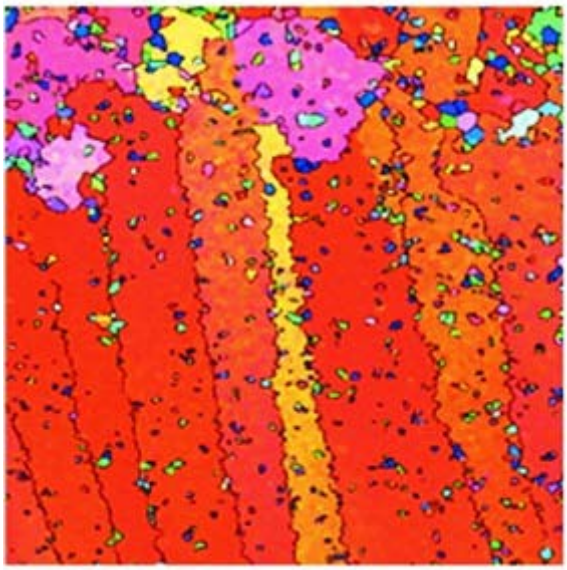

Figure 2-19 β grains in WAAM processed component [19]

Due to the difference in the grain size in the WAAM part, the parts made by WAAM process have an anisotropic characteristic. The mechanical properties may appear different in different directions.

2.2.3 Microstructure of rolled WAAM Ti-6Al-4V

Rolled Wire and Arc Additive Manufacturing mentioned here is a kind of WAAM technologies combining the application of rolling. Figure 2-20 is the rolled WAAM equipment.

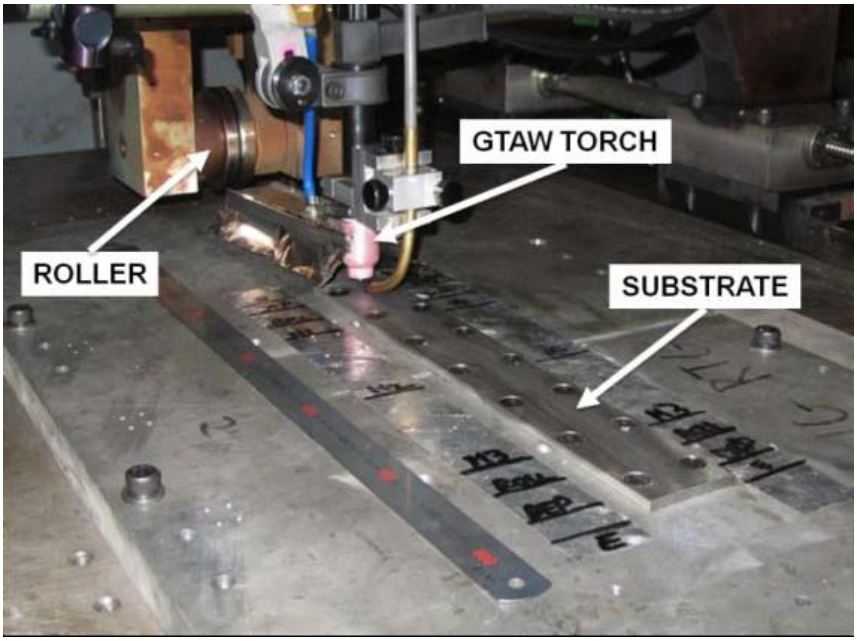

Figure 2-20 Rolling equipment at the Welding Engineering Research Centre, Cranfield University [17]

A roller is used to deform the deposited layer with a predefined load immediately after the deposition of each layer. β grain size is reduced through this process. Distortion and residual stress are also reduced as well. The effects of rolling on microstructure are shown in Figure 2-21, and Y-Z sections of a control sample without rolling, a wall rolled with a 50 kN load, and a wall rolled with a 75 kN load are shown in Figure 2-22. The grain is finer under higher load. Yield strength and ultimate tensile strength increase if the microstructure is finer. Figure 2-23 depicts the sizes change of grains with different loads. It can be seen that the sizes become smaller after rolling. Obviously the dimensions in different directions turn to be similar.

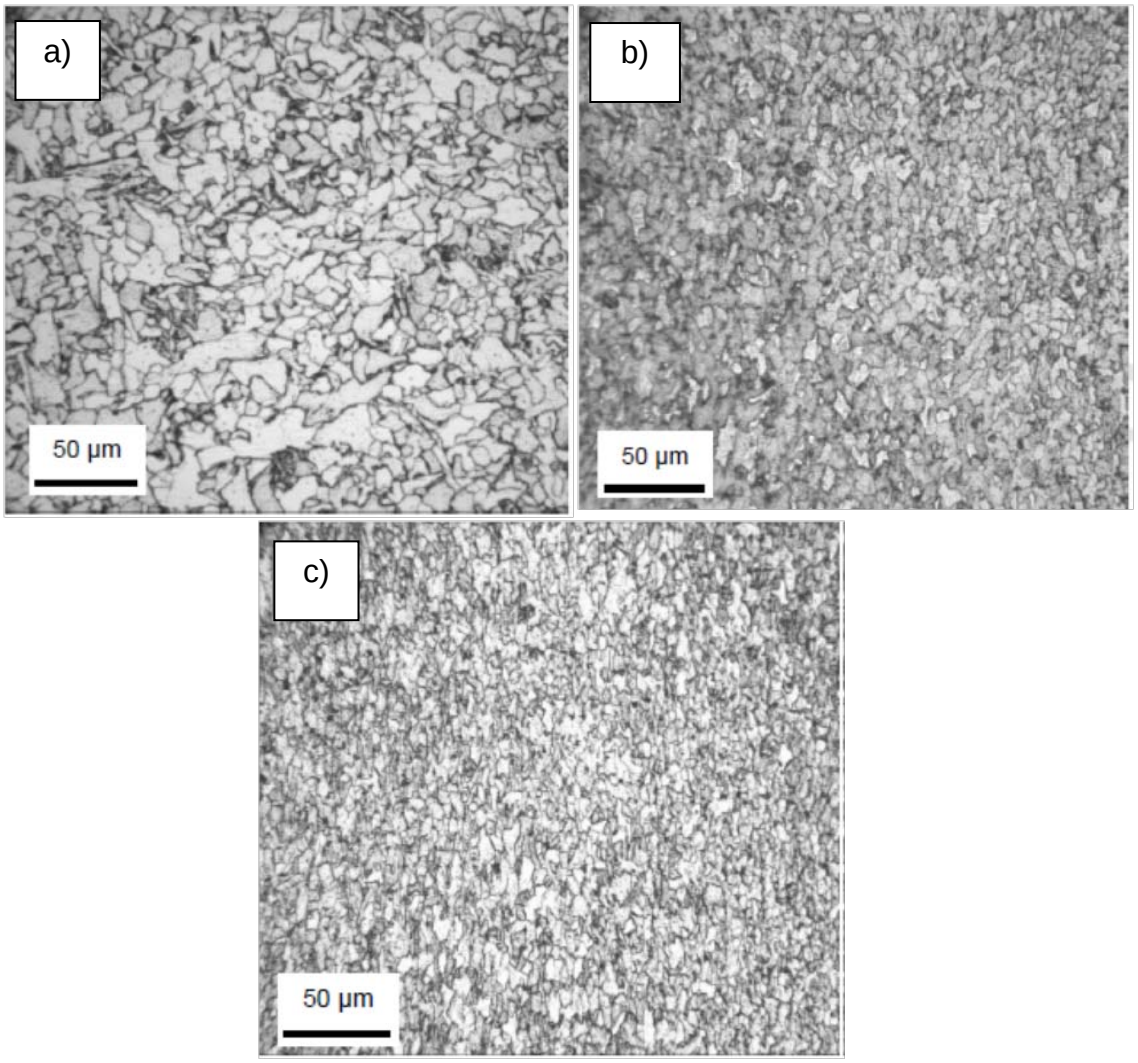

Figure 2-21 Microstructures from the refined region from the centre of the wall a) without rolling, b) 50 kN load, c) 75 kN load [33]

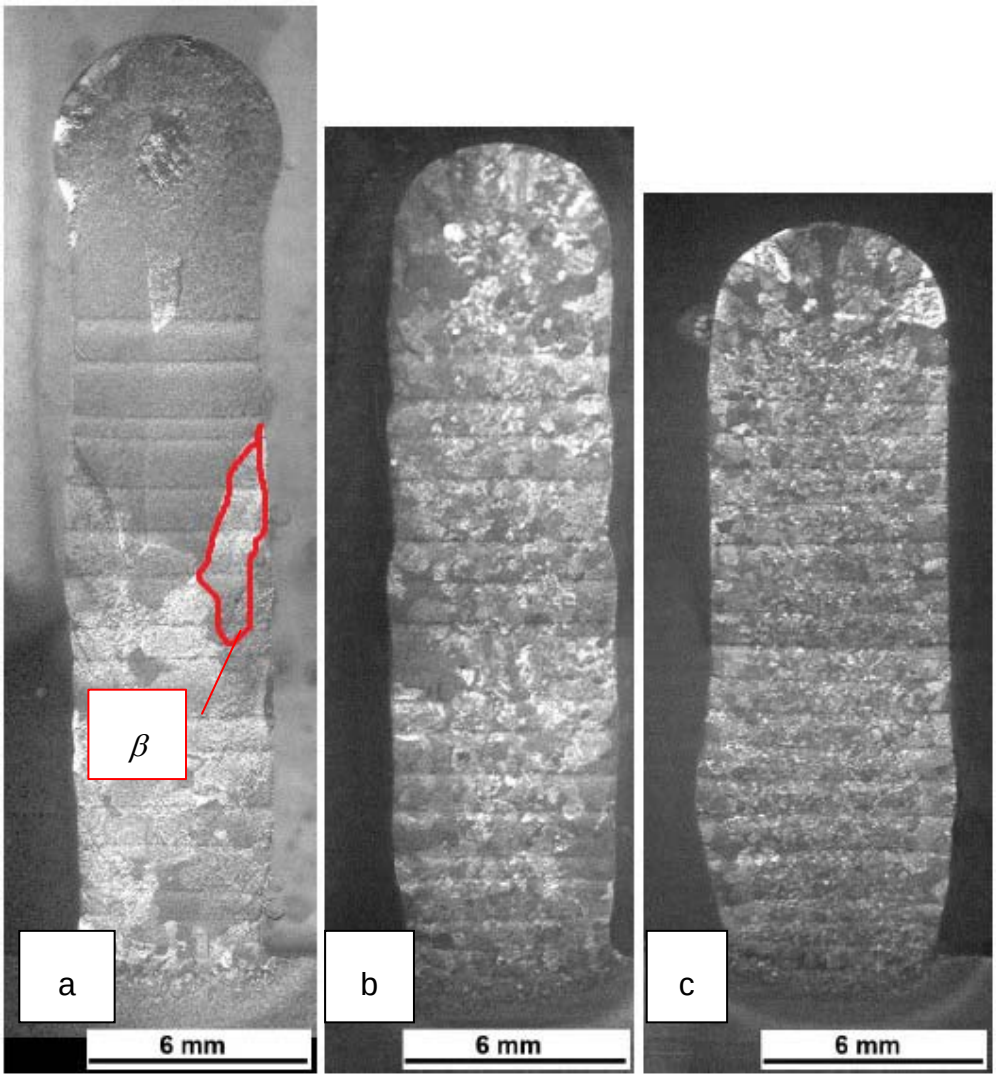

Figure 2-22 Y-Z sections a without rolling, b 50 kN load, c 75 kN [18]

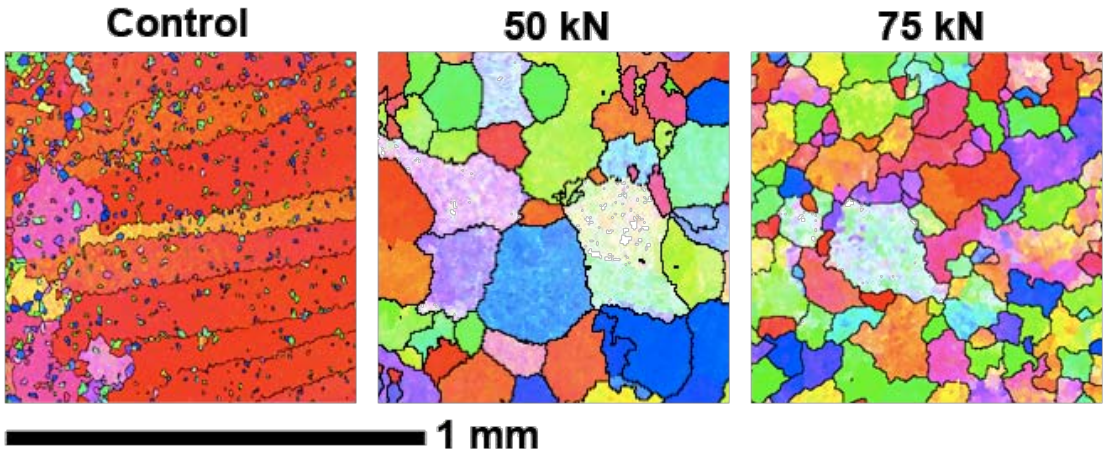

Figure 2-23 Grain sizes change with different loads, control means the unrolled one [19]

The microstructure at the top is obviously finer than that of unrolled WAAM. And comparing to the microstructure of a common low-carbon steel, the microstructure of WAAM processed component is even finer than the common one. Figure 2-24 is the comparison between the common low-carbon steel and steel by rolled WAAM. The grains sizes of rolled WAAM processed component with 75 kN rolling load are smaller than the grains sizes of common used one.

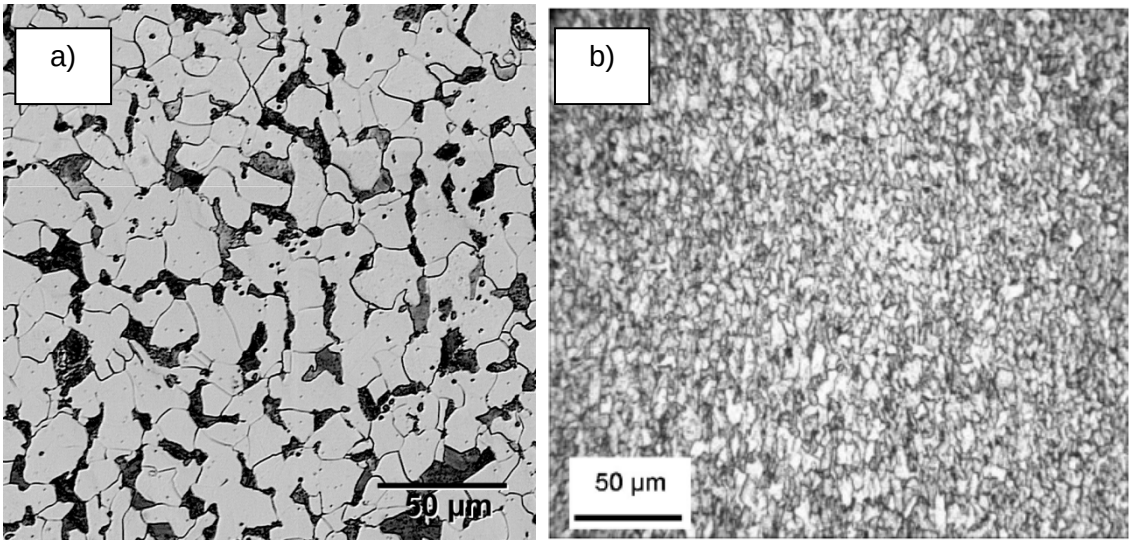

Figure 2-24 Microstructures of a) common low-carbon steel [34], b) 75 kN WAAM [33]

Due to recrystallisation phenomena under high-pressure, mechanical properties which are very close to isotropy can be obtained through rolling. This makes it possible to gain the industrial adoption of metal by additive manufacture.

2.3 Mechanical properties of additive manufactured materials

In the aerospace industry, all the materials must meet the specifications in the standards, and can be used on an aircraft. Table 2-4 lists the mechanical properties requirements in Aerospace Material Specification (AMS) 4911 [22].

Table 2-4 Mechanical property requirements for wrought Ti-6Al-4V in AMS 4911 [22]

Mechanical properties	Metric	Comments
Ultimate Tensile Strength (*UTS* or σ_b)	950 MPa	
Yield Tensile Strength (*YTS*	880 MPa	

or σ_y)		
Elongation at Break (ε)	14%	
Modulus of Elasticity (E)	113.8 GPa	
Fracture Toughness (K_{IC})	60 MPa.m$^{1/2}$	Plane-strain

Standard for annealed Ti-6Al-4V laser deposition products, AMS 4999 has been developed since 2002. Table 2-5 shows the mechanical properties requirements in AMS 4999 [35]. Note that the elongation at break is much lower than the wrought alloy.

Table 2-5 AMS 4999 – Titanium Alloy Laser Deposition Products 6Al-4V Annealed [35]

Mechanical properties	Longitudinal	Transverse
σ_b (MPa)	896	841
σ_y (MPa)	800	745
ε (%)	4	4

Several researches have been done to study the mechanical properties of the parts produced by Additive Manufacture in order to gain a satisfactory and stable result which can meet the standards. Then the manufacture can substitute the high cost and inefficient manufacture methods used today.

2.3.1 Mechanical properties of DLD material

Leuders et al. (2013) [36] researched the effects on mechanical properties by Selective Laser Melting (SLM) as a kind of Direct Laser Deposition (DLD) processes from which a good surface finish can be obtained, but the products volumes are limited to the size of the bed and the production rate is 50 grams per hour in average. SLM is characterized by medium productivity, high surface quality. Leuders and his team members used several Ti-6Al-4V specimens with standardized geometries made by powder with an average particle size of 40 μm in different heat treatment conditions. The one without heat treatment is referred to as "As-built", and the other samples were heat treated in vacuum or under Argon atmosphere at 800 ^{o}C (below β-transus), 1050 ^{o}C (above β-transus), and for hot isostatically pressed condition (HIP, at 920 ^{o}C at a pressure of 1000 bar for 2 h). Table 2-6 is the tensile test results. It can be seen

that 1050 ^{o}C heat treatment has the lowest strength but highest elongation at break.

Table 2-6 Ultimate tensile strength, yield strength and elongation at break of SLM produced Ti-6Al-4V [36]

Heat treatment	σ_b (MPa)	σ_y (MPa)	ε (%)
As-built	1080	1008	1.6
800 ^{o}C	1040	962	5
1050 ^{o}C	945	798	11.6
HIP condition	1005	912	8.3

The elongation at failure can be increased with the increased temperature, at the cost of decrease in the ultimate tensile strength.

In an earlier research by Sun et al. (2010) [37], they tested several components produced by SLM and obtained the properties, as shown in Table 2-7.

Table 2-7 Tensile test result [37]

Mechanical properties	Longitudinal	Transverse
σ_b (MPa)	1197	1122
σ_y (MPa)	1029	958
ε (%)	8.3	8.1
E (GPa)	116	111

All the research found that mechanical properties in the longitudinal direction are better than that in the transverse direction by SLM process. An isotropic property can be obtained by the HIP process. And the static properties are better than that of the wrought material, because that post heat treatment can reduce the anisotropy in mechanical properties and improve the ductility.

2.3.2 Mechanical properties of EBM material

Rafi et al. (2012) [38] studied the mechanical properties of the parts produced by EBM process. EBM can gain better mechanical properties than DLD does, but the surface finish quality is not as good as DLD. The EBM technology enables to manufacture three dimensional parts with properties comparable to wrought parts and better than casted products. The data in AMS 4999 is also

based on the EBM technology. The material Rafi used for their study was Ti-6Al-4V ELI (Extra Low Interstitial) powder with the average particle size of 60.8 µm [38]. Their specimens were manufactured for tensile and fatigue tests in longitudinal and transverse directions according to ASTM Standards E8M. The tensile test results are shown in table 2-8.

Table 2-8 Tensile test results [38]

Direction	Stress at Yield [Offset 0.2 %] (MPa)	Ultimate tensile stress (MPa)	Elongation at break (%)	*E*-Modulus (GPa)
As-built longitudinal	844	917	8.8	104
As-built transverse	782	842	9.9	101

The tensile properties in the longitudinal direction are better than those in transverse direction, except the elongation at break. Figure 2-25 shows the microstructures in both directions, and indicates that the grains in the longitudinal direction are much finer than in transverse direction.

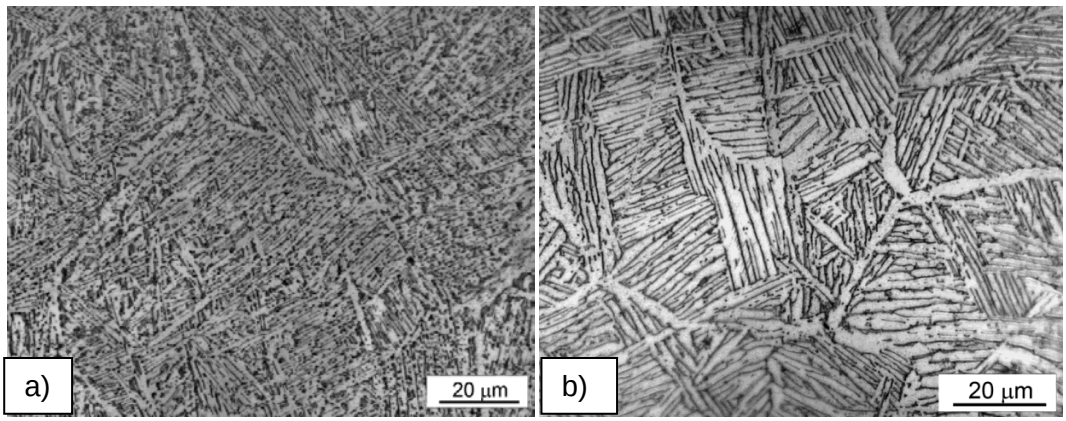

Figure 2-25 a) microstructure in longitudinal direction, b) microstructure in transverse direction [38]

2.3.3 Mechanical properties of WAAM material

Lorant (2010) [2] researched the mechanical properties of unrolled WAAM processed Ti-6Al-4V, her study was a part of a larger project, the “Ready-to-Use Additive Manufacturing” (RUAM) programme which was to facilitate the manufacturing of high precision ready-to-use functional parts [2]. The original

wire Lorant used was 1.2 mm diameter. She tested the tensile, fatigue and fracture properties both in the longitudinal and the transverse directions. In the tests, Lorant used 2 specimens per direction in each test and calculated the average value of the results. Table 2-9 is the tensile tests results.

Table 2-2 Tensile tests results [2]

Mechanical properties	Longitudinal		Transverse	
	Test1	Test2	Test1	Test2
σ_b (MPa)	918	928	897	914
Average σ_b (MPa)	923		906	
σ_y (MPa)	835	845	800	820
Average σ_y (MPa)	840		810	
ε (%)	7.7	9.2	10.8	12.3
Average ε (%)	8.5		11.6	
E (GPa)	123	124	117	136
Average E GPa	123.5		126.5	

The ultimate tensile strength and the yield strength are higher for the specimens tested in the longitudinal direction than for those tested in the transverse one. However the elongation is higher for the specimens tested in the transverse direction. Differences in the grain size could cause the observed differences in strength [2]. On the other hand, β grains are oriented in the transverse direction, and more grain boundaries are in the longitudinal direction. So the elongation is better in the transverse direction [2].

2.3.4 Mechanical properties of rolled WAAM material

Rolled WAAM process can reduce distortion and residual stress produced by the conventional AM process. Residual stress can exist in WAAM processed materials. This problem can be overcome by rolling each layer after it being deposited. Colegrove et al. (2013) [33] researched the effects on reducing residual stress through rolling. The specimens they used were based on the WAAM technology applied by a rolling process. They introduced several rolling processes which are listed in Table 2-10.

Table 2-3 Parameters used for the rolling experiments [33]

Experiment	Rolling loads (kN)	Application of rolling
Profiled Roller	25, 50, 75	After every layer
Slotted Roller	25, 50	After every layer
Profiled Roller - LL	50	Last layer only
Profiled Roller – 4L	50	Every 4 layers
Profiled Roller – IS	25, 50	Every layer, in situ – 120 mm behind welding torch

The two different rollers are shown in Figure 2-26.

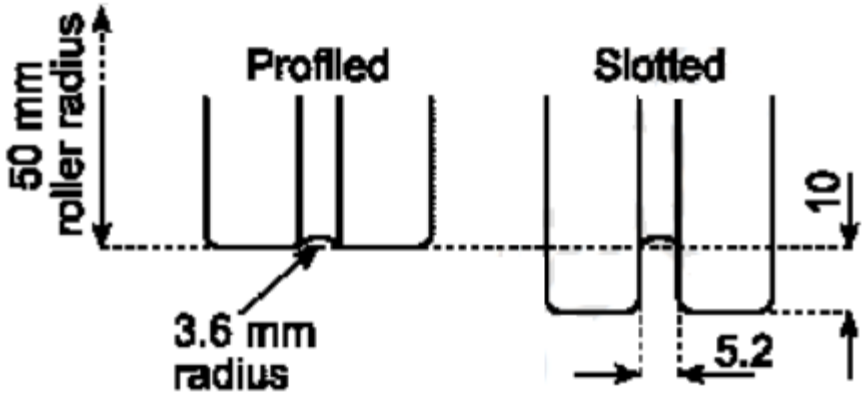

Figure 2-26 Roller designs applied to the WAAM deposits [33]

All the specimens (apart from the in-situ) were rolled once they had cooled below 50 ^{o}C. Figure 2-27 and 2-28 are the effects on reducing residual stress by rolling in both directions. In the figures, control means unrolled WAAM processed material.

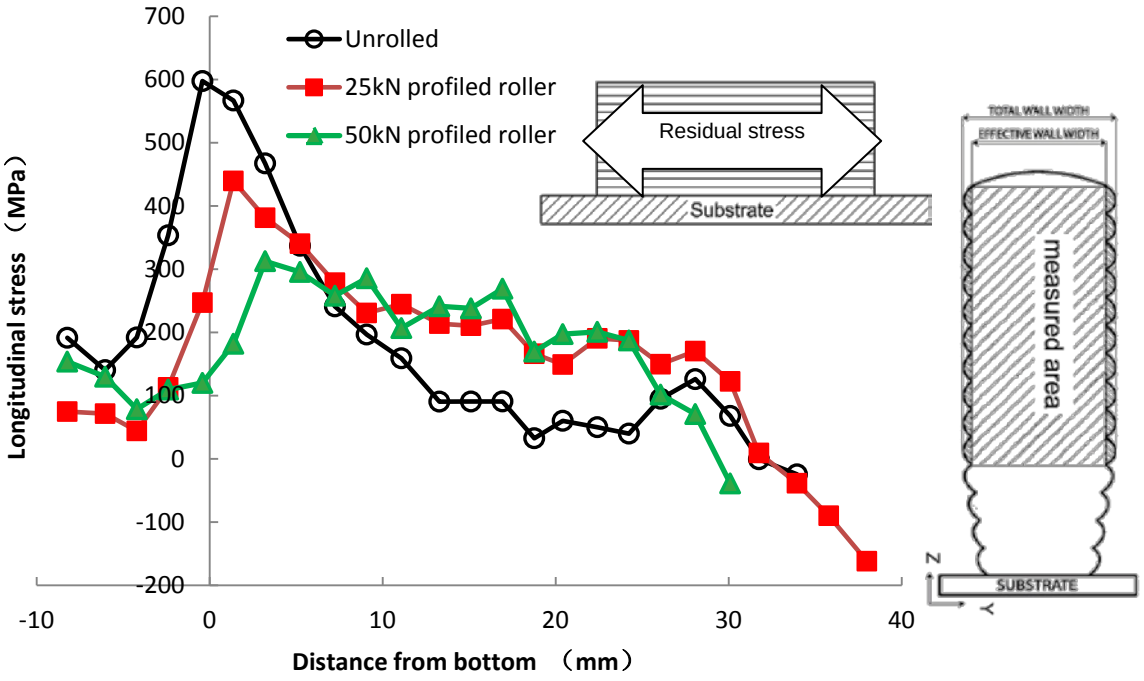

Figure 2-27 Effects on residual stress in longitudinal direction [33]

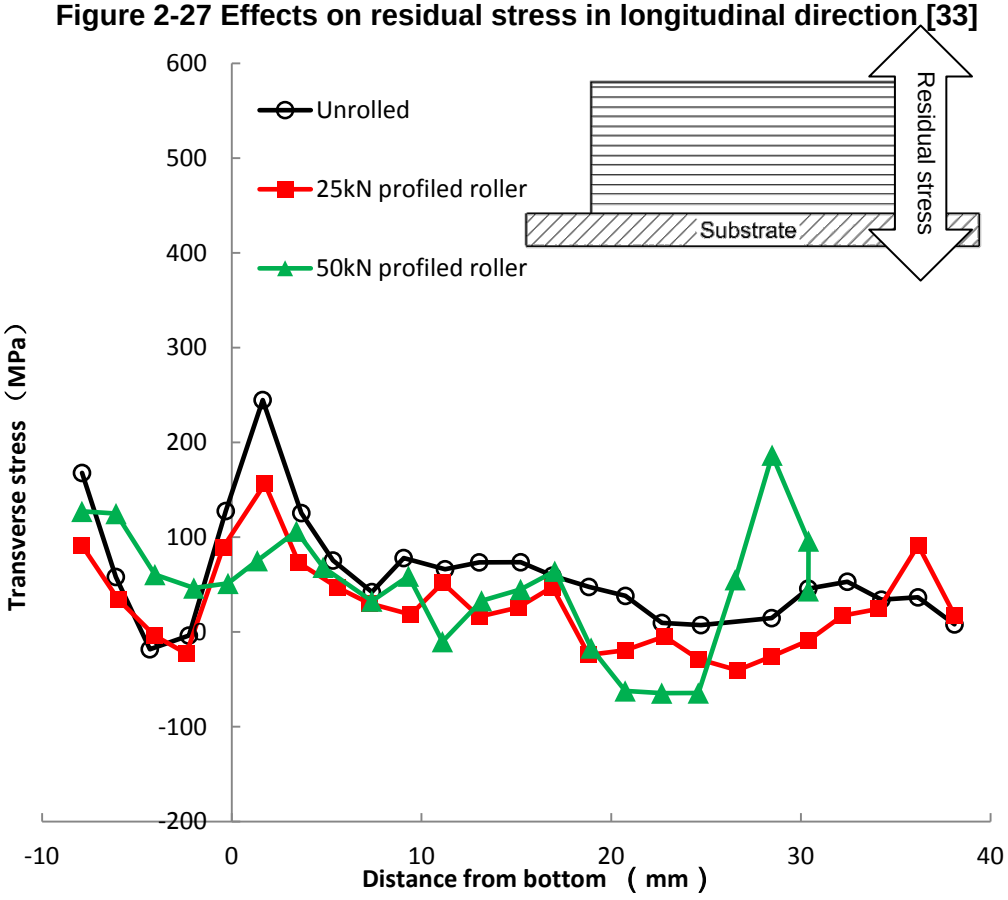

Figure 2-28 Effects on residual stress in transverse direction [33]

The peak residual stress in the longitudinal direction is significantly reduced by rolling from almost 600 MPa to around 250 MPa, reduced by more than 50%. They also found that rolling after every 4 layers had a similar effect on the distortion as rolling every layer, and rolling behind the deposition process (in-situ) has no effect on the distortion [33].

Filomeno Martina who took part in the RUAM project tested the tensile properties of rolled WAAM processed Ti-6Al-4V [19]. He tested the parts produced with 50 kN and 75 kN profiled roller. The results are listed in Table 2-11. Isotropy of tensile properties is obtained by 75 kN rolling. Figure 2-29 shows the mechanical properties of Ti-6Al-4V made by the rolled WAAM process with different rolling loads compared with the wrought Ti-6Al-4V.

Table 2-4 Tensile test results [19]

Rolling load (kN)	50	75	50	75
Test direction	Longitudinal		Transverse	
σ_b (MPa)	1009	1080	1028	1083
σ_y (MPa)	915	1029	923	997
ε (%)	10	13	14	13

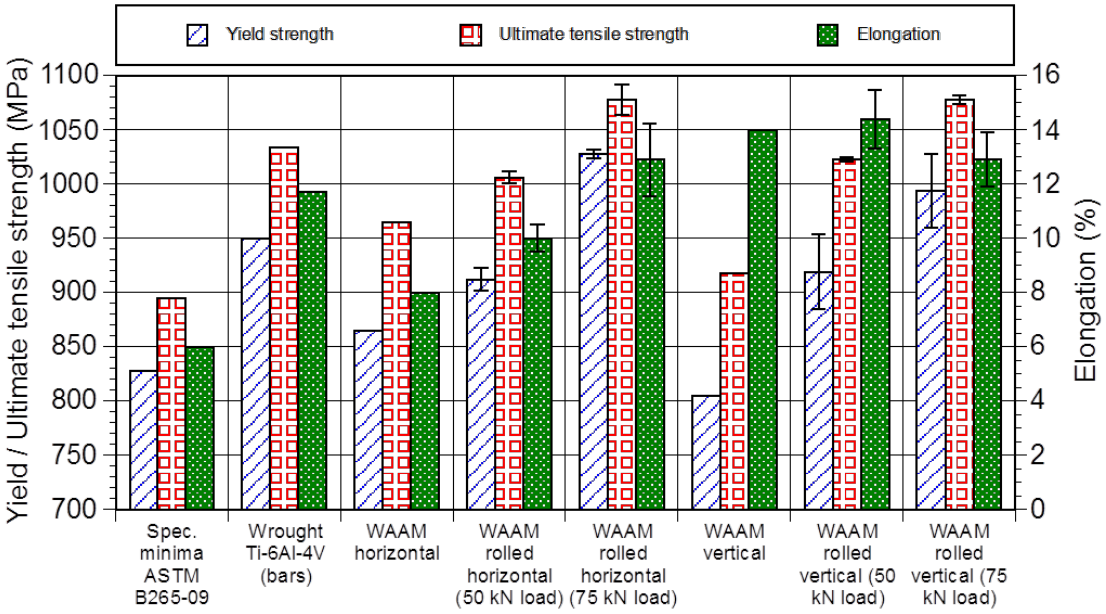

Figure 2-29 Comparison of tension properties of various load rolled WAAM and wrought Ti-6Al-4V [19]

Tensile properties by different processes are compared in Figure 2-30 with the standards AMS 4911 and AMS 4999 included. All the additive manufactures meet the requirements in AMS 4999. SLM, EBM and WAAM have met the strength requirements in AMS 4911, though SLM is obviously anisotropic. Rolled WAAM produces the elongation closest to AMS 4911.

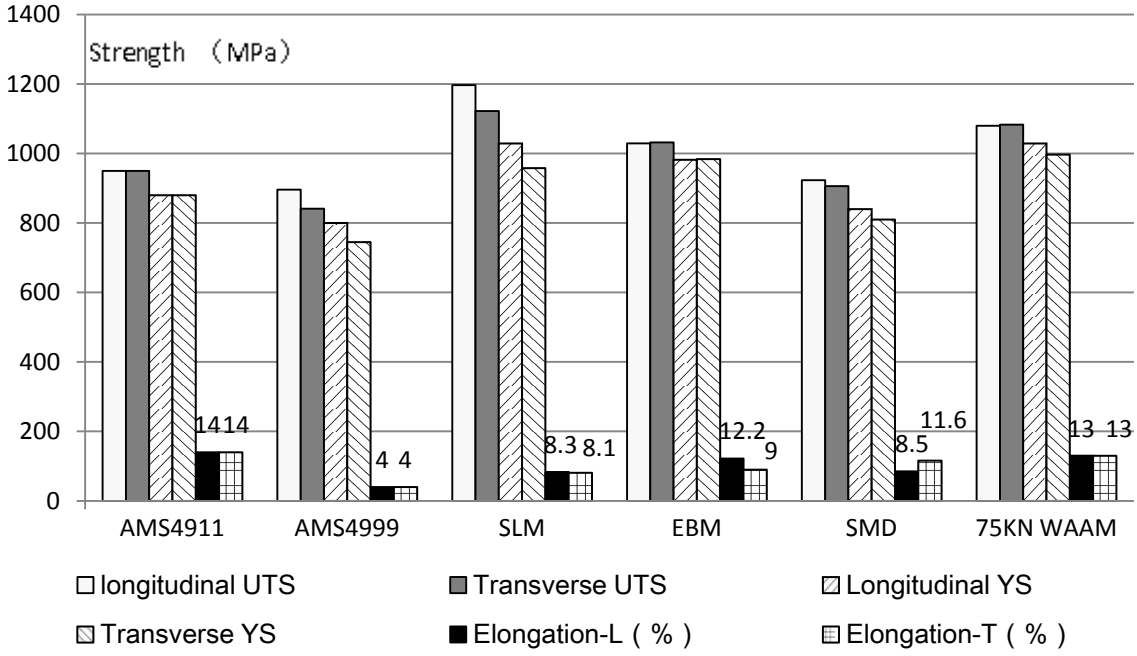

Figure 2-30 Comparison of the tensile properties by different processes

2.4 Fatigue behaviour

Failure due to repeatedly applied load is known as fatigue. It has long been known that a component subjected to fluctuating stresses may fail at stress levels much lower than its static elastic strength. If the loads are above a certain threshold, microscopic cracks will begin to form at the stress concentrators such as the surface, Persistent Slip Bands (PSBs), and grain interfaces. Eventually a crack will reach a critical size, and the structure will suddenly fracture [40]. The word ‘fatigue’ first used in 1839 [41]. It is believed that more than 95% of all mechanical failures can be attributed to fatigue. Mechanical failures due to fatigue investigated in more than 150 years [41]. In 1950s, British De Havilland Comet, the world’s first commercial jet airliner got four crashes in 1953-1955 [41]. It was the first example of metal fatigue due to high altitude flights.

There are three commonly recognized forms of fatigue: High Cycle Fatigue (HCF), Low Cycle Fatigue (LCF) and Thermal Mechanical Fatigue (TMF) [42]. HCF is the mode of material degradation when plastic strains are induced to an airframe component due to the service environment.

2.4.1 S-N curve

Based on the LCF local strain philosophy, fatigue cracks initiate as a result of repeated plastic strain cycling at the locations of maximum strain concentration. The fatigue performance of material is commonly characterized by an S-N curve [41]. S-N curve is a graph of the magnitude of a cyclic stress (S) against the logarithmic scale of cycles to failure (N). S-N curves are derived from tests on samples of the material to be characterized where a regular sinusoidal stress is applied by a test machine which also counts the number of cycles to failure.

2.4.2 Fatigue crack propagation rates properties

In engineering terms fatigue damage and life prediction is mainly dealt with by a combination of fatigue crack initiation and fatigue crack growth. Knowing fatigue crack propagation life is important for understanding and predicting fatigue behaviour of a structure, then failure of a component can be avoidable through inspections.

The fatigue crack propagation rate is defined as the crack size increment *da* during a small number of cycles *dN*. The propagation is described as $\Delta a/\Delta N$ or written as da/dN [43]. Some parameters are used to describe the crack growth. A cyclic plastic zone forms at the crack tip, and the growing crack leaves behind a plastic wake. If the plastic zone is small enough that it is embedded within an elastic singularity zone, the conditions at the crack tip are uniquely defined by the current stress intensity factor *K* value, and the crack growth rate is characterized by K_{min} and K_{max} [44], which are shown in Figure 2-31.

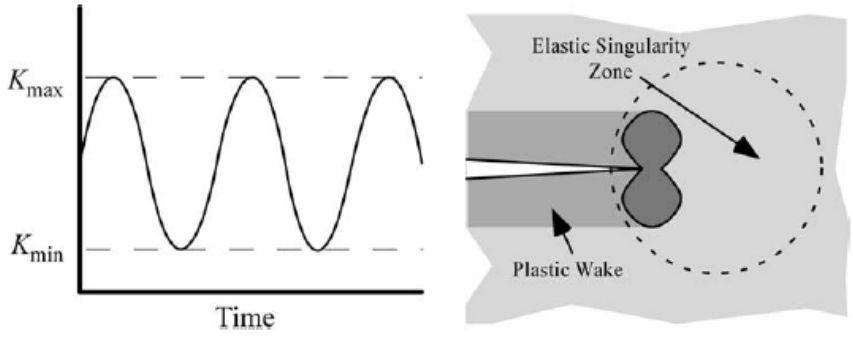

Figure 2-31 Constant amplitude fatigue crack growth under small-scale yielding conditions [44]

The relationship between ΔK and crack propagation rate is described in the following equation 2-1 [44].

$$\frac{da}{dN} = f(\Delta K, R) \quad \textbf{(2-1)}$$

Where $\Delta K=(K_{max}-K_{min})$, $R=K_{min}/K_{max}$

Figure 2-32 is the log-log plot of da/dN vs. ΔK, which describes the typical characteristics of fatigue crack growth rate.

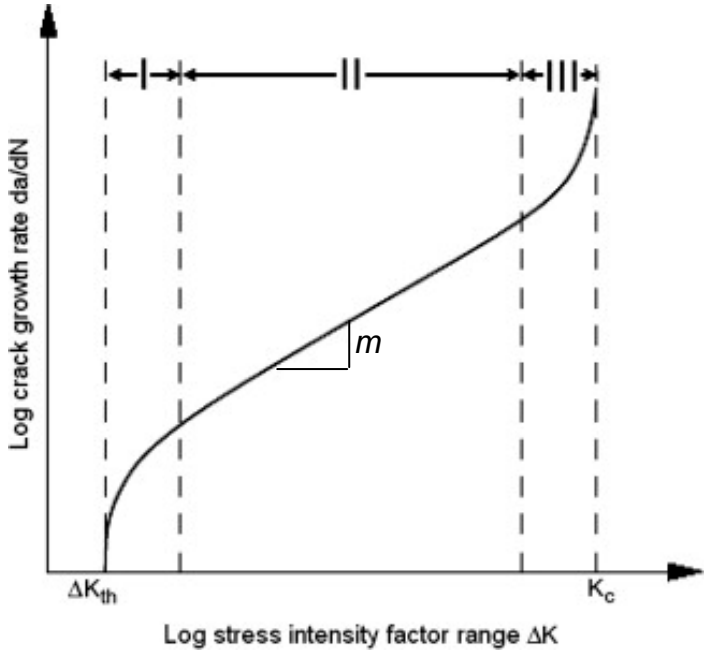

Figure 2-32 Typical fatigue crack growth behaviour in metals [44]

The curve is divided into three regions. Region I is a threshold stress intensity factor range ΔK_{th}, below which the crack does not grow. ΔK_{th} can be used in

the calculation of permissible crack length or stress applied to avoid fatigue crack growth [43]. This region is called the low stress Intensity region, crack growth rate increases rapidly once the ΔK value is above $\Delta K_{th.}$

In region II, the curve is linear and the crack growth rate is power function of ΔK (equation 2-2). Paris and Erdogan were apparently the first to discover the power-law relationship for fatigue crack growth in Region II, so this region is called the Paris Law region [44]. Studies over the past four decades have shown that m can range from 2 to 4 for most metals in the incorrosive environment.

$$\frac{da}{dN} = C\Delta K^m \quad \textbf{(2-2)}$$

Where C and m are material constants determined experimentally.

Region III is called the high stress Intensity region in contrast to region I. Crack growth rate curve rises to an asymptote in region III where the maximum stress intensity factor K_{max} equals to the critical stress intensity factor K_c [43]. Relationship for Region II and Region III is described as the following equations [44].

$$\frac{da}{dN} = \frac{C*\Delta K^m}{[(1-R)K_c - \Delta K]} \quad \textbf{(2-3)}$$

or

$$\frac{da}{dN} = \frac{C*\Delta K^{m-1}}{\left(\frac{K_c}{K_{max}} - 1\right)} \quad \textbf{(2-4)}$$

Region III behaviour results from a superposition of fracture and fatigue rather than plastic zone effects.

2.4.3 Fatigue properties of AM manufactured materials

Different methods were used in evaluating the fatigue properties of different AM manufacturing. The SLM and WAAM used fatigue growth rate for fatigue properties evaluation. In the tests of SLM, the stress ratio (R) used was 0.1, and

the stress intensity factor range (ΔK) was from 1 MPa.m$^{1/2}$ to 80 MPa.m$^{1/2}$, and the frequency was 40 Hz. From the tests, the average threshold stress intensity factor range value of as-built SLM was 1.4 MPa.m$^{1/2}$ with the crack in the longitudinal direction and 1.7 MPa.m$^{1/2}$ with the crack in the transverse direction when the fatigue crack growth rates of both specimens were 1X10^{-11} m/cycle. The fatigue crack growth rate in the longitudinal direction was greater than that in the transverse direction [36]. The fatigue crack growth rate results are shown in Figure 2-33.

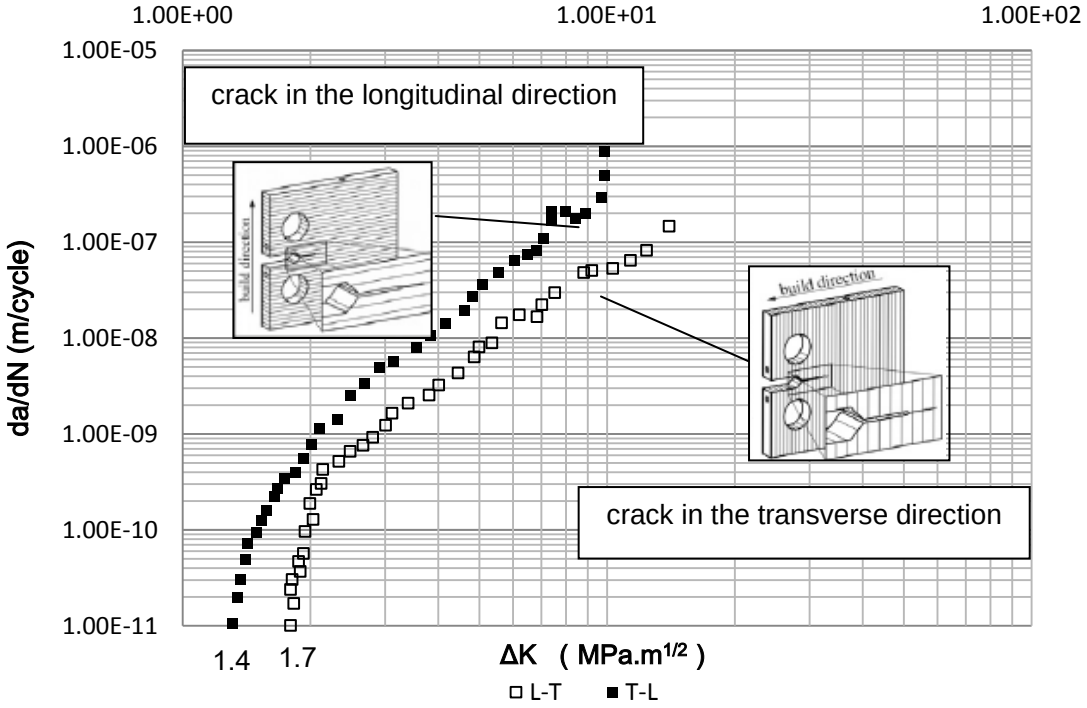

Figure 2-33 Fatigue crack growth rate results of SLM parts (as-built), [edited from Ref 36]

Experiments of WAAM processed specimens were carried out with an R ratio 0.1 and a frequency of 8 Hz. The ΔK_{th} was around 6.5 MPa.m$^{1/2}$. Under this conditions, da/dN were 1.1X10^{-9} m/cycle (crack in the longitudinal direction) and 1.4X10^{-9} m/cycle (crack in the transverse direction) [2]. The results of WAAM are shown in Figure 2-34. Fatigue crack growth rate seemed a little greater in the transverse direction. Wrought Ti-6Al-4V was tested with the R ratio 0.3 and a frequency of 30 Hz, The da/dN was 1X10^{-9} m/cycle at a stress intensity factor range value of 6.5 MPa.m$^{1/2}$ [2].

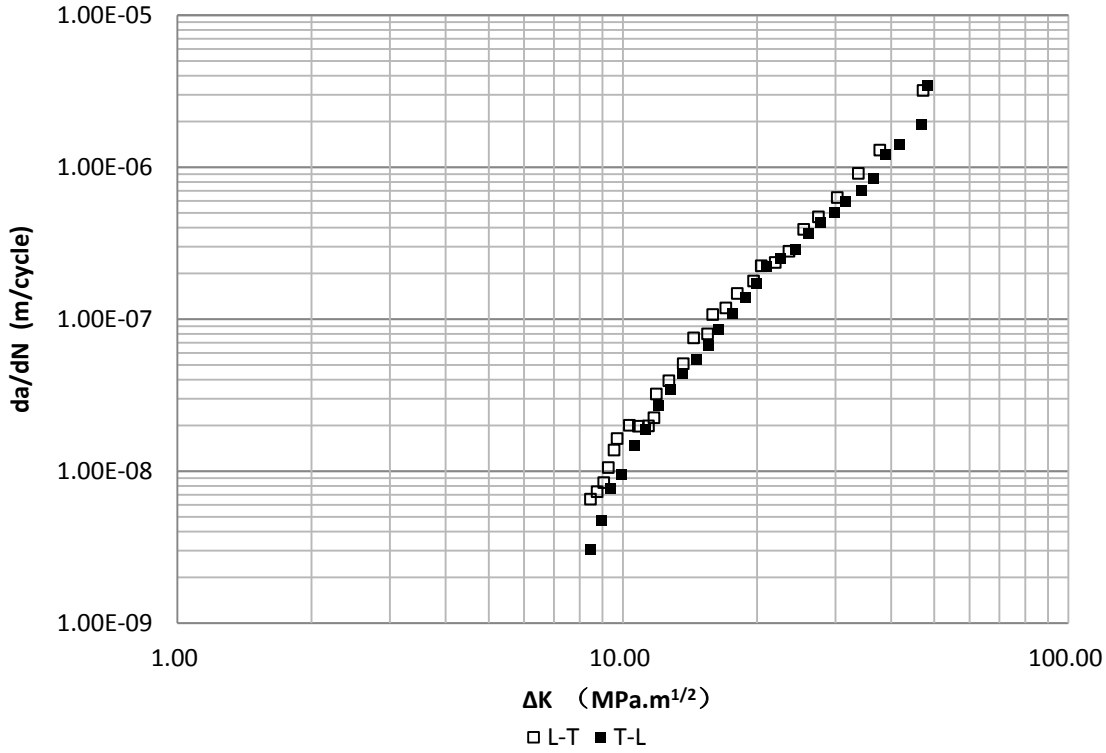

Figure 2-34 Fatigue crack growth rate test results of WAAM, [edited from Ref 2]

According to Lorant's analysis, crack propagated along the β grain boundaries, the grain size was much bigger in the transverse direction than in the longitudinal direction. So the L-T specimens whose test load was along the longitudinal direction and crack in the transverse direction did not have a fatigue crack growth performance as good as T-L specimens. Figure 2-35 shows the crack propagation in L-T specimen.

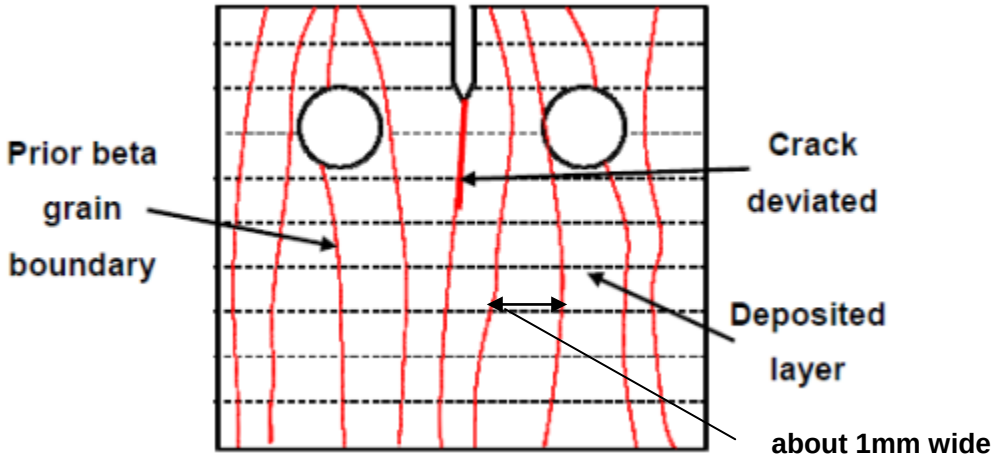

Figure 2-35 Crack growth in L-T specimen [2]

EBM specimens were evaluated through "Stress amplitude Vs. log cycles" method: S-N curves. The result is shown in Figure 2-36.

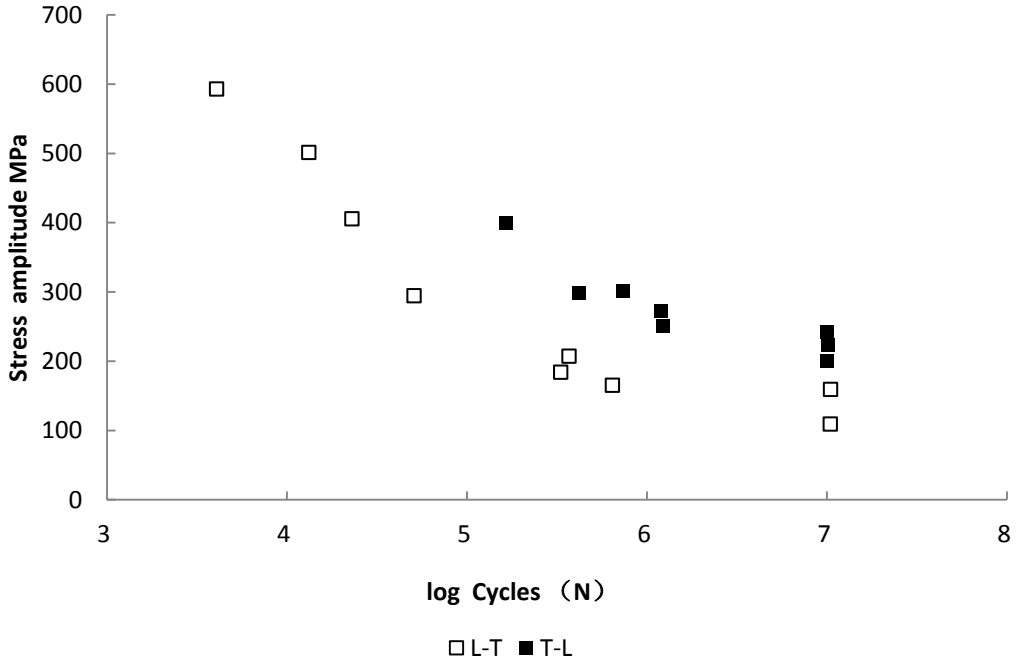

Figure 2-36 Fatigue characteristics of EBM specimens, [edited from Ref 38]

The specimens with the crack in the longitudinal direction had a better performance in fatigue properties.

Both WAAM and EBM obtained better fatigue performance in the longitudinal direction, but SLM had a better fatigue performance in the transverse direction. Fatigue properties of rolled WAAM processed Ti-6Al-4V have not been tested. One of the purpose of this project is to evaluate the fatigue properties of rolled WAAM processed Ti-6Al-4V and compare the results with unrolled WAAM processed one. The fatigue properties of the materials made by different AM manufacturing are summarized in Table 2-12.

Table 2-5 Fatigue properties of AM processed Ti-6Al-4V

Manufacturing	Crack growth in the longitudinal direction	Crack growth in the transverse direction
SLM	Faster	Lower
WAAM	Lower	Faster
EBM	Lower	Faster

2.5 Fracture toughness

Tensile fracture can be stated as a critical stress intensity factor K_c. K_c value depends on the thickness constraint [43]. The limited value of K_c for maximum constraint (plane strain) is K_{IC} which can be considered as a property of material characterizing the crack resistance, and is called the plane strain fracture toughness [43]. Knowledge of K_{IC} can be helpful to predict failure for different combinations of stress and crack size and different geometries. K_c has a decreasing trend with the increasing thickness, until K_{IC}, which is a transition from plane stress to plane strain at the crack tip. Figure 2-37 describes the trend, and Figure 2-38 shows the effect of thickness on fracture surface.

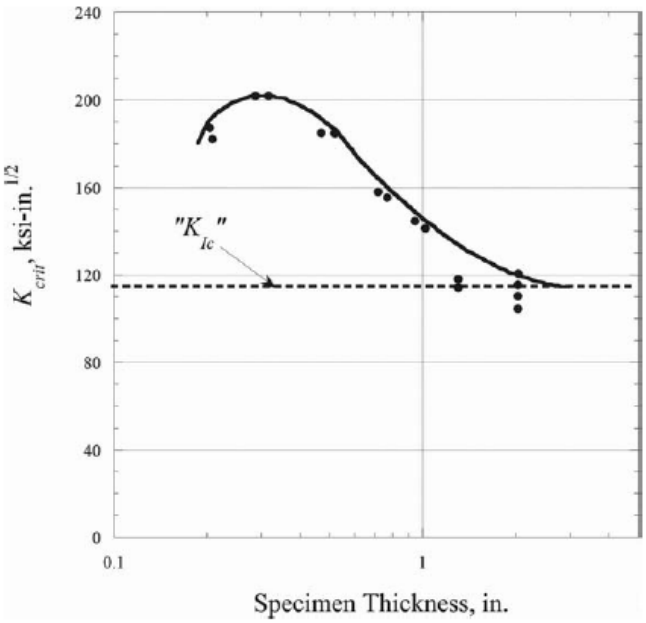

Figure 2-37 Variation of measured fracture toughness with specimen thickness for an unspecified alloy [44]

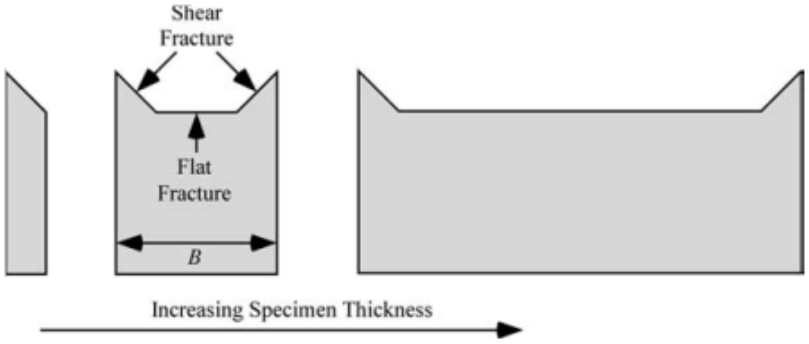

Figure 2-38 Effect of specimen thickness on fracture surface [44]

Only WAAM processed Ti-6Al-4V was tested for the fracture toughness by Lorant [2], she carried out the tests according to ASTM Standard E399 (Standard Test Method for Plane-Strain Fracture Toughness of Metallic Materials) and compact tension specimens were used in her tests. But the dimensions of the specimens did not meet the plane strain condition. According to ASTM Standard E399, the thickness (*B*) and width (*W*) of the compact tension C (T) specimen must meet the requirement:

$$2 \leq W/B \leq 4$$

And in the standard, the specimen thickness *B* must meet the following requirement before obtaining the plane strain result.

$$B > 2.5\left(\frac{K_{IC}}{\sigma_y}\right)^2$$

Referred from the wrought Ti-6Al-4V, K_{Ic} was 60 MPa.m$^{1/2}$ and the minimum σ_y referred from ALM [2] was 810 MPa. So the minimum B value should be 14 mm.

The drawing of the C (T) specimens Lorant used is shown in Figure 2-39.

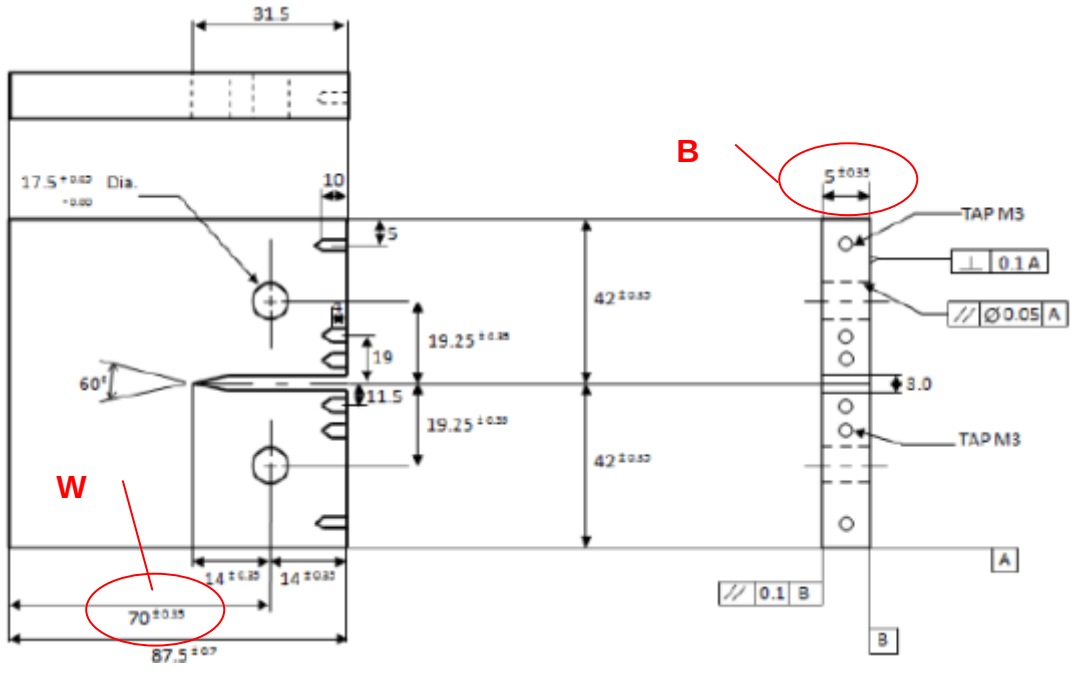

Figure 2-39 C (T) specimens used by Lorant [2]

The *W* value of the specimen was 70 mm and the *B* value was only 5 mm, *W/B* equals to 14 which was beyond the range in ASTM E399. So the test results were valid with the particular thickness.

The testing procedures were operated according to ASTM E399. In this test, crack length was measured by the Direct Current Potential Drop technique and checked optically. A “Howden” Pulsed Direct Current Crack Length Measurement System was used in this test. Figure 2-40 shows the principle of this technique.

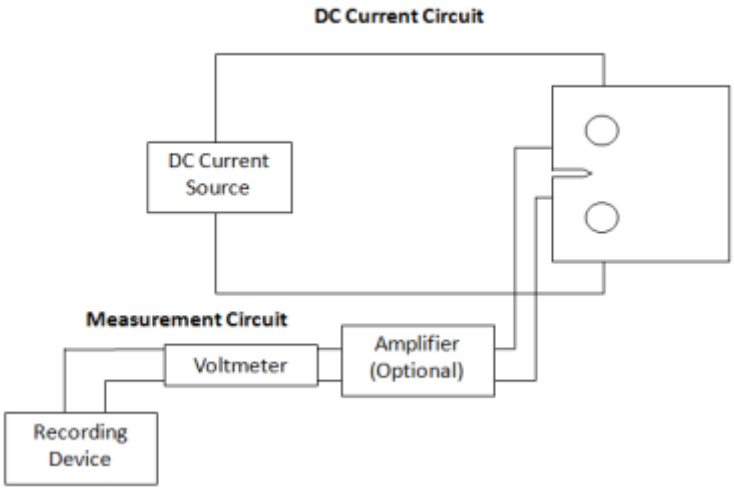

Figure 2-40 DC Current System [45]

Electrical field in a cracked specimen with a current flowing through it is a function of the geometry, and in particular the crack size. For a constant current flow, the electric potential or voltage drop across the crack plane will increase with increasing crack size due to modification of the electric field and associated perturbation of the current streamlines. The change in voltage can be related to crack size through analytical or experimental calibration relationship [45].

Incremental polynomial method [45] is introduced to compute *da/dN* involving fitting a second-order polynomial (parabola) to set of (2n+1) successive data points. The form of the equation for the local fit is as followed.

$$\hat{a}\imath = b_0 + b_1\left(\frac{Ni - C1}{C2}\right) + b_2\left(\frac{Ni - C1}{C2}\right)^2 \quad \textbf{(2-5)}$$

Where $-1 \le \left(\frac{Ni-C1}{C2}\right) \le +1$, and b_0, b_1 and b_2 are the regression parameters that are determined by the least squares method over the range $a_{i-n} \le a \le a_{i+n}$. The value $\hat{a}\imath$ is the fitted value of crack length at N_i. The parameter $C_1=0.5(N_{i+n}+N_{i-n})$ and $C_2=0.5(N_{i+n}-N_{i-n})$ are used to scale the input data, thus avoiding numerical

difficulties in determining the regression parameters. The rate of crack growth at N_i is given by the following equation [45].

$$(\frac{da}{dN})_{\widehat{ai}} = \frac{b1}{C1} + \frac{2b_2(Ni - C1)}{C_2^2} \quad \textbf{(2-6)}$$

The value of ΔK associated with this da/dN is calculated as the equation below.

$$\Delta K = \frac{\Delta P}{B\sqrt{W}} * \frac{(2+\alpha)}{(1-\alpha)^{\frac{3}{2}}}(0.886 + 4.64\alpha - 13.32\alpha^2 + 14.72\alpha^3 - 5.6\alpha^4) \quad \textbf{(2-7)}$$

Where $\alpha = a/W$, B is the specimen thickness, ΔP is the load range.

According to ASTM E399, The rate of increase of stress intensity is within the range 0.55 to 2.75 MPa·m$^{1/2}$/s [45]. The maximum stress intensity factor K_{max} in this test is calculated from the following expression [46].

$$K_{max} = (P_{max}/BW^{1/2}) * f(a/W) \quad \textbf{(2-8)}$$

Where

$$f(a/W) = \frac{(2+a/W)(0.886+4.64a/W-13.32a^2/W^2+14.72a^3/W^3-5.6a^4/W^4)}{(1-a/W)^{3/2}} \quad \textbf{(2-9)}$$

B, a and W are shown in Figure 2-41. P_{max} is the maximum load determined from ASTM E399 Calculate 2.5 $(K_Q/\sigma_y)^2$, if this quantity is less than both the specimen thickness and the crack length, then K_{max} is equal to K_{Ic}.

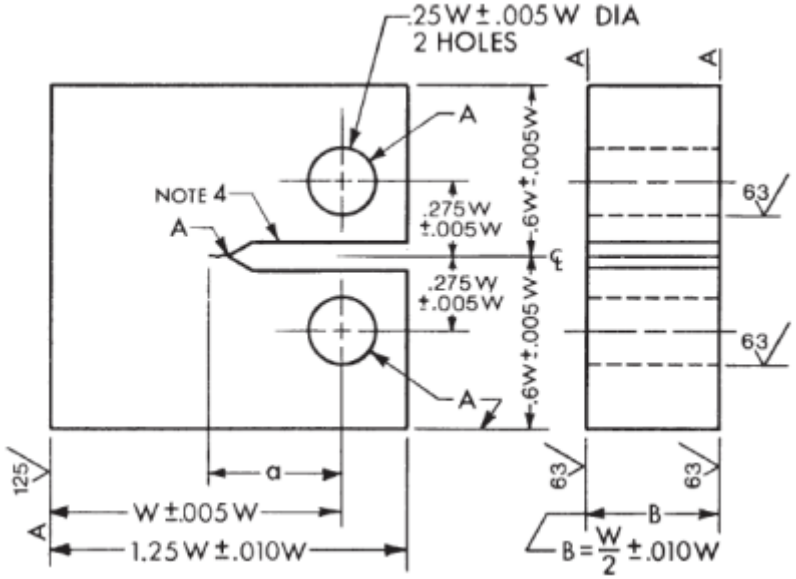

Figure 2-41 Specimen dimension requirement in ASTM E399 [46]

In Lorant's tests [2], C (T) specimens were pre-cracked by fatigue carried out on a DMG servo-hydraulic machine, and the maximum load was 20 kN. The crack length was equal to the average value of 0.50*W for pre-cracking. The test started at a high value of stress intensity to complete the pre-cracking immediately, for time saving. Then, the stress intensity was decreased each time the crack grew by 0.5 mm. After pre-cracking, the test was performed on an Instron Electro-Mechanical machine, with a maximum load of 100 kN. Figure 2-42 below shows the test equipment used in this test.

Figure 2-42 C (T) specimen and Displacement Gage used in Fracture Toughness tests [2]

According to ASTM Standard E399 which advises to use a loading rate between 0.55 and 2.75 MPa.m$^{1/2}$/s, the loading rate was chosen as 6 mm/min. And the tests results are listed in Table 2-13. Four specimens with each two in one direction were tested. The directions of the specimens are shown in Figure 2-43.

Table 2-6 Load range ΔP and fracture toughness K_{IC} for each specimen tested [2]

	L-T testing direction		T-L testing direction	
	Test 1	Test 2	Test 1	Test 2
ΔP (N)	11500	10800	10000	10300
K_{IC} (MPa.m$^{1/2}$)	84.8	78.9	73.0	74.8

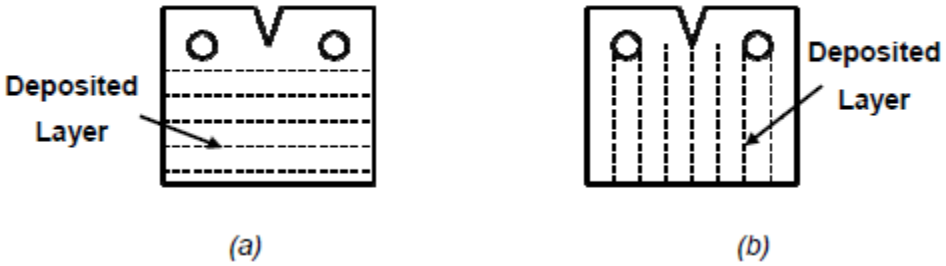

Figure 2-43 Directions of the specimens, (a) L-T, (b) T-L [2]

Because of the thickness of the specimen was only 5mm which did not fulfil the plane strain condition (greater than $2.5*(K_{IC}/\sigma_y)^2$ [46]), the fracture toughness tests is under conditional load P_{max}. The average fracture toughness value of specimens tested in the L-T direction was equal to 81.9 MPa.m$^{1/2}$; it was equal to 73.9 MPa.m$^{1/2}$ for specimens tested in the T-L direction [2]. It was found in the tests that a crack propagating in the T-L specimen spent most of its life in one layer. But a crack propagating in the L-T compact tension specimen propagated through more layer boundaries. Lorant explained that fracture toughness increased when the α grain size increased in alloys. So L-T compact tension specimens had greater fracture toughness values than T-L compact tension specimens. Figure 2-44 shows crack propagating through a specimen.

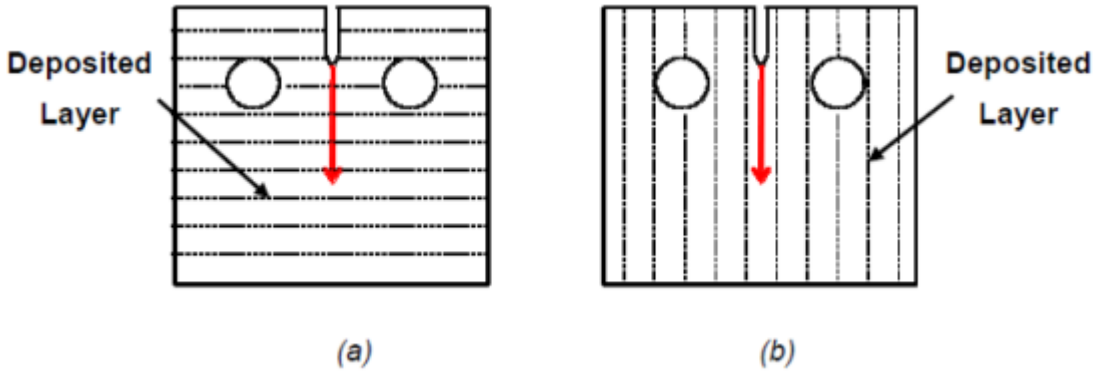

Figure 2-44 Crack propagation in compact tension specimen a）L-T specimen, b) T-L specimen [2]

As mentioned before, β grain size is greater in the transverse direction, so the crack in L-T specimen crosses much more α grains than in T-L specimen, in which the crack crosses more β grains.

3 MATERIALS AND TESTING PROCEDURES

This chapter is about the materials and manufacturing of the specimens as well as the testing procedures of the fatigue crack growth rate tests. In order to investigate the fatigue crack growth rates of rolled WAAM processed Ti-6Al-4V and estimate whether the fatigue properties are isotropic, four specimens were used, two for the longitudinal direction and two for the transverse direction. All the specimens were manufactured from the same initial wall produced by rolled WAAM.

3.1 Original material and manufacturing method

The initial Ti-6Al-4V wall was built in Welding Engineering and Laser Processing Centre (WELPC) of Cranfield University. The WELPC was Established in 1961 specializes in fundamental, strategic and applied research in the area of advanced fusion joining processes and high deposition rate additive built structures. The initial wall was made by rolled WAAM process. VBC Interpulse Tungsten Inert Gas power source was used as a process of WAAM. VBC Interpulse Tungsten Inert Gas Welding uses an alternative current at a high frequency. The current signal is a square wave as shown in Figure 3-1.

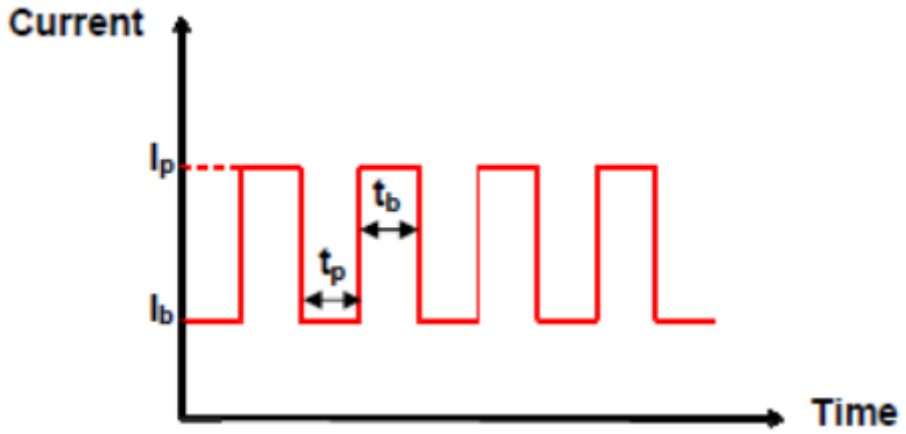

Figure 3-1 Current signal used in the VBC Interpulse Tungsten Inert Gas Welding

The type of VBC Interpulse Tungsten Inert Gas Welding system used in this project is a TIG COMMANDER 400AC/DC. Figure 3-2 shows the welding system used to build the wall. The main parameters of the welding system used to build the wall are listed in Table 3-1.

Figure 3-2 TIG COMMANDER 400AC/DC

Table 3-1 Parameters used to build the wall

Parameter	Value
Peak value of current I_p	150 A
Bottom value of current I_b	70 A
Interpulse current	125 A
Time of peak current t_p	0.05 s
Time of bottom current t_b	0.05 s
Frequency f	10 Hz
Travel speed	3.5 mm/s
Rolling speed	8 mm/s

The batch number of the original Ti-6Al-4V wire was K71M. The diameter of the original wire was 1.2 mm. The wire feeder type was MIGATRONIC KT4. The feed speed was 1.8 m/min. Figure 3-3 is the machine used to build the wall.

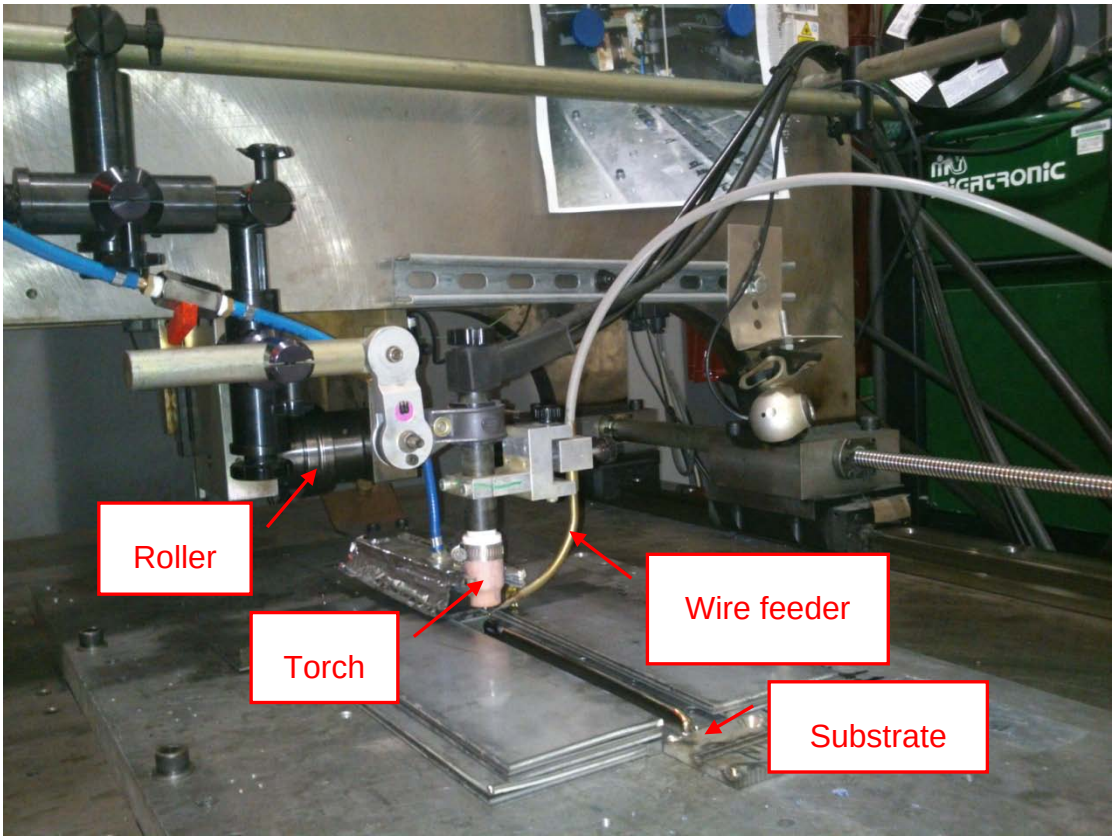

Figure 3-3 Machine used to build the wall

The roller used was a profile roller and the type was Profile 5. The initial wall was rolled layer by layer. The rolling load was 75 kN. Figure 3-4 shows the dimensions of the roller. The thickness of each layer was 0.8 mm after being rolled.

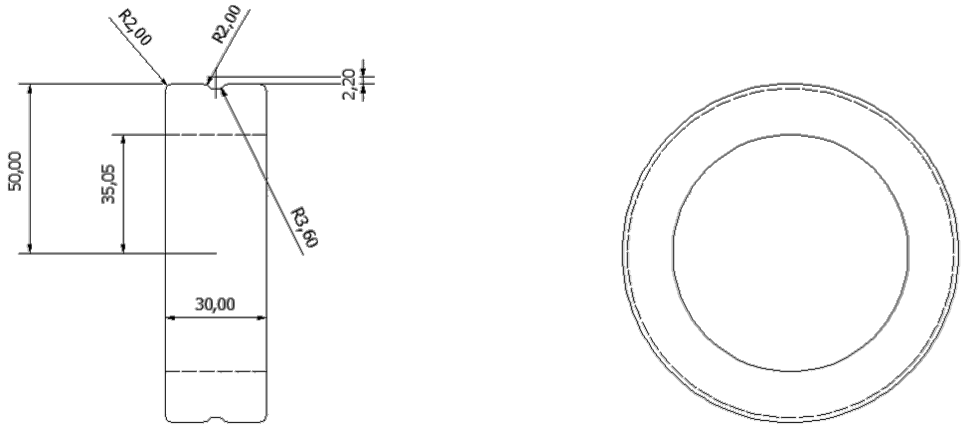

Figure 3-4 Roller used to build the wall

The final dimensions of the initial wall were 340*150*7 mm as shown in Figure 3-5. Figure 3-6 is the picture of the initial wall after being cut from the substrate.

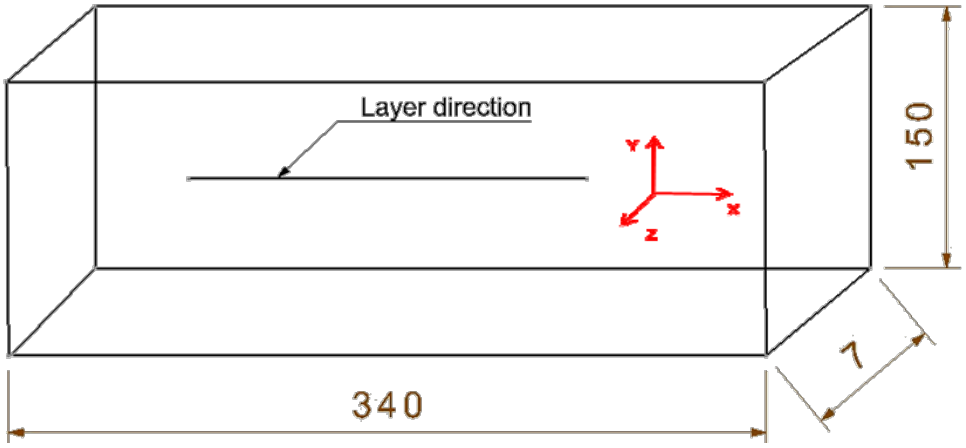

Figure 3-5 Final dimensions of the wall

Figure 3-6 The initial wall

It was significantly different from the unrolled WAAM processed Ti-6Al-4V wall shown in Figure 3-7 that *β* grain in the rolled one is unobvious on the surface of the wall. And the thickness of each layer of unrolled wall was 1.1 mm, but the thickness of each layer of rolled one was only 0.8 mm.

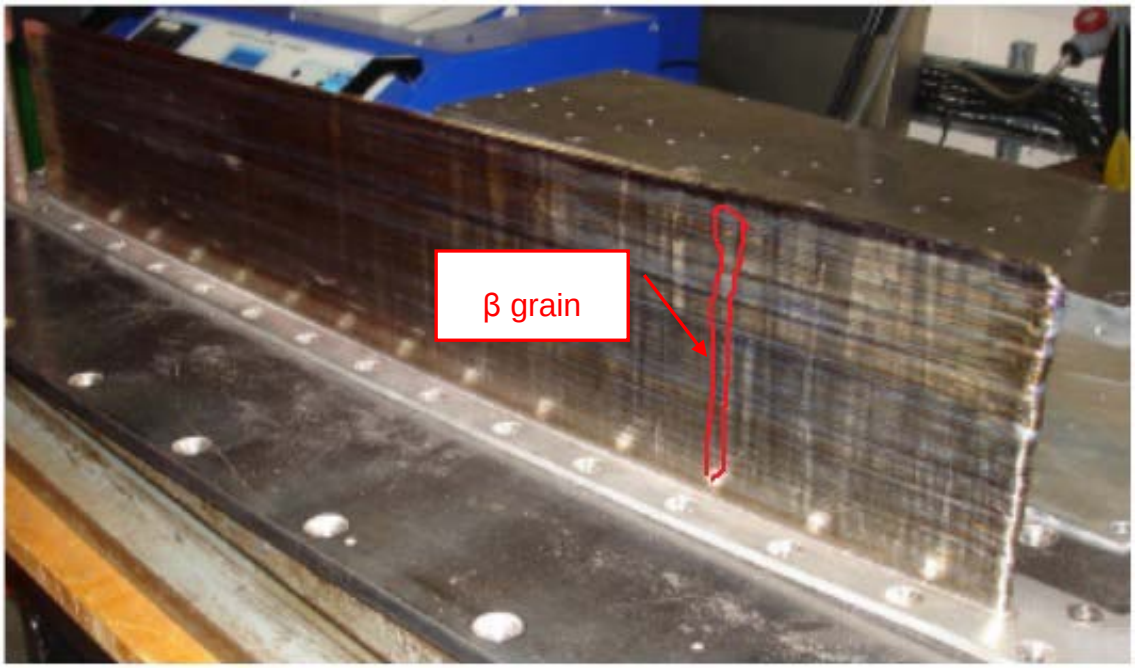

Figure 3-7 Unrolled WAAM processed Ti-6Al-4V wall [2]

3.2 Specimen machining

Compact tension specimens were designed for the fatigue crack growth rate tests. The specimens were manufactured by spark machining of a company who cooperates with School of Applied Science of Cranfield University. The dimensions of the specimen were designed according to ASTM Standard E647 (Standard Test Method for Measurement of Fatigue Crack Growth Rates).

According to ASTM E647, the dimensions of the C (T) specimens must meet the requirements in Figure 3-8.

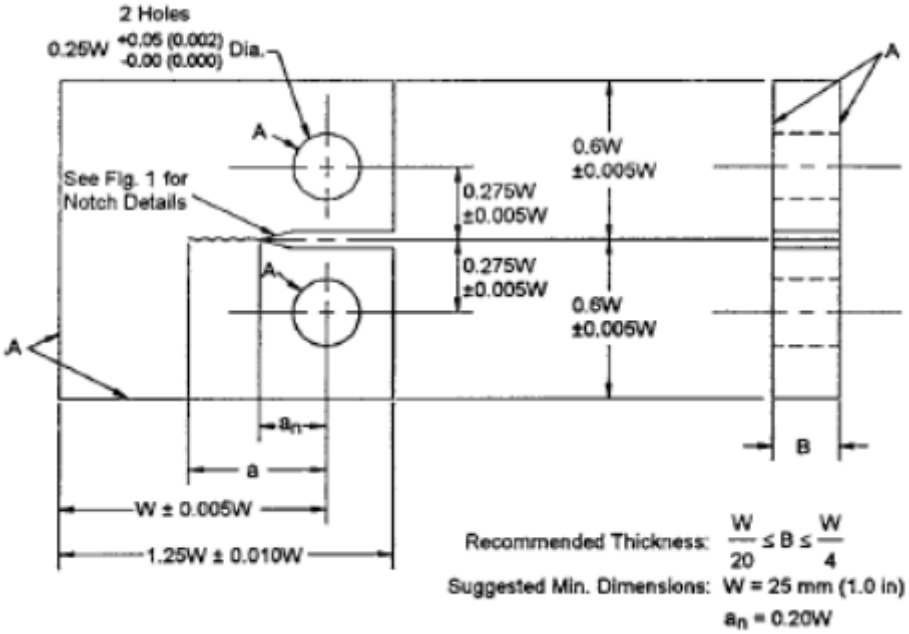

Figure 3-8 Dimensions requirements in ASTM E647 [45]

Since the rolled WAAM process is quite a new additive manufacturing and the process is still in investigation, the manufacturing can only build the initial wall with the maximum thickness of 7 mm (the current roller can only build 7 mm wall, it need time to design new roller to get satisfactory quality of microstructure of different thickness). Considering the surface roughness requirement, the wave surfaces of the both sides of the initial wall as shown in Figure 3-9, must be skimmed away. So the effectual thickness of the initial wall was 5 mm.

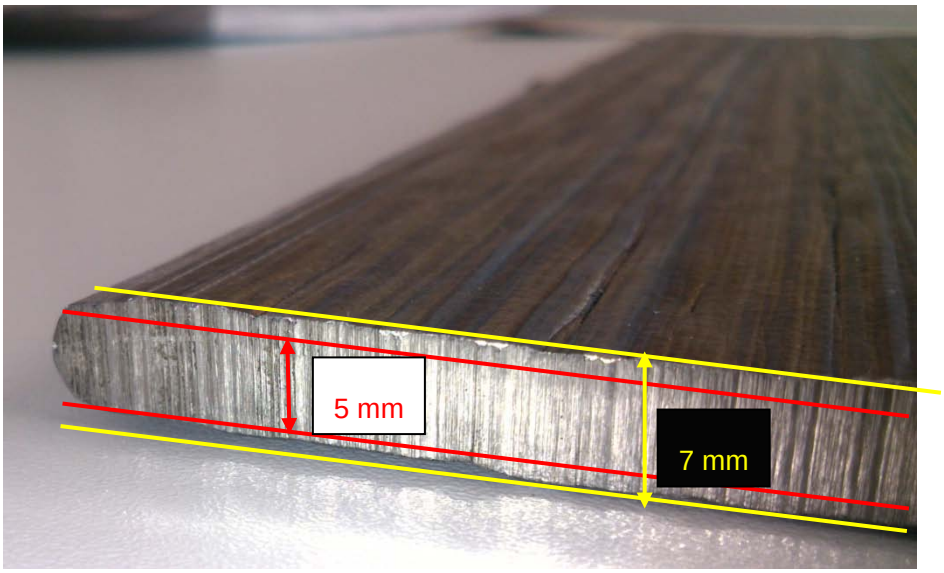

Figure 3-9 Wave surface of the initial wall

50.8 mm was chosen for the *W* value of the specimens according to ASTM E647. Figure 3-10 is the layout of the specimens. Details of the layout are presented in Appendix A.

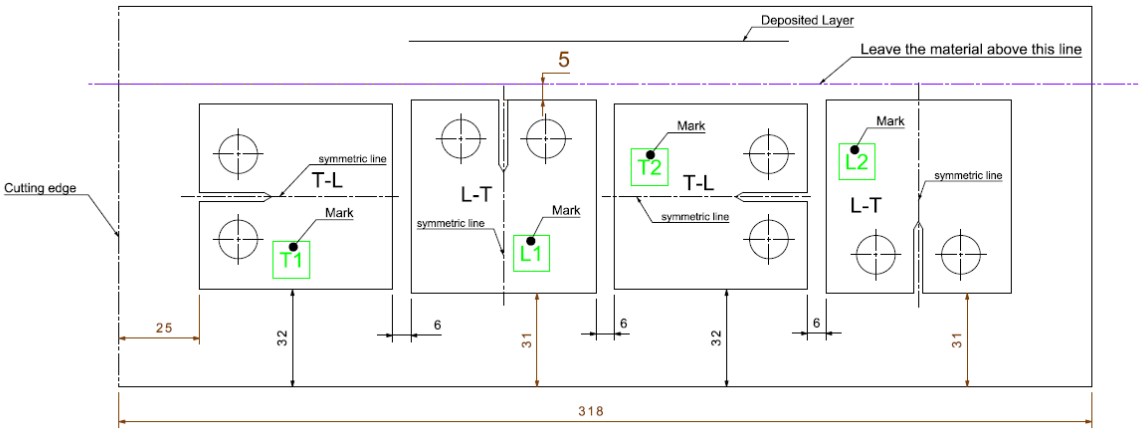

Figure 3-10 Layout of the specimens

The specimens were marked by T1, L1, T2 and L2. T meant T-L specimens with the load in the transverse direction and the crack in the longitudinal direction. L meant L-T specimens with the load in the longitudinal direction and the crack in the transverse direction. Considering whether the crack position in the wall (top or bottom) had any effect on the fatigue properties and the randomicity, all the crack directions were designed differently. The crack in L1 was from top to bottom, and the crack in L2 was from bottom to top. The crack in T1 was from left to right, and the crack in T2 was from right to left. The dimensions of the specimens are shown in Figure 3-11. Details of the specimen drawing are presented in Appendix A.

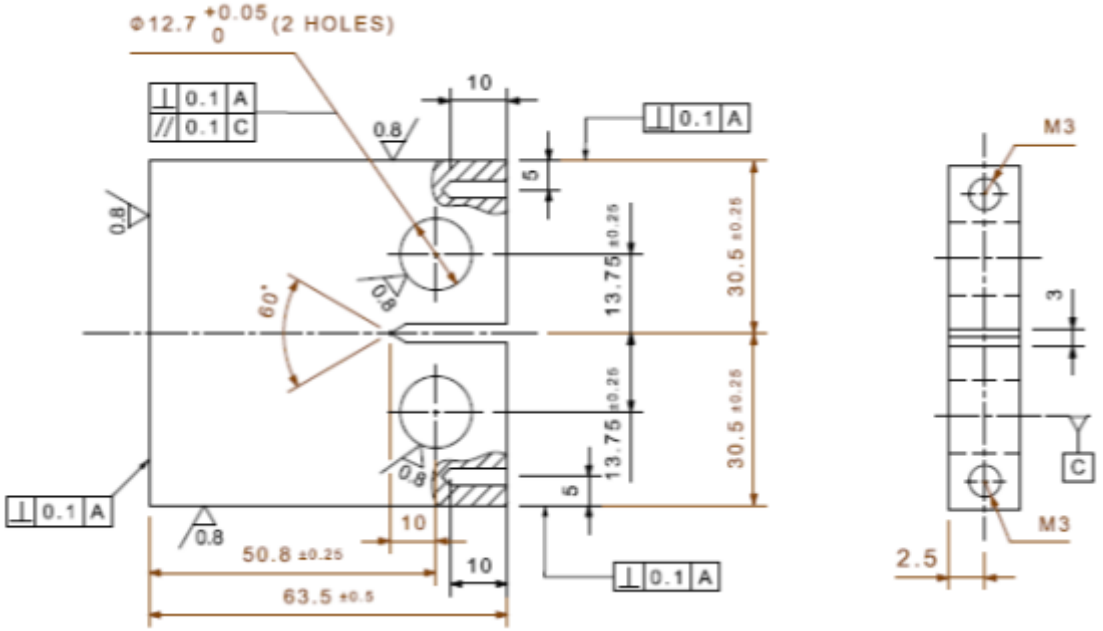

Figure 3-11 Dimensions of the specimens

The manufacturing procedures were designed as follows:

- Machine out the “Cutting edge” as a datum plane for following work. The cutting edge should be perpendicular to deposited layer.

- Skim the wall to the required thickness and surface roughness.

- Machine the specimens. The symmetric lines of T-L specimens should be perpendicular to cutting edge. The symmetric lines of L-T specimens should be parallel to cutting edge. Make a clear mark in each specimen before machining.

Notes in machining:

- All the dimensions are in millimetres, except the surface roughness in micrometers.

- The notch tip should be as sharp as possible.

- Marks should be visible on finished specimens.

3.3 Test method

The purpose of the fatigue crack growth rate tests is to study fatigue behaviours of Ti-6Al-4V made by rolled WAAM process. The tests were carried out according to ASTM Standard E647.

The aim of the fatigue crack growth rate tests is to record the crack length growth and the number of fatigue cycles corresponding to the crack length, use the data to draw the *da/dN* curves, and then analyze the fatigue properties of rolled WAAM processed Ti-6Al-4V parts.

3.3.1 Measurement

The crack length were observed by a microscope and recorded manually. The specimens were scribed every one millimetre in order to measure the crack length, as shown in Figure 3-12. For every 5 mm, a line which was 0.5 mm to the line of 5 mm was scribed to make the line of 5 mm being clearly found during the test. Through this way, it was easy to record the length of the crack. Figure 3-13 shows the scribed lines in the specimens. The surfaces painted blue to make the lines clearer.

Figure 3-12 Scribing the specimens using the vernal gauge

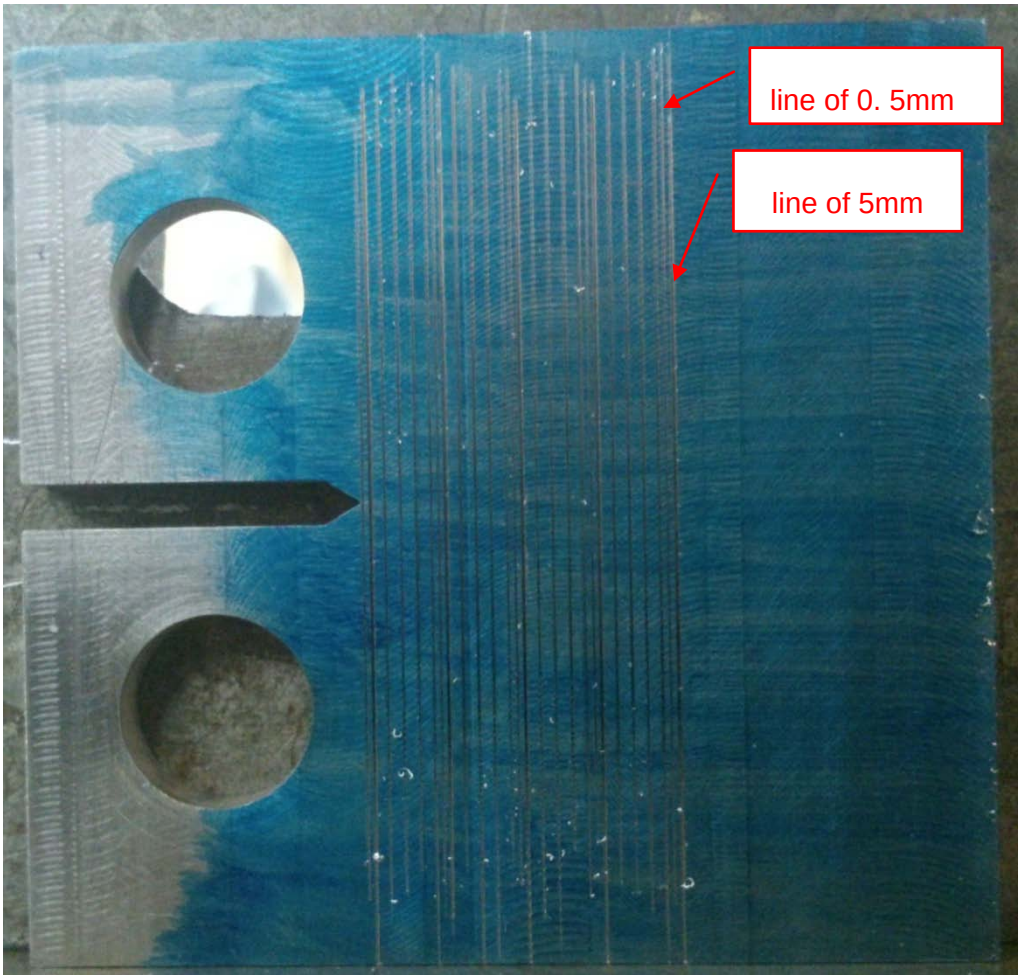

Figure 3-13 Scores in the specimens

3.3.2 Equipment for the fatigue crack growth rate tests

The fatigue crack growth rate tests were carried out on an INSTRON 8031 machine. The maximum load of this machine was 100 kN. The tolerance on the load of test machine was 0.5%. According to ASTM E647, a clevis and pin assembly was used at both the top and bottom of the specimen to allow in-plane rotation as the specimen was loaded. This specimen and loading arrangement was to be used for tension-tension loading only. Figure 3-14 is the clevis used in the tests.

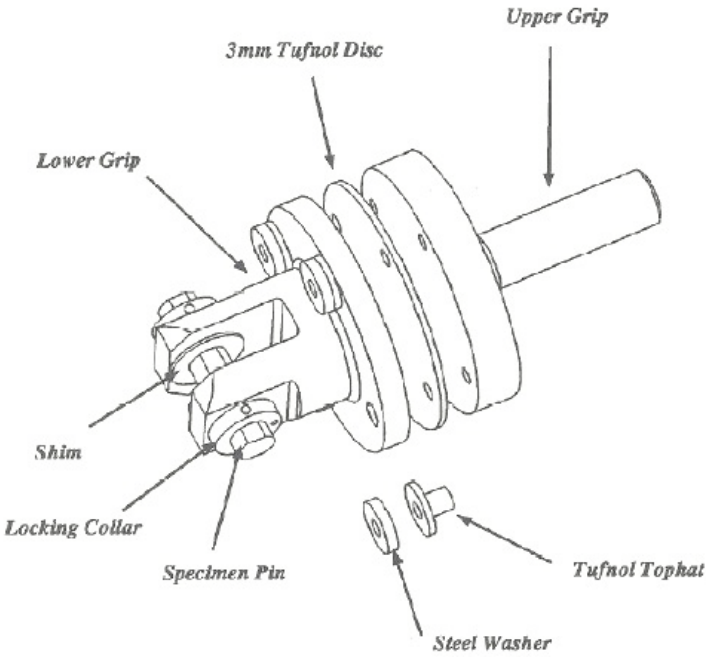

Figure 3-14 Clevis used in the tests

The size of the specimens tested was too smaller to be assembled in the clevis, so two median grips were used during the tests. The two median grips were assembled on the clevis, and the specimen was assembled to be tested in the median grips. Figure 3-15 shows a C (T) specimen being held in the grips. Figure 3-16 shows the scribed lines being observed from the microscope.

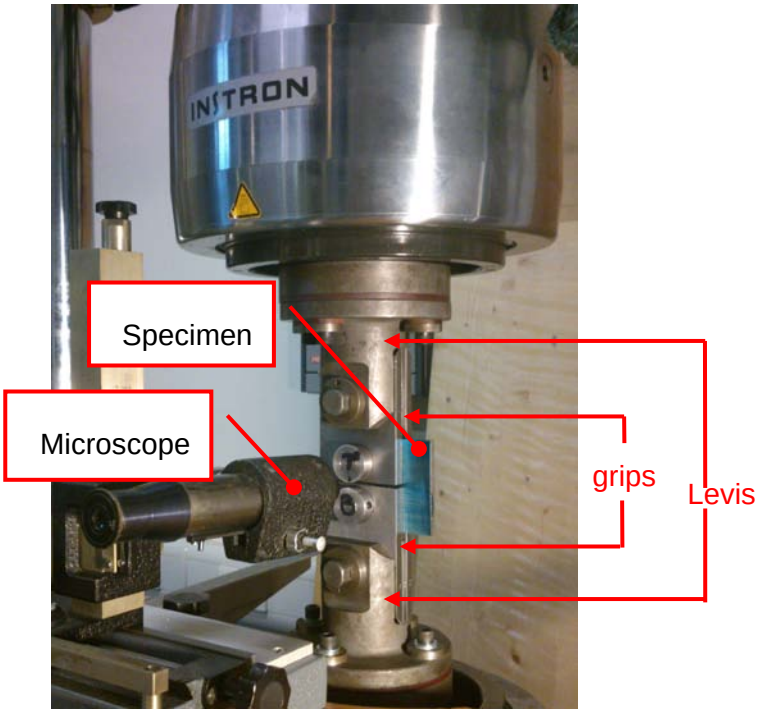

Figure 3-15 C (T) specimen, microscope, levis and grips in the INSTRON machine

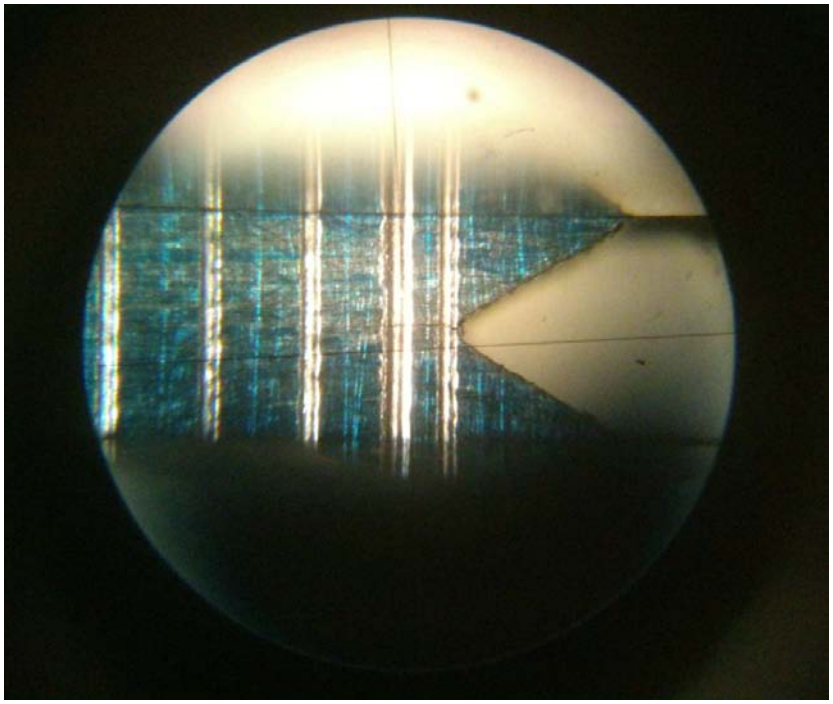

Figure 3-16 Scribed lines observed from the microscope

3.3.3 Parameters of the fatigue crack growth rate tests

According to ASTM E647, some parameters must be chosen before the fatigue crack growth rate test is carried out. Some of the parameters are used for the inputs for the test machine which affect the testing results. Other parameters are used to calculate the results.

All the four fatigue crack growth rate tests were carried out at constant load range ΔP. This load range was calculated from the initial value of stress intensity required. Equation 3-1 is from ASTM E647 for calculating the load range of the C (T) specimens.

$$\Delta P = \Delta K * B * \sqrt{W} * \frac{(1-\alpha)^{3/2}}{(2+\alpha) * (0.886 + 4.64 * \alpha - 13.32 * \alpha^2 + 14.72 * \alpha^3 - 5.6 * \alpha^4)} \quad \textbf{(3-1)}$$

The average ΔK of unrolled WAAM processed Ti-6Al-4V, 15 MPa.m$^{1/2}$ [2] tested by Lorant was used to calculate the initial testing load. Then the ΔP value was equal to 3.6 kN by applying this ΔK value to Equation 3-1. Considering time saving, the R ratio value of 0.5, which is the ratio of minimum load P_{min} over the maximum load P_{max} was chosen, and 10 Hz was chosen for the cycling

frequency. A pre-crack was required in ASTM E647 as shown in Figure 3-17, therefore 2 mm was chosen for the pre-crack.

Figure 3-17 Pre-crack requirement in ASTM E647 [45]

3.3.4 Testing

All the four specimens were compact tension specimens. The compact specimen C (T) was a single edge-notch specimen loaded in tension [45]. The C (T) specimen had the remarkable advantage that the least amount of test material was required to evaluate the crack growth behaviour.

Considering time saving during the first test for specimen L1, a high load was used for pre-cracking. 10.8 kN was chosen for initial maximum load P_{max}. When the crack length grew by 1 mm, the maximum load P_{max} was reduced to 9 kN. Then decreased the P_{max} to 7.2 kN, when the crack length grew by 2 mm. After that the value P_{max} =7.2 kN was used as a constant maximum load for the fatigue crack growth rate test.

After the first test, 10 kN was chosen for initial P_{max}. Then turned down to 8 kN, when the crack had 1 mm increment. And then changed the P_{max} to 6 kN, when the crack grew by 2 mm. After that the value P_{max} =6 kN was used as a constant P_{max} for the fatigue crack growth rate tests. The R ratio was 0.5. Table 3-2 sums up the main parameters of the 4 C (T) specimens.

Table 3-2 Parameters of specimens used in fatigue crack growth rate tests

Specimen	L1	L2	T1	T2
Width (mm)	50.8	50.8	50.8	50.8
Thickness (mm)	5	5	5	5
Initial P_{max} (kN)	10.8	10	10	10
ΔP (kN)	3.6	3	3	3
Constant P_{max} (kN)	7.2	6	6	6
Frequency (Hz)	10	8	10	8
R ratio	0.5	0.5	0.5	0.5

During each test, the cycling numbers were recorded each time the crack length had 1 mm increment, until the crack length grew to 30.5 mm. Then the recorded data was used to calculate the stress intensity factor ΔK corresponding to certain crack length through applying the data to Equation 2-7. The order of the tests was L1, T1 then L2 and T2. After L1 and T1, it was found that 10 Hz was a little high for recording data. This was because the test machine had to be paused by hand before the data was recorded each time. Consequently the frequency reduced to 8 Hz for L2 and T2.

4 TEST RESULTS

This chapter describes the results gained from the fatigue crack growth rate tests. The *a* - *N* and *da/dN* curves of the four rolled WAAM processed Ti-6Al-4V specimens are presented in this chapter. Figure 4-1 shows the fatigue crack observed from the microscope.

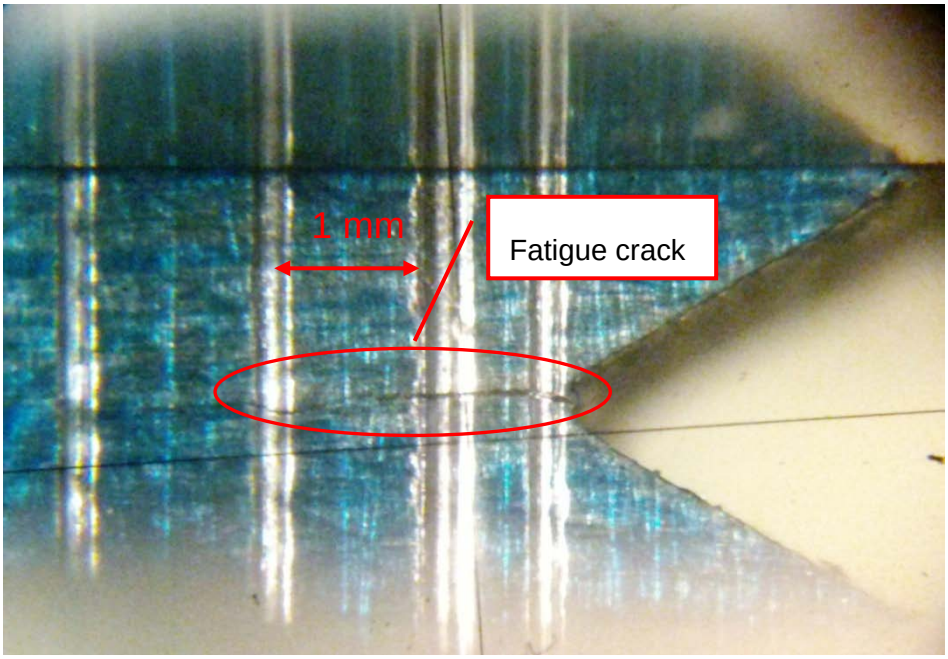

Figure 4-1 Fatigue crack in the test observed through a microscope (vertical lines indicate the scribes at 1 mm distance)

First, the crack length versus cycle number curve was directly measured. The crack growth rate curve was calculated according to the ASTM E647 [45]. There are two methods of data reduction techniques. One is the Incremental Polynomial Method, which is described in Section 2.5; the other is the Secant Method. The secant or point-to-point technique for computing the crack growth rate simply involves calculating the slope of the straight line connecting two adjacent data points on the "*a* versus *N*" curve. It is more formally expressed as Equation 4-1.

$$(da/dN)_{\bar{a}} = (a_{i+1} - a_i)/(N_{i+1} - N_i) \quad \textbf{(4-1)}$$

Because there was less scatter in the test measured *a* – *N* data, Secant Method was chosen to calculate the fatigue crack growth rates.

4.1 Results of L-T specimens

This section presents the fatigue crack growth rate properties of rolled WAAM processed Ti-6Al-4V with the load in the longitudinal direction and the fatigue cracks in the transverse direction.

L-T specimen is defined as the applied load being in the longitudinal direction and the fatigue crack in the transverse direction. The so-called longitudinal direction is perpendicular to the material build-up direction. Figure 4-2 shows the definition of L-T specimen. The two L-T specimens were marked as L1 and L2. To see whether the fatigue crack position would have any effect on the material's fatigue behaviour, specimens with different crack locations were obtained, i.e. either near to the substrate plate, or to the wall's top. Figure 4-3 shows the locations in the initial wall of the two L-T specimens. The final shapes of L1, L2 are shown in Figure 4-4.

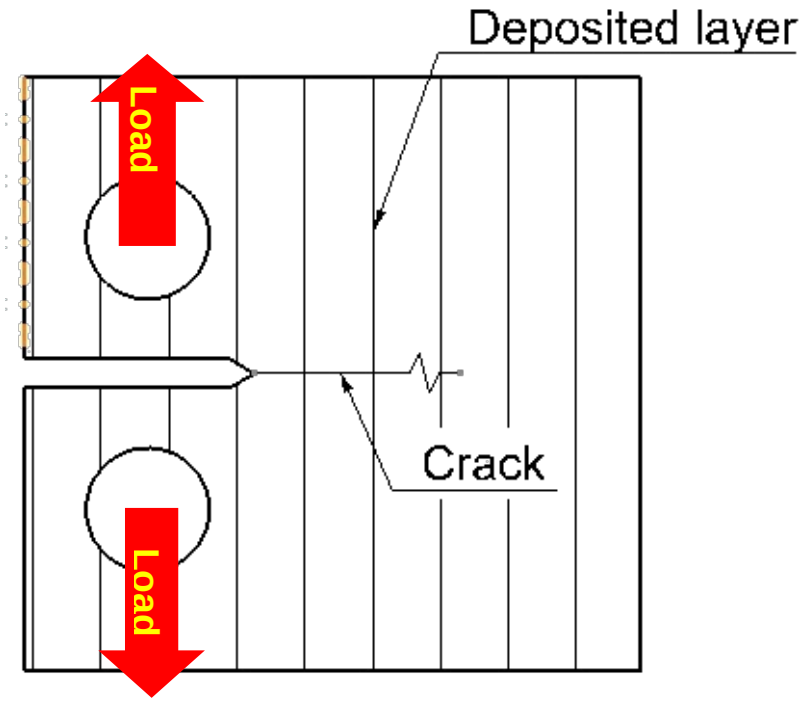

Figure 4-2 Definition of L-T specimen

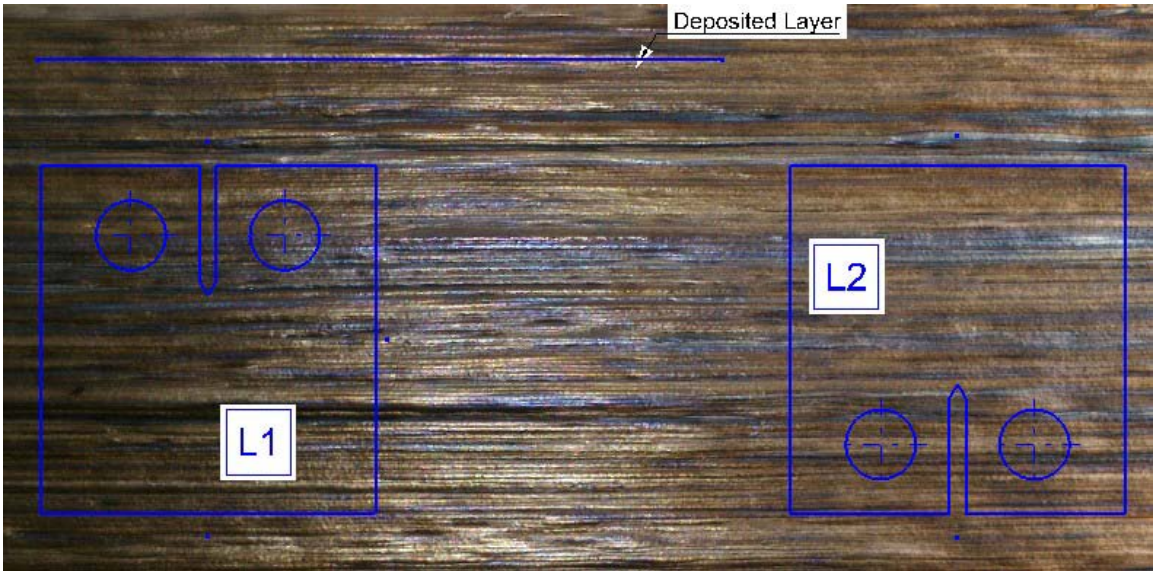

Figure 4-3 Locations of L-T specimens as they were cut off from the "wall"; crack in L1 specimen was from the wall's top to bottom, crack in L2 specimen was from the wall's bottom (near the substrate plate)

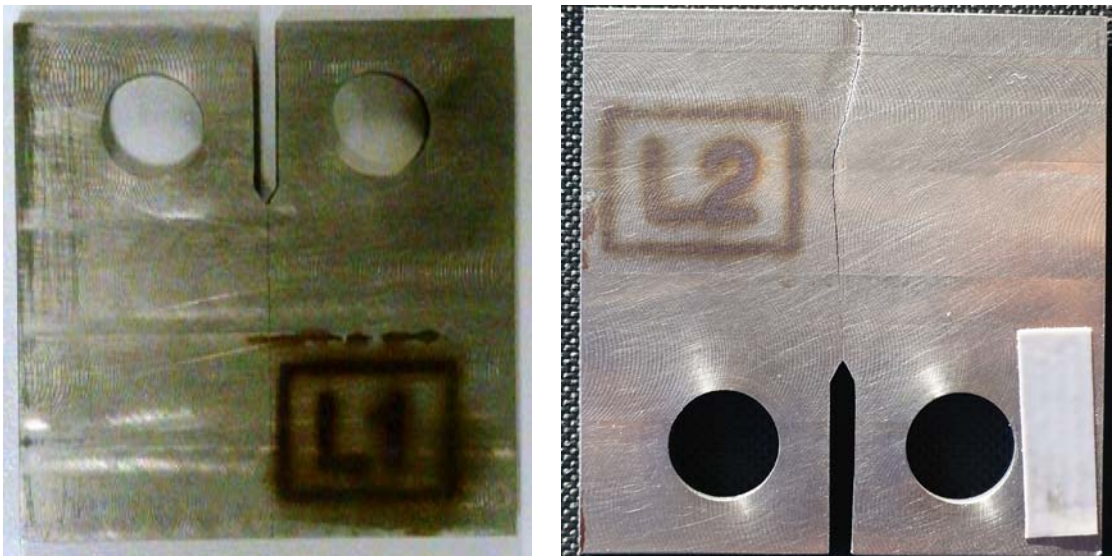

Figure 4-4 Photo of the L1, L2 specimens

4.1.1 Crack growth life

Curve of the crack length versus the number of cycles describes the life time of a specimen. Figure 4-5 shows the *a*-*N* curves of the L1 and L2 specimens.

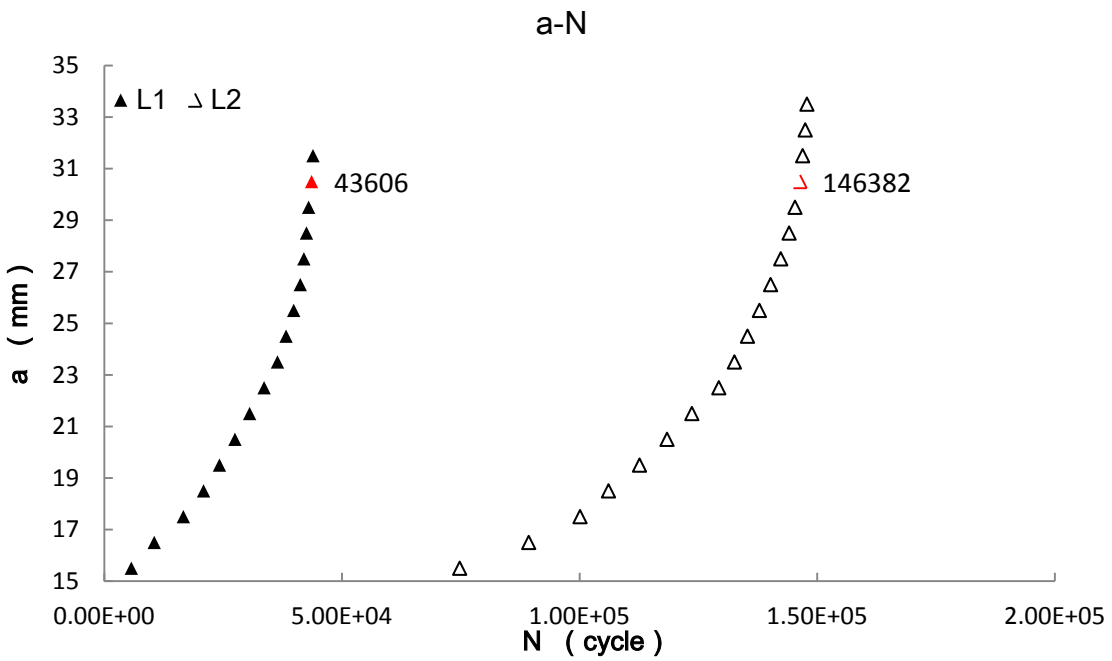

Figure 4-5 Test measured *a-N* curves of L1 and L2

From the curves, it can be found that L2 has a longer life time than L1. At a crack length of 30.5 mm, the life time of L2 is over 3 times longer than that of L1 (146382 cycles for L2 to 43606 cycles for L1).

Since the applied load ranges are different between L1 and L2 (3.6 kN for L1 and 3 kN for L2), the different fatigue lives may not only be caused by the different crack locations in the initial wall. For example, ΔK is function of load, *da/dN* is function of ΔK. Hence increase in load will cause increase in ΔK, da/dN, and decrease in *N*.

4.1.2 Fatigue crack growth rates

Figure 4-6 shows the fatigue crack growth rate curves of L1 and L2.

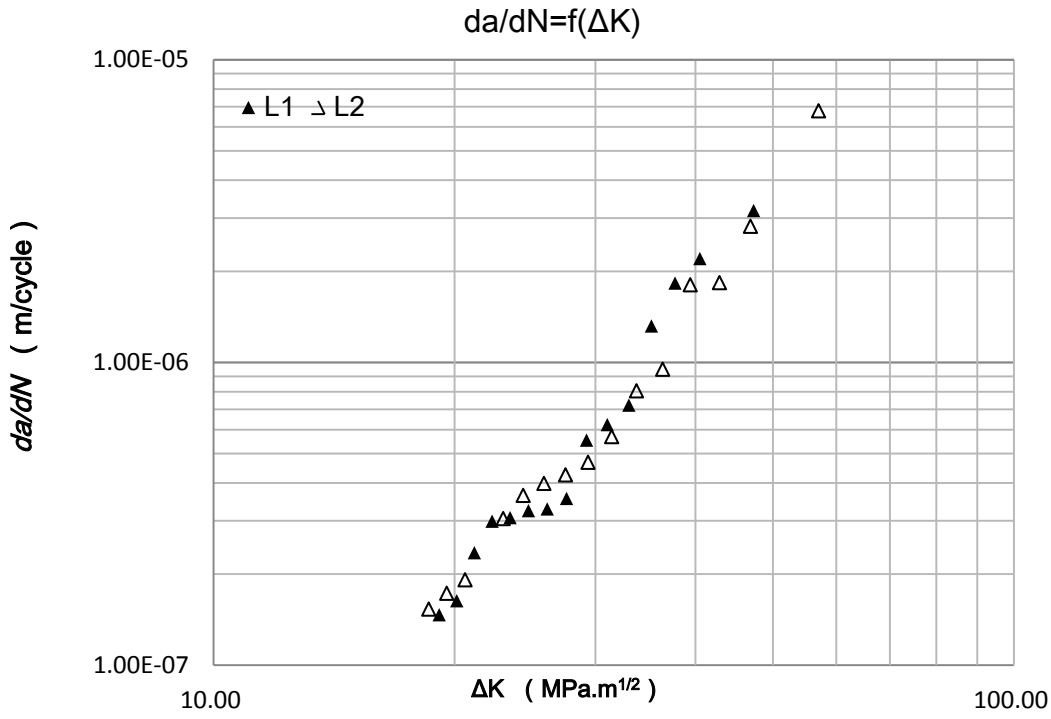

Figure 4-6 Fatigue crack growth rate curves of L1 and L2

The test were carried with a high load range (3.6 kN and 3 kN) and high R ratio (0.5), the curves begin from around 18 MPa.m$^{1/2}$ which is beyond the low stress intensity region. The curves are in the Paris Law region, the fatigue behaviour of L2 is slightly better than L1. The experimental Paris Law described in Equation 4-2 was calculated for the specimens.

$$\frac{da}{dN} = C * (\Delta K)^m \quad \textbf{(4-2)}$$

In the equation, *C* and *m* are two constants. These values were gained by approximating the linear portion of a curve with the least squares method. The experimental value for each test is shown in Table 4-1. ΔK_1 is the minimum stress intensity range value to determine the Paris Law; ΔK_2 is the maximum stress intensity range value.

Table 4-1 The Paris Law constants of the L-T specimens

Specimen	L1	L2
Log (*C*)	-10.7	-11.2
m	3.1	3.4
ΔK_1 (MPa.m$^{1/2}$)	18.2	17.6
ΔK_2 (MPa.m$^{1/2}$)	33.0	36.4
Correlation Coefficient	0.949	0.977

L1 has slightly greater rates than L2. For instance, at a stress intensity of 29 MPa.m$^{1/2}$, the fatigue crack growth rate of L1 is 5.54*10^{-7} m/cycle and the rate of L2 is 4.68*10^{-7} m/cycle, which is 15% smaller than that of L1.

da/dN vs. ΔK relation brings the two tests together even the applied load is very different. Similitude is reserved if ΔK is used as control parameter. Applying Equation 2-7 to Equation 4-2, the following equation can be obtained.

$$\frac{da}{dN} = C * \left(\frac{\Delta P}{B\sqrt{W}} * \frac{(2+\alpha)}{(1-\alpha)^{\frac{3}{2}}} (0.886 + 4.64\alpha + 13.32\alpha^2 + 14.72\alpha^3 - 5.6\alpha^4) \right)^m \quad \textbf{(4-3)}$$

At a α of 0.4, constants of L1 in Table 4-1 and L2's ΔP (3 kN) are applied to Equation 4-3, the fatigue crack growth rate of L1 obtained is 1.95*10^{-7} m/cycle, while *da/dN* of L2 at the same α value and ΔP is 1.5*10^{-7} m/cycle, which is 23% smaller than that of L1.

Since the data was recorded manually, less data points were recorded during the high stress intensity region. Thus the high stress intensity region is not well visible in the above curves. The test machine stopped automatically when the specimens fractured. Also, the maximum output load of the test machine is 100 kN, but the maximum testing load is only 10.8 kN. All these factors could have some effects on the accuracy of the experiment results.

Figure 4-7 and Figure 4-8 are the pictures of the specimens when they fractured. It can be seen that the fatigue cracks grew almost strictly along the symmetric lines of the specimens before fracture.

Figure 4-7 Specimen L1 after the test

Figure 4-8 Specimen L2 after the test

4.2 Results of T-L specimens

These results are to describe the fatigue properties of rolled WAAM processed Ti-6Al-4V with the load in the transverse direction and fatigue cracks in the longitudinal direction.

T-L specimen is defined as the load being introduced in the transverse direction with the fatigue crack parallel to the longitudinal direction. Figure 4-9 explains the definition of T-L specimen.

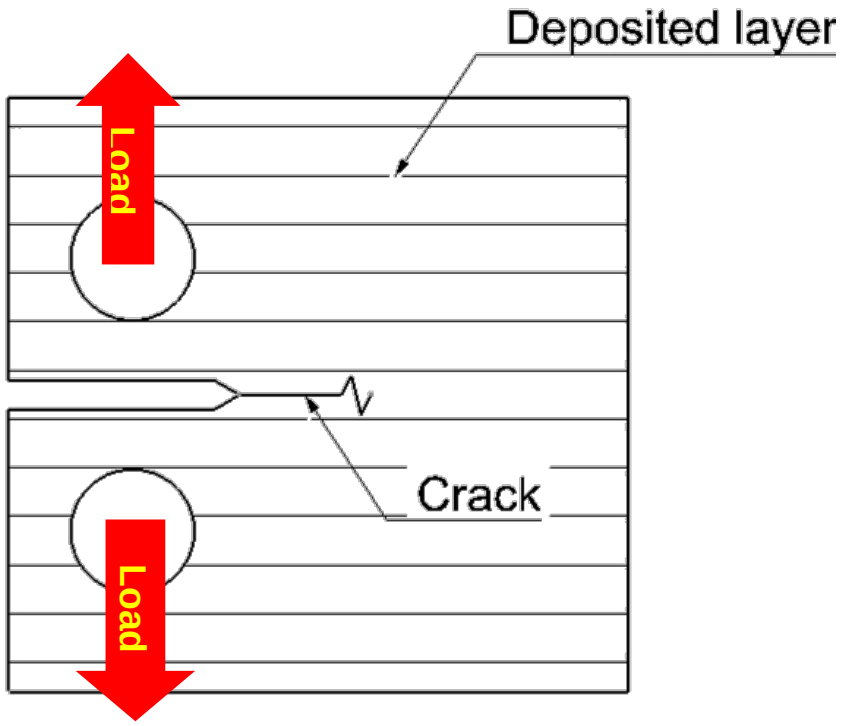

Figure 4-9 Definition of T-L specimen

To see whether the randomicity had any effect on the material's fatigue behaviour, specimens with different crack locations were obtained. The T-L specimens were marked as T1 and T2. Figure 4-10 shows the locations in the initial wall of the two T-L specimens. The final shapes of T1, T2 are shown in Figure 4-11.

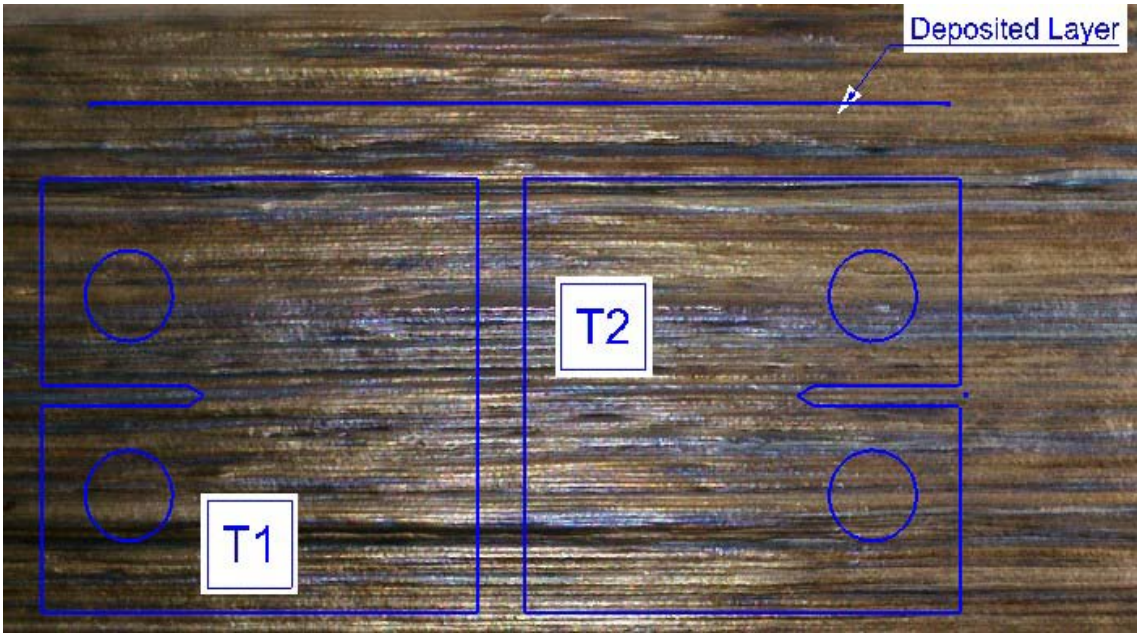

Figure 4-10 Locations of T-L specimens, crack in T1 was from left to right, crack in T2 was from left to right

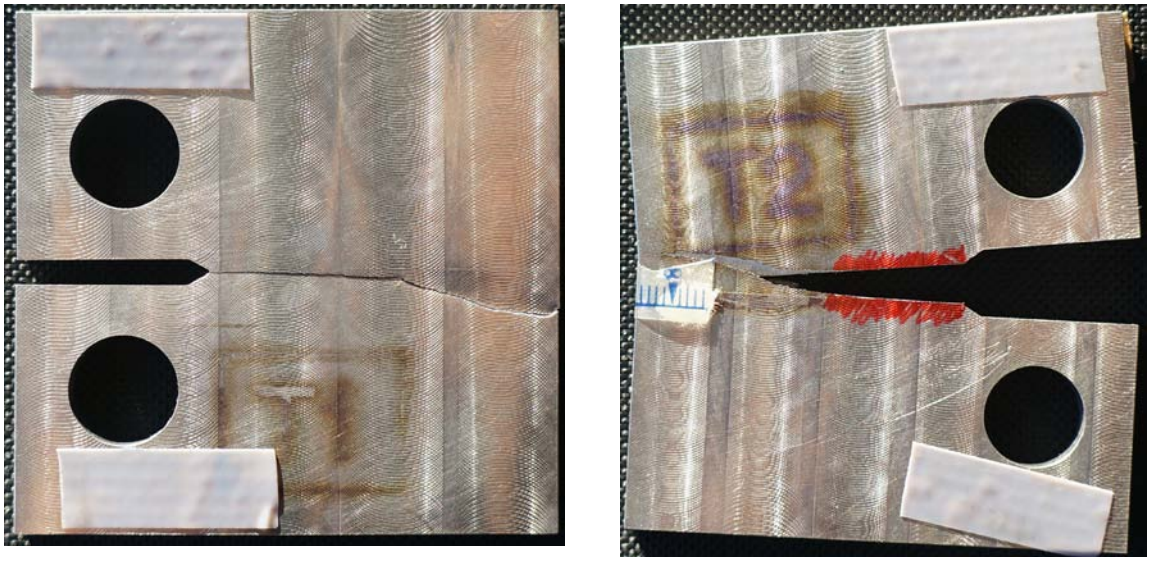

Figure 4-11 Final shapes of T1, T2

If it were not the marks, there is little difference between the L-T specimens and T-L specimens from the appearance.

4.2.1 Crack growth life

Figure 4-12 show the a-N curves of T1and T2.

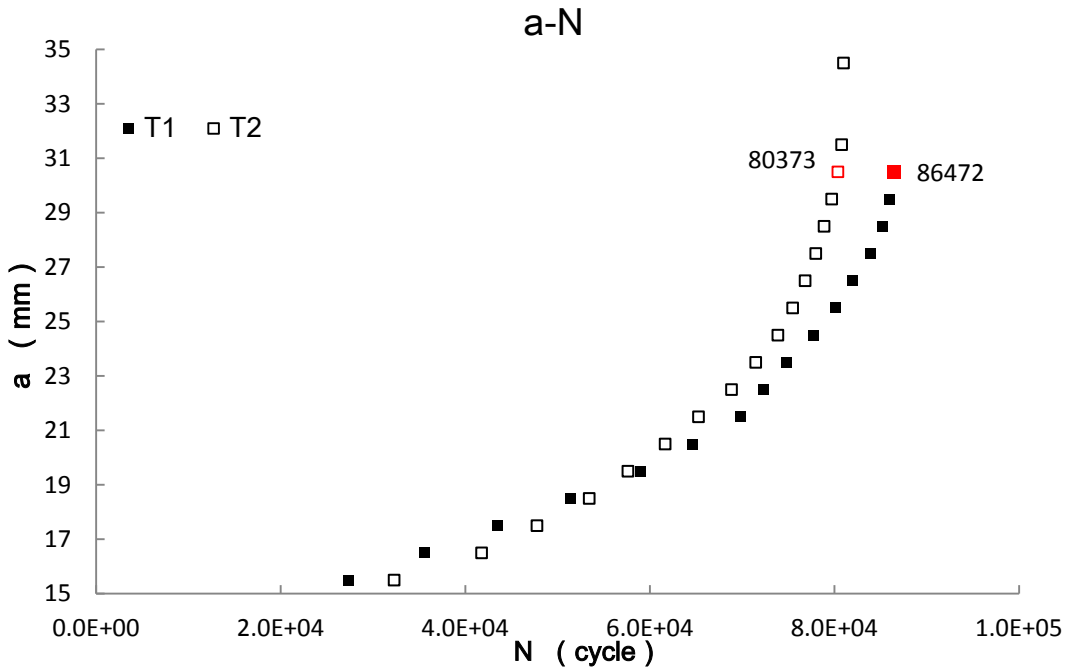

Figure 4-12 a-N curves of T1 and T2

The fatigue lives of these two T-L specimens are almost the same, T1 seems to have slightly longer life time than T2. For example the number of cycles required to get a crack length of 30.5 mm is 86472 for T1 and 80373 for T2. The life of T1 is only 7% longer than that of T2. The fatigue crack direction which is from right to left or from left to right has little effect on the fatigue life time.

4.2.2 Fatigue crack growth rates

Figure 4-13 shows the fatigue crack growth rate curves of T1 and T2.

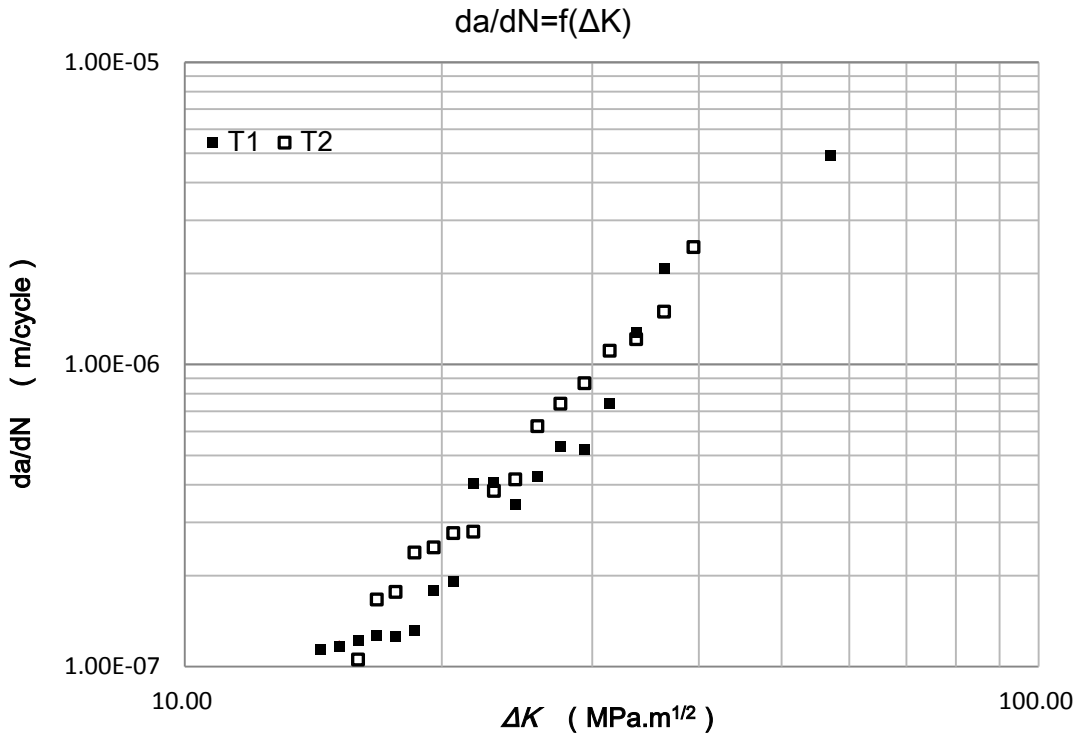

Figure 4-13 Fatigue crack growth rate curves of T1 and T2

Like the two L-T specimens, the tests were carried with a high load range (3 kN) and high R ratio (0.5), the curves begin from around 15 MPa.m$^{1/2}$ which is beyond the low stress intensity region. The curves are in the Paris Law region. The fatigue behaviour of T1 is slightly better than that of T2. The experimental value for each test is shown in Table 4-2, where ΔK_1 is the minimum stress intensity range value to determine the Paris Law; ΔK_2 is the maximum stress intensity range value.

Table 4-2 The Paris Law constants of the T-L specimens

Specimen	T1	T2
Log (*C*)	-10.4	-11.1
m	2.9	3.5
ΔK_1 (MPa.m$^{1/2}$)	18.57	17.65
ΔK_2 (MPa.m$^{1/2}$)	33.77	29.37
Correlation Coefficient	0.955	0.967

T2 has greater rates than T1. For instance, at a stress intensity of 29 MPa.$m^{1/2}$, the fatigue crack growth rate of T1 is $5.21*10^{-7}$ m/cycle and the rate of T2 is $8.67*10^{-7}$ m/cycle. T2 is 66% greater than T1.

Same as the tests of L-T specimens, the data of T-L specimens was recorded manually, less data points were recorded during the high stress intensity region. The high stress intensity region is not well visible in the curves above. The test machine stopped automatically when the specimens fractured.

Figure 4-14 and Figure 4-15 are the pictures of the specimens when they fractured. Like the tests of the L-T specimens, the fatigue cracks grew strictly along the symmetric lines of the specimens before fracture.

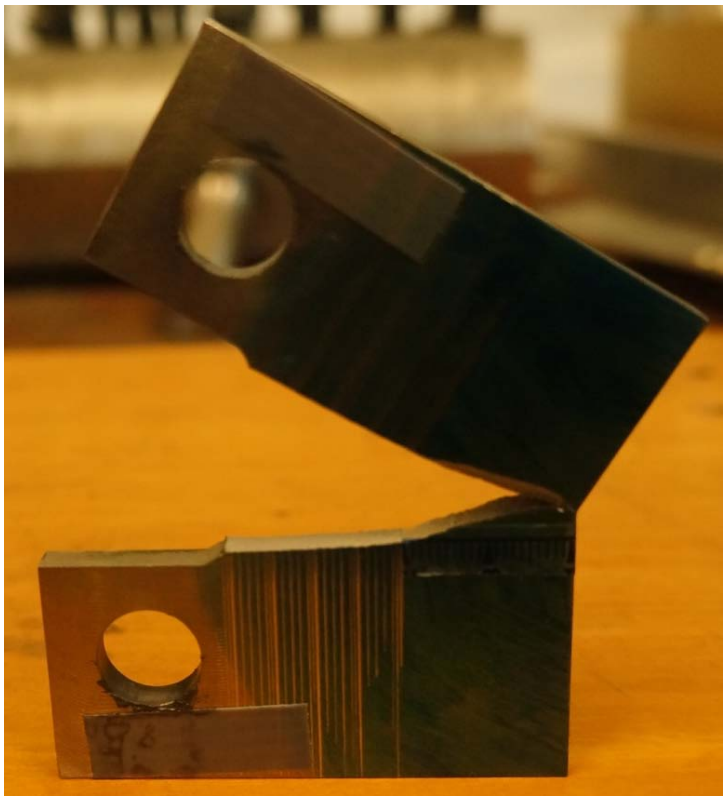

Figure 4-14 Specimen T1 after the test

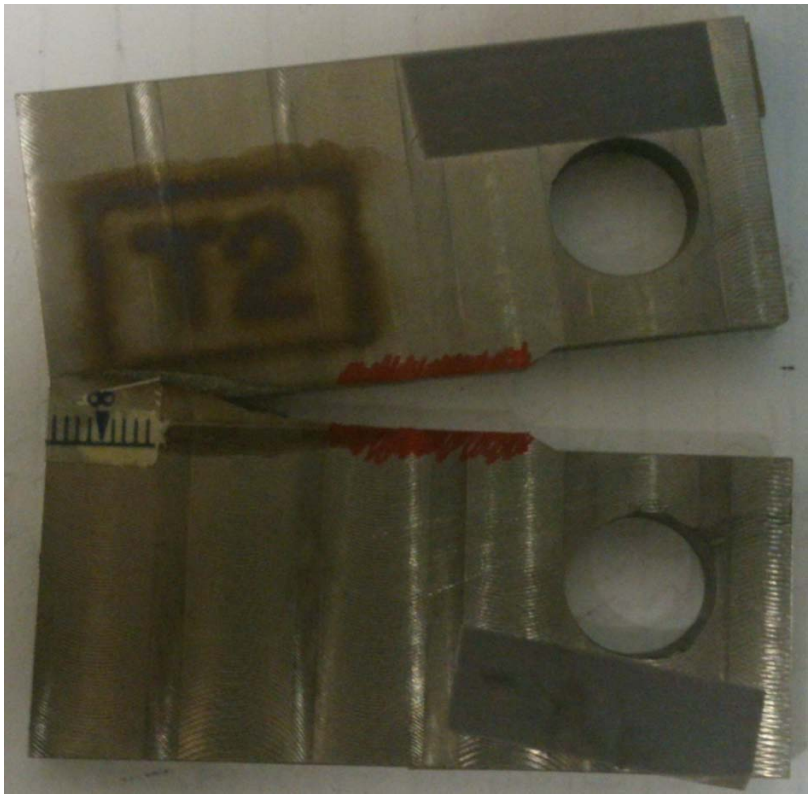

Figure 4-15 Specimen T2 after the test

5 DISCUSSION

This chapter aims at discussing about the results gained from this project. The fatigue crack growth rate tests results of the L-T specimens are compared with the results of T-L specimens to discuss the fatigue properties of the Ti-6Al-4V parts made by rolled WAAM manufacturing in longitudinal and transverse directions. Then, the fatigue properties of rolled WAAM processed Ti-6Al-4V are compared with unrolled WAAM processed Ti-6Al-4V to discuss the effects of rolling on Ti-6Al-4V made by Wire and Arc Additive Manufacturing.

5.1 Comparison between L-T and T-L

Martina [47] tested the tensile properties and hardness of the rolled WAAM processed Ti-6Al-4V. The results are listed in Table 5-1.

Table 5-1 Tensile properties and hardness of rolled WAAM processed Ti-6Al-4V

Specimen	Longitudinal	Transverse	AMS 4911
Ultimate Tensile Strength (MPa)	1080	1080	950
Yield Strength (MPa)	1025	995	880
Elongation (%)	13	13	14
Hardness (HV)	377		349

The tensile properties and hardness of the rolled WAAM processed Ti-6Al-4V have met the requirements in the aerospace material specification. And isotropy of static mechanical properties was gained by 75 kN rolling on WAAM processed Ti-6A-4V.

5.1.1 a-N curves

The fatigue life time of the four specimens were summarized in Figure 5-1.

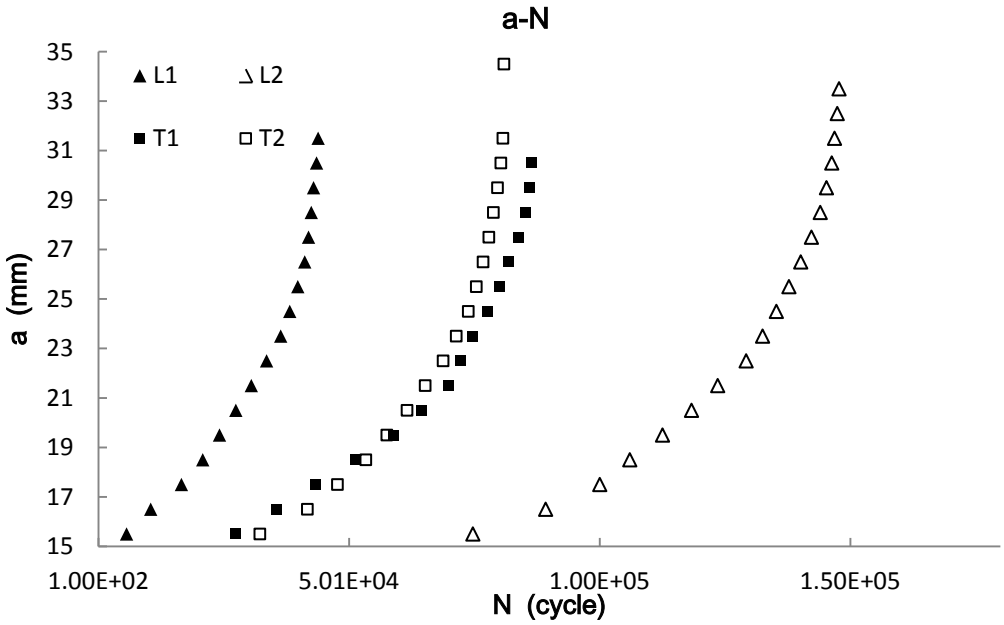

Figure 5-1 Summary of a-N

L-T specimens: It is clear that the life time of the two L-T specimens had a big difference. Specimen L1 had the shortest fatigue life and specimen L2 had the longest fatigue life which is over 300% that of L1. The different testing loads can cause the different fatigue lives. The load range was 3.6 kN for L1 and 3 kN for L2. According to Equation 2-7, ΔK increases with the increasing ΔP. For example, at the same fatigue crack length a=20.5 mm, the ΔK is 23.5 MPa.m$^{1/2}$ for L1and 19.5 MPa.m$^{1/2}$ for L2. The stress intensity factor range is increased by 20%, and the da/dN is 3.1*10^{-7} m/cycle for L1 and 1.73*10^{-7} m/cycle for L2.

T-L specimens: The two T-L specimens had almost the same life. The fatigue life of T1 is only 6% longer than that of T2.

The parameters such as the load range ΔP, R ratio and the initial maximum load P_{max} used in the fatigue crack growth rate test of specimen L2 were the same as those used in the tests of specimens T1 and T2. So it seems that the Ti-6Al-4V made by rolled WAAM process has a longer fatigue life time with the load in the longitudinal direction than in the transverse direction.

Although the fatigue crack growth rates test of specimen L1 used higher load, it is hard to say that the tests results were only influenced by the different loads. Because the cracks locations in the initial wall were different, the microstructures may have some effect on the results. Figure 5-2 shows the microstructures of the initial wall.

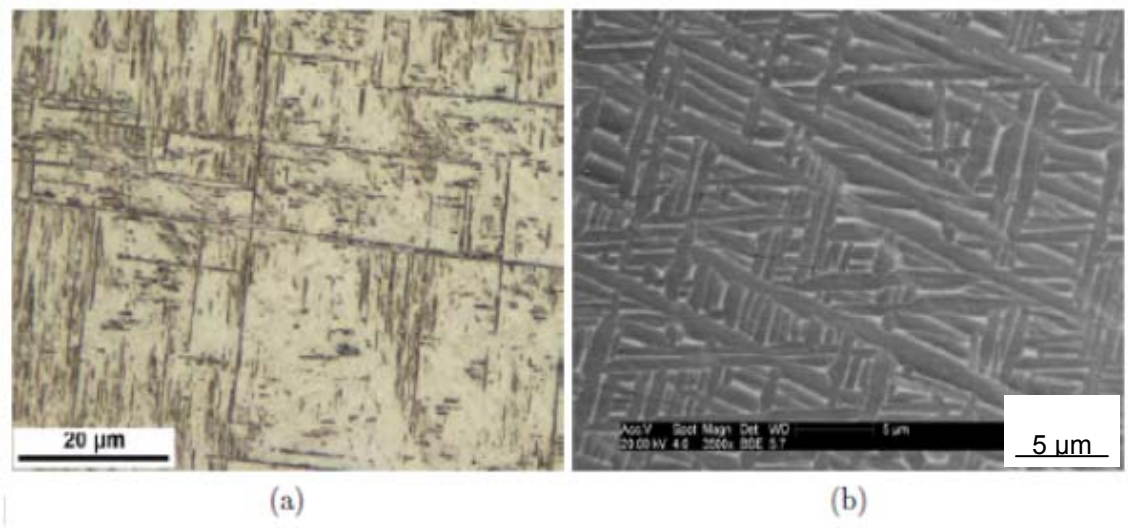

Figure 5-2 (a) Microstructure observed in the top of the initial wall and (b) microstructure observed in the rest of the wall [47]

The microstructure in the top area was different from the rest of the wall. But the top area was only in a range of 6 mm from the top of the wall [47] as shown in Figure 5-3.

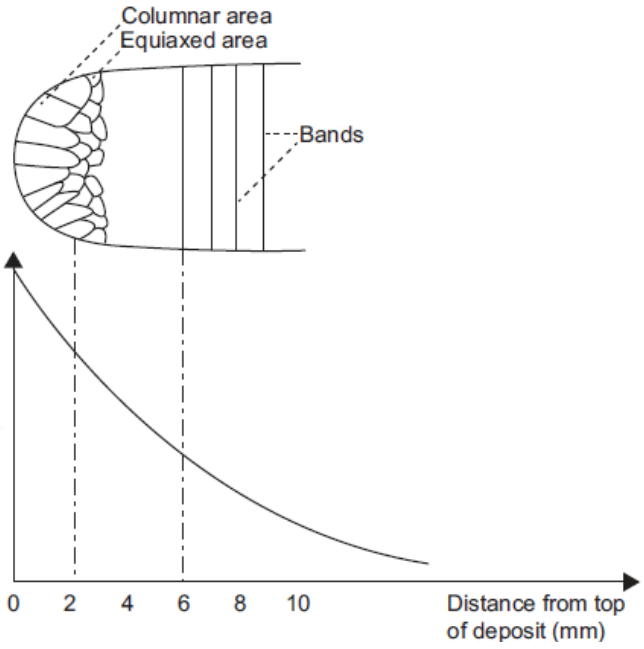

Figure 5-3 The range of top the area [47]

The distance between each specimen and the top of the initial wall was more than 30 mm as shown in Figure 5-4. So specimen L1 should have the same microstructure with other three specimens, and the different microstructures in the initial wall had little effect on the tests.

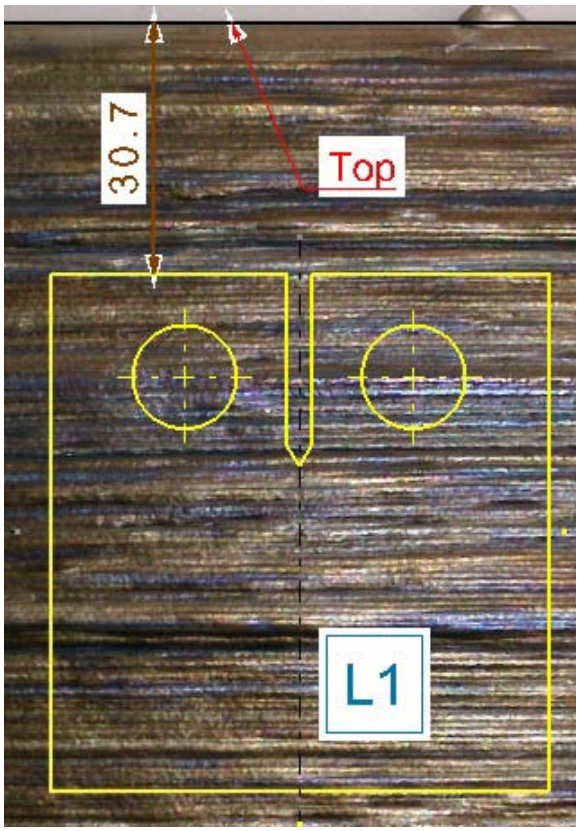

Figure 5-4 Distance between the top of initial wall and the specimen

Martina [47] investigated the residual stress of rolled WAAM processed Ti-6Al-4V. The residual stress was measured in the initial wall in the longitudinal direction after welding (the wall was not separated from the substrate). Figure 5-5 describes the residual stress in the wall. Although the residual stress of the wall made by 75kN rolling was not measured in the investigation, it can be seen that the residual stress in the longitudinal direction reduced with the increasing distance from the bottom of the measured area to the top. The residual stress even turned to negative after 30mm. Negative residual stress could decrease the tensile load in the longitudinal direction during the fatigue crack growth rates test on L-T specimens, while positive residual stress could increase the testing load.

Since the crack in specimen L1 was from the top to the bottom and crack in specimen L2 was from the bottom to the top, the testing loads were increased in L1 and decreased in L2. This may have some effect on the test results. Though the test machine outputs the same loads to specimens L2, T1 and T2, the actual stress at the crack tip of L2 was lower than the other two specimens.

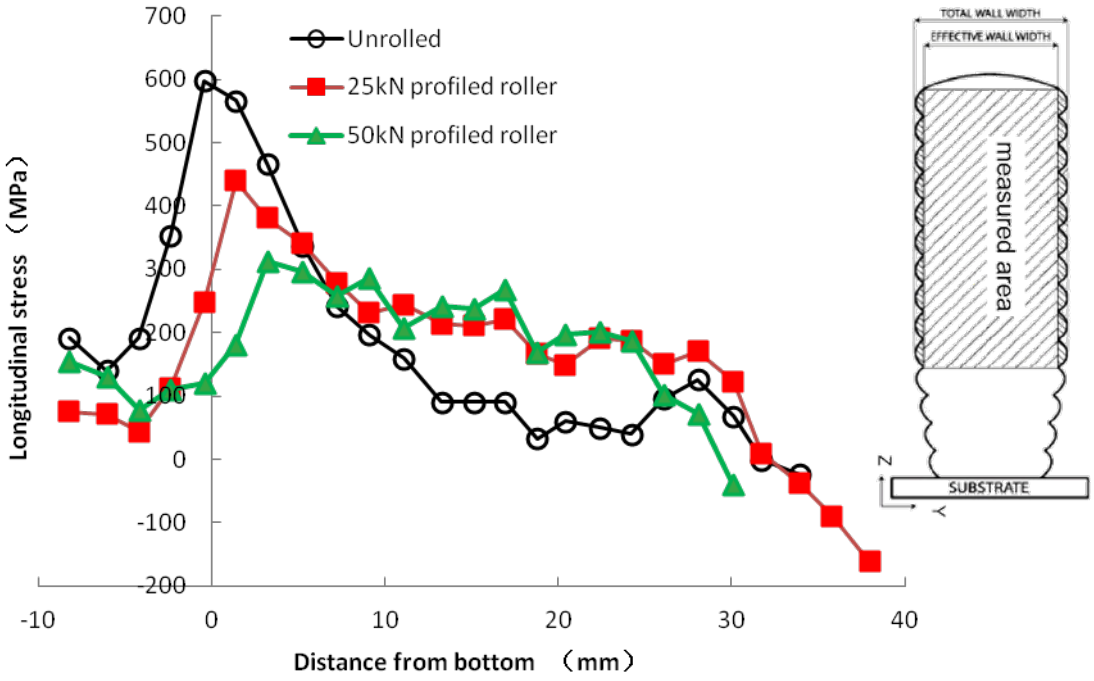

Figure 5-5 Longitudinal residual stress in measured area [47]

The residual stress in the longitudinal direction may be reduced after the wall being cut from the substrate. Ding et al. analyzed the residual stress in rolled WAAM processed steel plates. Though the material was different, the trend should be similar. The residual stress in the longitudinal direction was decreased, and the stress value almost kept constant when the distance was more than 10 mm from the bottom as shown in Figure 5-6 [48].

Since the initial wall in this project was separated from the substrate and the distance between each specimen and the bottom of the initial wall was more than 30 mm as shown in Figure 5-7, the effects of the longitudinal stress on L1 and L2 should be the same, if the rolled WAAM processed Ti has the same thermo-mechanical properties with the steel. Then the difference in the fatigue life time of the two L-T specimens should be cause by the different test loads.

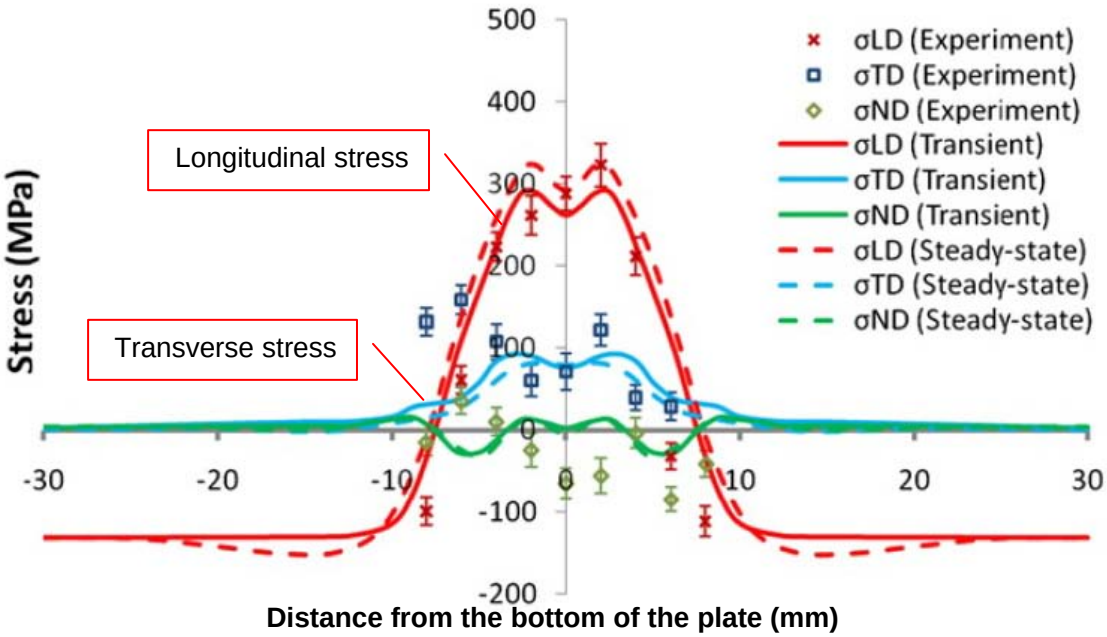

Figure 5-6 Residual stress in the longitudinal (LD) direction [48]

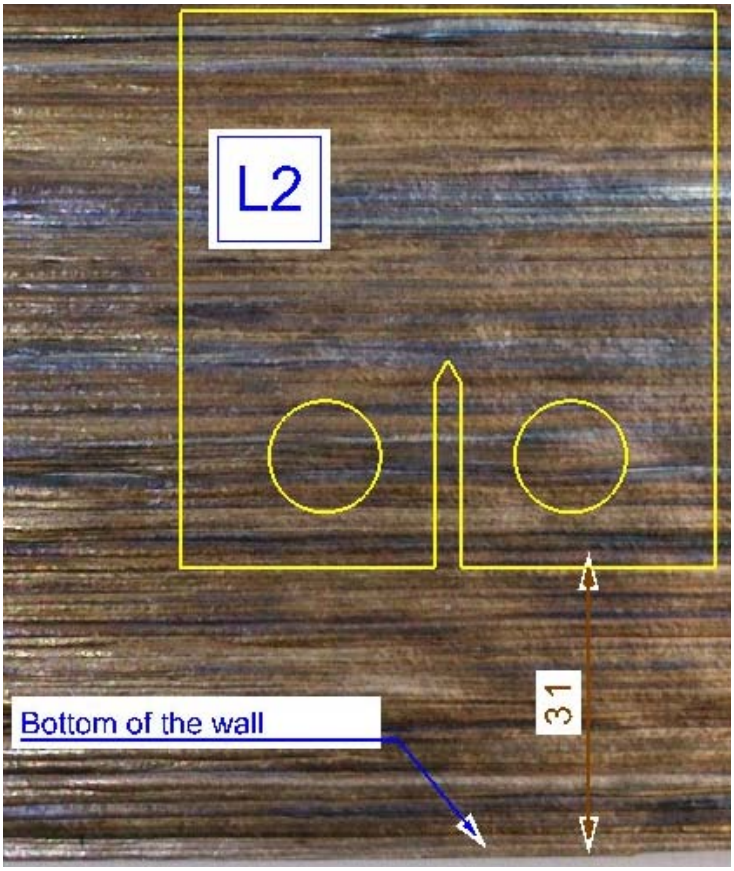

Figure 5-7 Distance between the specimen and the bottom of the wall

Comparing L2 with the two T-L specimens, the fatigue life time of L2 is 1.5 times of the average life time of T-L. The L-T specimen seems to have a longer

fatigue life time than the T-L one with the condition of same load and R ratio. However the test machine stopped twice accidently during the test of L2, and the load reduced to zero at that time. This might have some effect on the test result of L2. A dark area can be seen on the fracture profile of L2, but there is no such an area on the fracture profile T-L specimen, as shown in Figure 5-8. The dark area should have some relationship with the fatigue life time. Scanning Electron Microscope should be used to observe the fracture profiles and to find the relationship between the dark area and fatigue life time in future work, for the Scanning Electron Microscope is unavailable in this project.

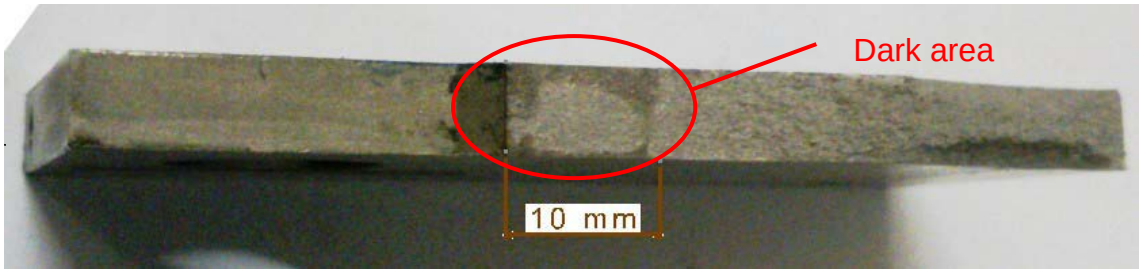

a)

b)

Figure 5-8 Fracture profiles a) L2, b) T1

5.1.2 da/dN curves

Figure 5-9 is the summary for the *da/dN* curves of the four specimens. The fatigue crack growth rates of the four specimens had no obvious difference between different directions.

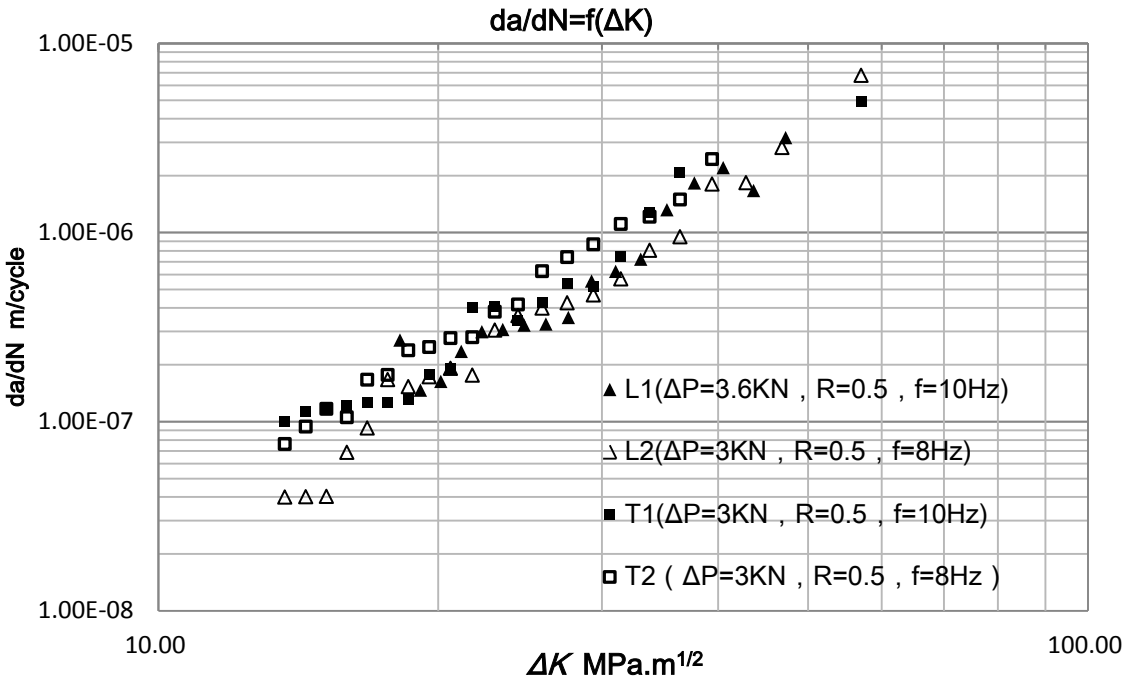

Figure 5-9 Summary for the *da/dN* curves

The Paris Law parameters of the L-T and T-L specimens are compared in Table 5-2. It can be seen that the fatigue crack growth rates for T2 are greater than other three specimens in the Paris Law region. For example, at the ΔK=29.4 MPa.m$^{1/2}$, the fatigue crack growth rate was 4.68*10^{-7} m/cycle for L2 and 8.67*10^{-7} m/cycle for T2.

Table 5-2 Comparison of the Paris Law parameter

Specimen	L1	L2	T1	T2
Log (*C*)	-10.7	-11.2	-10.4	-11.1
m	3.1	3.4	2.9	3.5
ΔK_1 (MPa.m$^{1/2}$)	18.2	17.6	18.57	17.65
ΔK_2 (MPa.m$^{1/2}$)	33.0	36.4	33.77	29.37
Correlation Coefficient	0.949	0.977	0.955	0.967

Fatigue crack growth rate properties of the four specimens are compared in Table 5-3.

Table 5-3 Comparison between fatigue crack growth rates of the four specimens

	Fatigue crack growth rate（m/cycle）			
ΔK (MPa.m$^{1/2}$)	L1	L2	T1	T2
18	1.46E-07	1.13E-07	1.84E-07	1.78E-07
19	1.72E-07	1.35E-07	2.16E-07	2.15E-07
20	2.01E-07	1.61E-07	2.51E-07	2.57E-07
22	2.70E-07	2.23E-07	3.31E-07	3.57E-07
25	4.00E-07	3.45E-07	4.80E-07	5.56E-07
30	7.01E-07	6.41E-07	8.18E-07	1.05E-06

It can be seen from the table that the L-T and T-L specimens made by rolled WAAM manufacturing seem to have similar fatigue crack growth rates. The T-L specimens have slightly greater (39% greater than L-T on average) fatigue crack growth rates. Isotropic fatigue crack growth behaviour can be obtained through rolling.

5.2 Comparison between unrolled and rolled WAAM

The first obvious difference between unrolled and rolled WAAM specimens is the β grains. Unrolled specimens have significantly larger β grains which can be seen from the surfaces of both the specimens and initial wall. But hardly any β grain can be seen on the surface of either the initial wall or machined specimens. Figure 5-10 is the example for the appearances of specimens made by the two manufacturing processes. The interface between two deposited layers is invisible on rolled specimens after machining.

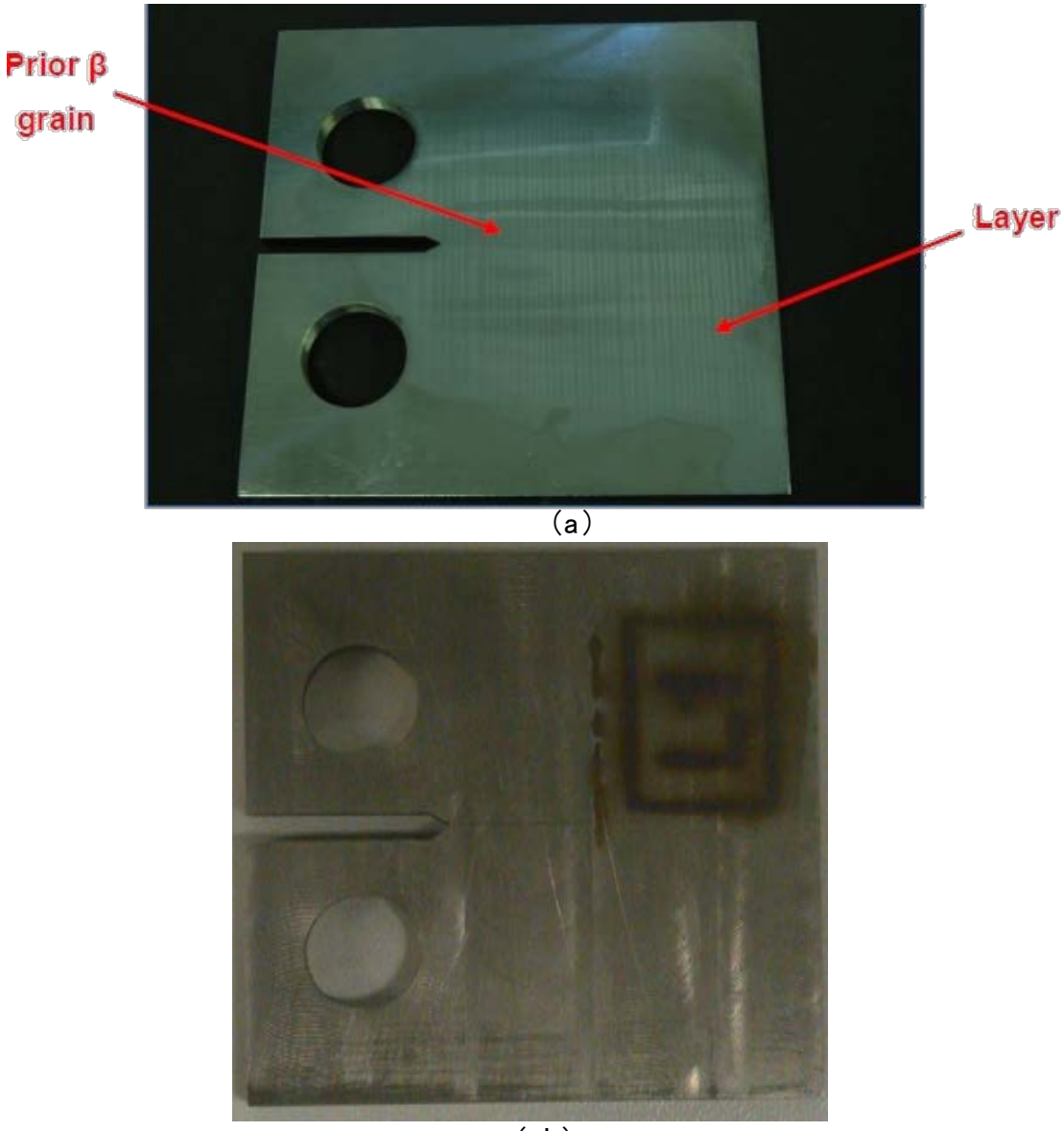

Figure 5-10 (a) unrolled L-T specimen (b) rolled L-T specimen

Lorant [2] carried out the fatigue crack growth rate tests on unrolled WAAM processed Ti-6Al-4V specimens. She found that the fatigue crack grew along the β grain edge, as shown in Figure 5-11. The fatigue crack growth path in a rolled specimen was strictly along the symmetric line no matter it was L-T or T-L specimen.

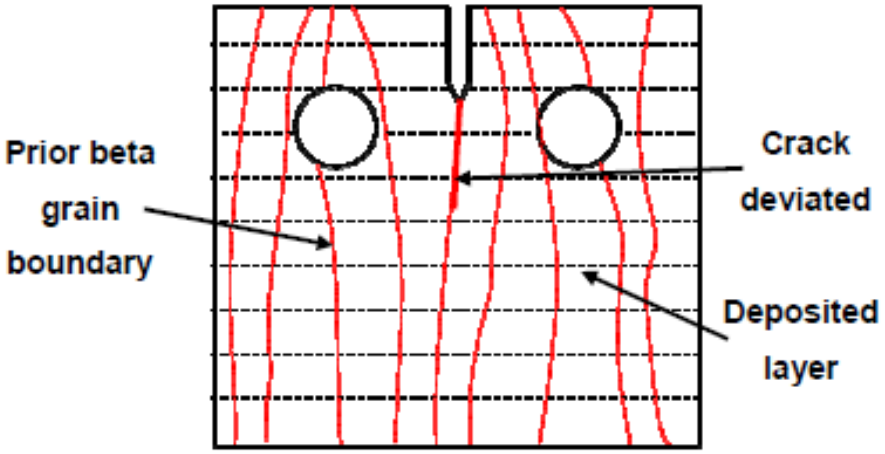

Figure 5-11 Crack growth path in the unrolled specimen [2]

The comparison of the *da/dN* curves between the rolled and unrolled Ti-6Al-4V specimens as shown in Figure 5-12.

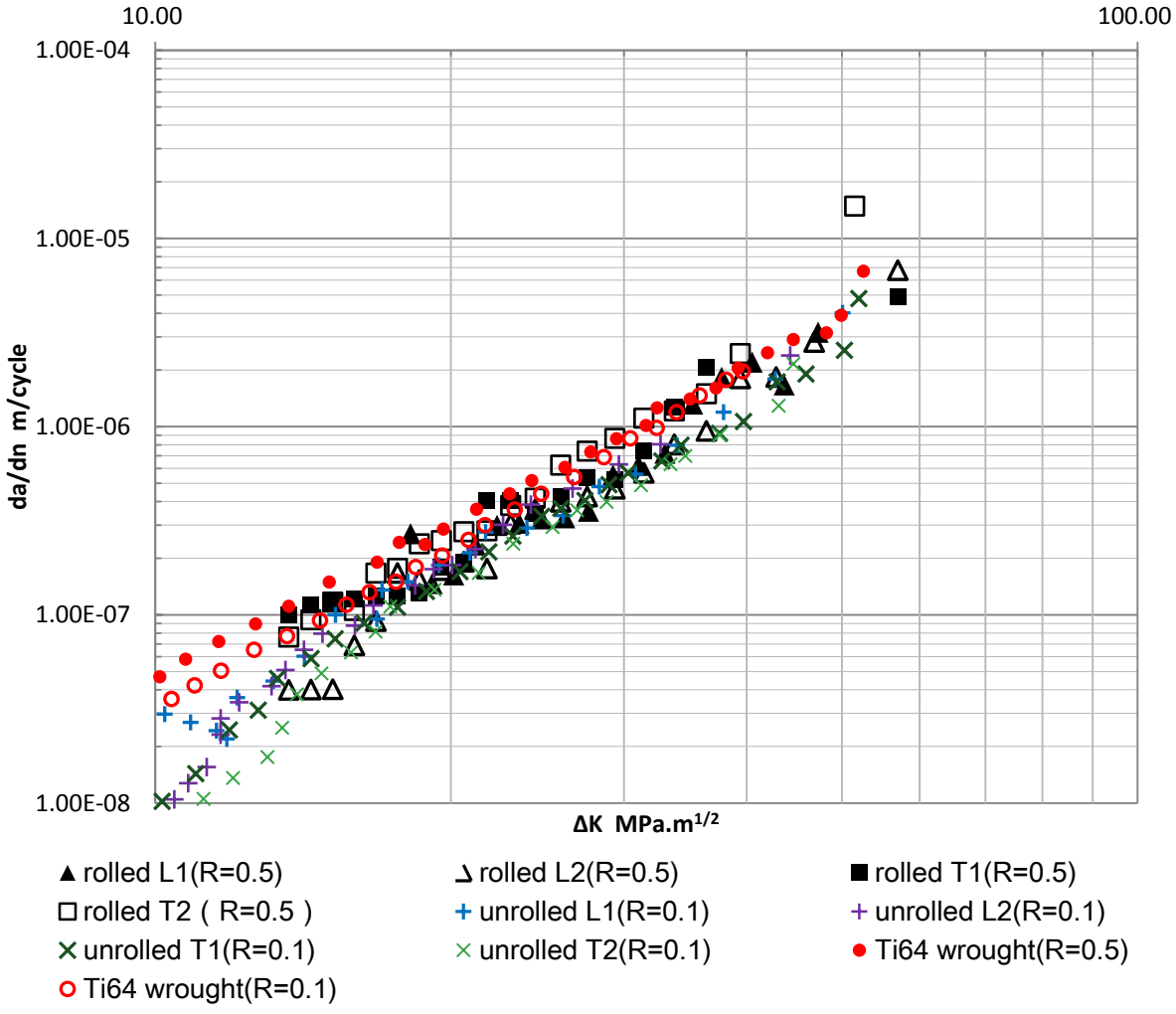

Figure 5-12 Comparison of the *da/dN* curves between the rolled and unrolled Ti-6Al-4V specimens, also compare with Ti64 wrought

The *da/dN* versus *ΔK* curves have little difference between rolled and unrolled WAAM processed Ti-6Al-4V, rolled specimen T2 had slightly greater fatigue crack growth rates compared with other specimens. But the R ratio used in the test of unrolled one is 0.1 and the load range is 2.16 kN which is much smaller than the rolled one. So in general it appears rolling has a positive effect on fatigue crack growth rate of WAAM processed Ti-6Al-4V. Fatigue crack growth rate properties of the specimens made by different WAAM processes are compared in Table 5-4.

Table 5-4 Comparison of fatigue crack growth rates of rolled and unrolled Ti

	Fatigue crack growth rate（m/cycle）							
	Rolled WAAM				Unrolled WAAM			
ΔK (MPa.m$^{1/2}$)	L1	L2	T1	T2	L1	L2	T1	T2
18	1.46E-07	1.13E-07	1.84E-07	1.78E-07	1.50E-07	1.44E-07	1.10E-07	1.11E-07
19	1.72E-07	1.35E-07	2.16E-07	2.15E-07	1.84E-07	1.75E-07	1.33E-07	1.36E-07
20	2.01E-07	1.61E-07	2.51E-07	2.57E-07	2.14E-07	1.84E-07	1.70E-07	1.67E-07
22	2.70E-07	2.23E-07	3.31E-07	3.57E-07	2.75E-07	3.01E-07	2.16E-07	2.39E-07
25	4.00E-07	3.45E-07	4.80E-07	5.56E-07	3.37E-07	3.85E-07	3.34E-07	2.93E-07
30	7.01E-07	6.41E-07	8.18E-07	1.05E-06	5.59E-07	6.30E-07	5.68E-07	4.89E-07

It can be seen that within the same range of stress intensity factor, the rolled specimens which were tested with higher load range and R ratio obtained similar results with the unrolled ones which tested with lower load range and R ratio.

The unrolled specimens were tested on a test machine with the maximum output of 20 kN, and the data during the tests of unrolled specimens were recorded by a computer. But the rolled specimens were tested on a test machine with maximum output of 100 kN, and all the data were observed and recorded manually. This measurement method may increase the possibility of scatter in the data.

Comparing the curves with those of the wrought Ti-6Al-4V, the curves of rolled specimens are better than the wrought one tested with the R ratio of 0.5. The curves are similar with the wrought one tested with the R ratio of 0.1. So again the rolling process appears to produce Ti-6Al-4V with better fatigue crack growth rate behaviour than wrought Ti64. However the number of samples tested is quite small and further testing is recommended.

6 CONCLUSIONS

Current understanding of WAAM processed titanium from the literature is as follows:

- Ti-6Al-4V made by Rolled Wire and Arc Additive Manufacturing has a finer microstructure. The β grains are not obviously visible as compared to the microstructure of titanium made by the Wire and Arc Additive Manufacturing alone (without rolling).
- Rolling can improve the mechanical properties under tension loads; the ultimate tensile strength and yield strength are both improved through rolling, by 19% and 26% respectively.
- Isotropy in tensile properties is achieved, i.e. tensile properties in the longitudinal and transverse directions are similar.

From this project, following conclusions can be drawn:

- Fatigue crack growth rate properties in both directions are improved (reduced) by in process rolling compared to those of unrolled WAAM titanium obtained in the literature.
- The rolling process produces Ti-6Al-4V with improved fatigue crack growth rate properties compared to wrought material.
- Isotropy in the fatigue crack growth rate properties is observed. The difference between the longitudinal and transverse directions was reduced by rolling.

7 SUGGESTION FOR FUTURE WORK

- Tension tests should be carried out to obtain the Young's modulus, tensile strength in different material directions. In fact, two specimens have been designed for tension tests, but due to resource constraint, tests have not been carried out.
- It could be interesting to measure the residual stress of the Ti-6Al-4V structures made by 75 kN rolling. The relationship between the residual stress and fatigue behaviours should be studied.
- More specimens for fatigue crack growth rate tests should be built to confirm the isotropy in fatigue properties. Future specimen dimension should be much larger than that used in this study in order to use the 50 kN test machine, or keep the same dimension but use 20 kN machine. The latter option was not available at the time of this project.
- Thicker specimens are required for the fracture toughness test on the rolled WAAM specimens.
- Fatigue crack growth rate properties of the joint area between the substrate plate and deposited layer should be investigated.
- Fracture profiles should be investigated to analyze the different fatigue crack growth behaviour in different directions.

REFERENCES

[1]: Jian Chen, Hybrid Design based on Wire and Arc Additive Manufacturing in the Aircraft Industry, 2012, MSc thesis, School of Applied Science, Cranfield University.

[2]: Emilie Lorant, Effect of microstructure on mechanical properties of Ti-6Al-4V structures made by Additive Layer Manufacturing, 2010, School of Applied Sciences, Cranfield University

[3]: P. Erin and B.S. Barry, Three-dimensional reconstruction of microstructures in α+β titanium alloys, 2008, Graduate Program in Materials Science and Engineering, The Ohio State University.

[4]: Tapany Udomphol, Titanium and its alloys, 2007, Suranaree University of Technology.

[5]: Don Sherman, The truth about titanium, 1993, Church of the Science of God, La Jolla, California 92038-3131.

[6]: Wang RongMin, Application of titanium in aviation, 2007, WORLD NONFERROUS METAL, pp. 65-67.

[7]: Light Metals Lecture：18
Titanium, http://app.eng.ubu.ac.th/~edocs/f20061122Suriya96.pdf (accessed on 5th May 2013)

[8]: S. Seong, O. Younossi, B. W. Goldsmith and T. Lang, M. Neumann, Titanium Industrial Base, Price Trends, and Technology Initiatives, 2009, PROJECT AIR FORCE, RAND Corporation.

[9]: Andrea Cini, Scribe Marks at Fuselage joints Initiation and propagation of fatigue cracks from mechanical defects in aluminum alloys, 2007, Internal Progress Review Report, School of Applied Sciences, Cranfield University.

[10]: M. Kazemi, B. Jabbari Poor, M. H. Sadeghi, B. Moetakef Imani, Surface Integrity of Thin-Walled Titanium Parts Machined by Peripheral Milling, 2007,

Dept. Of Mechanical Engineering, Tarbiat Modares University, Tehran,Iran, Dept. Of Mechanical Engineering, Ferdowsi University, Mashad , Iran.

[11]: R. Dehoff, C. Tallman, C. Duty, Case Study: Additive Manufacturing of Aerospace Brackets, 2008, U.S. Department of Energy, Office of Energy Efficiency and Renewable Energy, Advanced Manufacturing Office.

[12]: Bernd Baufeld, Omer Vanderbiest, Rosemary Gault, Additive manufacturing of Ti–6Al–4V components by shaped metal deposition: Microstructure and mechanical properties, 2009, Materials and Design 31 (2010) S106–S111.

[13]: R. Lupoi, M. Sparkes, A. Cockburn, W. O'Neill, High speed titanium coatings by supersonic laser deposition, 2011, Materials Letters 65 (2011) 3205-3207.

[14]: Joe Hiemenz, EBM Offers a New Alternative For Producing Titanium Parts And Prototypes, 2006, Time-Compression Technologies, www.timecompress.com

[15]: Bernd Baufeld, Omer van der Biest, Rosemary Gault, Microstructure of Ti-6Al-4V specimens produced by shape metal deposition, 2009, Car Hanser Verlag GmbH & Co.KG ISSN 1862-5282.

[16]: F. Wang, S. Williams, M. Rush, Morphology investigation on direct current pulsed gas tungsten arc welded additive layer manufactured Ti6Al4V alloy, 2011, International Journal of Advanced Manufacturing Technology Volume 57, Numbers 5-8, 597-603

[17]: Alphons. A. Antonysamy, Microstructure, Texture and Mechanical Property Evolution during Additive Manufacturing of Ti6Al4V Alloy for Aerospace Applications, 2012, School of Materials, University of Manchester.

[18]: F. Martina, P. Colegrove, S.W. Williams, Grain refinement and distortion reduction of Ti-6Al-4V wire and arc additively manufactured parts through high-pressure rolling, Welding Engineering and Laser Processing Centre (WELPC), Cranfield University.

[19]: Filomeno Martina, Application of rolling to additively manufactured parts, Welding Engineering and Laser Processing Centre (WELPC), Cranfield University.

[20]: G. Lutjering and J. Williams, Titanium, 2003, New York: Springer-Verlag.

[21]: V. Joshi, Titanium Alloys: An Atlas of Structures and Fracture Features, 2006, Fla. Boca Raton: CRC Press, Taylor and Francis Group.

[22]: Aerospace material specification, 2012,"Titanium Alloy, Sheet, Strip, and Plate 6AI - 4V Annealed", Specification AMS 4911.

[23]: W.A. Glaeser, Bernard H. Lawless, Behavior of alloy Ti–6Al–4V under pre-fretting and subsequent fatigue conditions, 2001, Wear 250 (2001) 621–630.

[24]: M. Motyka, K. Kubiak, J. Sieniawski and W. Ziaja, Hot Plasticity of Alpha Beta Alloys, Chapter 5, Titanium Alloys - Towards Achieving Enhanced Properties for Diversified Applications, 2012, Edited by A.K.M. Nurul Amin.

[25]: M. Tane a, S. Akita a, T. Nakano b, K. Hagihara b, Y. Umakoshi b, M. Niinomi c, H. Mori d and H. Nakajima a, Low Young's modulus of Ti–Nb–Ta–Zr alloys caused by softening in shear moduli c0 and c44 near lower limit of body-centered cubic phase stability, 2010, Acta Materialia 58 (2010) 6790–6798.

[26]: R.K. NALLA, B.L. BOYCE, J.P. CAMPBELL, J.O. PETERS, and R.O. RITCHIE, Influence of Microstructure on High-Cycle Fatigue of Ti-6Al-4V: Bimodal vs. Lamellar Structures, 2002, METALLURGICAL AND MATERIALS TRANSACTIONS A, VOLUME 33A.

[27]: G. Lutjering, Influence of Processing on Microstructure and Mechanical Properties of (α+β) Titanium Alloys, 1998, Materials Science and Engineering A, A243: p. 32-45.

[28]: O.M. Ivasishin, and P. E. Markovsky, Enhancing the Mechanical Properties of Titanium Alloys with Rapid Heat Treatment, 2006, JOM. 48: p. 48-52.

[29]: E. Brandla, C. Leyensb, F. Palma, Mechanical properties of additive manufactured Ti-6Al-4V using wire and powder based processes, 2004, Materials Science and Engineering 26 (2011) 012004.

[30]: P.M. Sequeira Almeida, S. Williams, Innovative Process Model of Ti-6Al-4V Additive Layer Manufacturing Using Cold Metal Transfer (CMT), 2012, Welding Engineering Research Centre (WERC), Cranfield University.

[31]: B. Baufelda, E. Brandlb and O. VanderBiest, Wire based additive layer manufacturing: Comparison of microstructure and mechanical properties of Ti–6Al–4V components fabricated by laser-beam deposition and shaped metal deposition, 2011, Journal of Materials Processing Technology 211 (2011) 1146–1158.

[32]: B. Baufeld and O. Vanderbiest, Mechanical properties of Ti-6Al-4V specimens produced by shaped metal deposition, 2009, Sci. Technol. Adv. Mater. 10 (2009) 015008 .

[33]: Colegrove, P.A., Coules, H.E., Fairman, J., Martina, F., Kashoob, T., Mamash, H., Cozzolino, L.D., Microstructure and residual stress improvement in wire and arc additively manufactured parts through high-pressure rolling, Journal of Materials Processing Technology (2013)

[34]: Optical Microscopy

http://www.pearson-studium.de/books/3827370597/cd01/Gallery/Images/OM.htm (accessed on 10th July 2013).

[35]: T. Reutzel, R. Martukanitz, S. Kelly,etc, Recent Advances in Laser Deposition for Repair and Additive Manufacturing, 2012, Applied Research Laboratory, Pennsylvania State University.

[36]: S. Leuders et al, On the mechanical behaviour of titanium alloy TiAl6V4 manufactured by selective laser melting: Fatigue resistance and crack growth performance, 2013, International Journal of Fatigue 48 (2013) 300–307

[37]: S. Sun, Q. Liu, M. Bringezu, etc, Microstructure and Mechanical Properties of Ti-6Al-4V Parts Built by Selective Laser Melting, 2010, RMIT University, DSTO, La Trobe University, DMTC.

[38]: Khalid Rafi. H, Karthik N.V, Thomas L. Starr and Brent E. Stucker, Mechanical property evaluation of Ti-6Al-4V parts made using Electron Beam Melting, 2012, Department of Industrial Engineering, Department of Chemical Engineering, J. B. Speed School of Engineering, University of Louisville, Louisville, KY 40292.

[39]: Nikolas Hrabe, Ryan Kircher and Timothy Quinn, Effects of Processing on Microstructure and Mechanical Properties of Ti-6Al-4V Fabricated using Electron Beam Melting (EBM): Orientation and Location, 2012, National Institute of Standards and Technology (NIST), Boulder, CO, Medical Modeling Inc., Golden, CO.

[40]: Kim, W.H, Laird, C,Crack Nucleation and State I Propagation in High Strain Fatigue- II Mechanism, 1987, Acta Metallurgica. p.789-799

[41]: Valeria La Saponara, Introduction to Fracture Mechanics and Fatigue, 2010, MAE @ UCD

[42]: D.P. DeLuca, Understanding Fatigue, United Technologies Pratt & Whitney.

[43]: M. Janssen, J. Zuidema and R. J. H. Wanhill, Fracture mechanics, 2002, Vereniging voor Studie-en Studentenbelangen te Delft.

[44]: T.L. Anderson, Ph. D, Fracture Mechanics Fundamentals and Applications, Third edition, 2005, Taylor & Francis Group, LLC.

[45]: ASTM E647-11, Standard Test Method for Measurement of Fatigue Crack Growth Rates, 2011, ASTM International, United States.

[46]: ASTM E399-90, Standard Test Method for Plane-Strain Fracture Toughness of Metallic Materials, 1997, ASTM International, United States.

[47]: Filomeno Martina, High-pressure rolling reduces grain size and distortion, improves mechanical properties and produces isotropy in Ti-6Al-4V wire+arc additively manufactured parts, 2013, Welding Engineering And Laser Processing Centre, Cranfield University

[48]: J. Ding a, P. Colegrove, J. Mehnen, S. Ganguly, P.M. Sequeira Almeida, F. Wangb, S. Williams, Thermo-mechanical analysis of Wire and Arc Additive Layer Manufacturing process on large multi-layer parts, 2011, Computational Materials Science, 50 (2011) 3315–3322

APPENDICES

Appendix A Drawing

Drawing for Compact Tension specimens used for Fatigue Crack Growth Rate tests is presented in this section.

The Compact Tension specimens used for Fatigue Crack Growth Rates tests

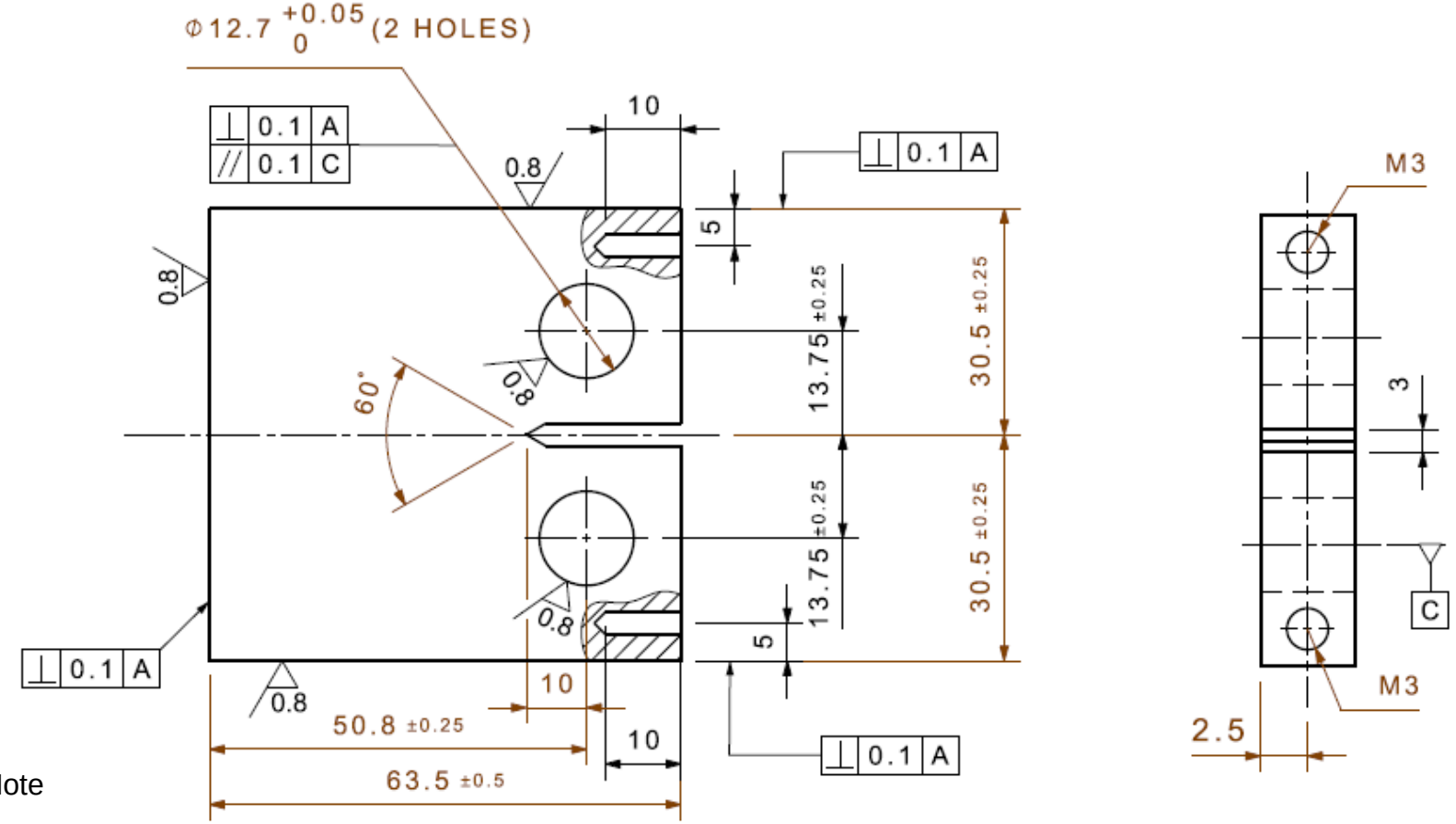

Note

1. All the dimensions are in millimetres, except the surface roughness in micrometers.
2. The notch tip should be as sharp as possible.
3. Marks should be visible on finished specimens.

Surface and thickness requirements on the initial wall

Disposition of specimens in the wall

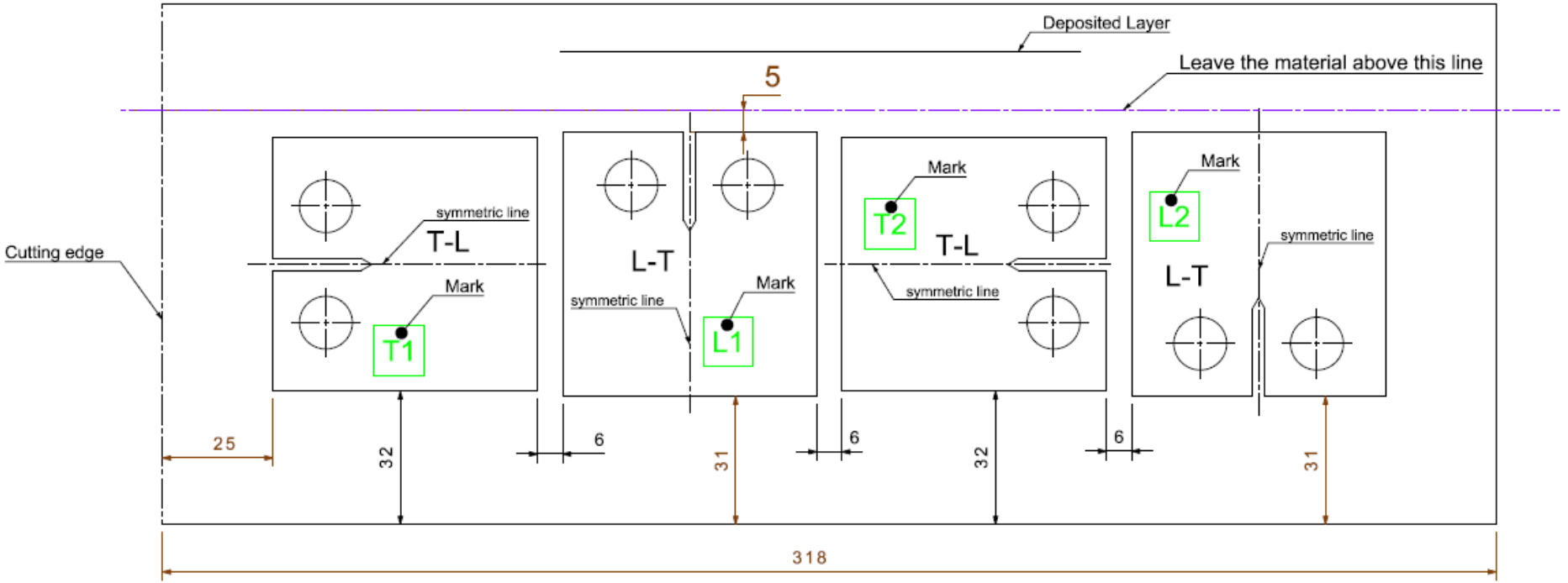

Procedure

1. Machine out the “Cutting edge” as a datum plane for following work. The cutting edge should be perpendicular to deposited layer.
2. Skim the wall to the required thickness and surface roughness.
3. Machine the specimens. The symmetric lines of T-L specimens should be perpendicular to cutting edge. The symmetric lines of L-T specimens should be parallel to cutting edge. Make a clear mark as shown in the drawing on each specimen before machining.